University of Bologna

PhD Thesis in

Civil and Environmental Engineering

Cycle XXVI

Modelling and analysis of thin-walled beams in the context of the Generalized Beam Theory

PhD Candidate:

Alejandro Gutierrez

Advisor:

Prof. Stefano de Miranda

PhD coordinator:

Prof. Alberto Lamberti

Co-Advisor:

Prof. Francesco Ubertini

March 29, 2014

Universitá di Bologna

Tesi di Dottorato di Ricerca in

Ingegneria Civile e Ambientale

XXVI Ciclo

Settore Scientifico-Disciplinare ICAR/08

Settore Concorsuale 08/B2

Modellazione e analisi di travi in parete sottile nell'ambito della Generalized Beam Theory

Candidato:

Alejandro Gutierrez

Relatore:

Prof. Stefano de Miranda

Coordinatore:

Prof. Alberto Lamberti

Correlatore:

Prof. Francesco Ubertini

March 29, 2014

Contents

List of Figures

Dedication

En memoria del Catire Gutiérrez, la Vieja Candelaria, El Látigo Negro y El Loro, quienes se fueron del mundo sin verme hecho un hombre completo. Yo guardaré sus nombres y su memoria siempre con orgullo.

Acknowledgements

I would like to thank the European Commission for financing the first three years of my stay in Italy through the "Ánimo, ¡Chévere!" scholarship program. I thank also the Department of Civil and Environmental Engineering at the University of Bologna for financing the rest of my PhD studies.

Thanks to Professor Stefano de Miranda for his inexhaustible patience and for the guidance he has provided in these years, not only on the matters dealt with in this work, but on the many commonly overlooked aspects of being a scientific researcher. Thanks also to Professor Francesco Ubertini for his advice and the trust he has given me on this endeavour. Also, I thank the gang at the department of Civil Engineering: Nicholas, Marco, Rosario, Alessandro, Ilaria, and the others. Without you guys, without the friendship and hospitality you have so freely given, this would have been much more difficult and considerably less fun!

I thank my old Venezuelan engineering comrades as well. Many of whom have, like myself, left behind our land looking for new horizons. Time and geography may have sundered our paths, but the bonds we once made will endure. Special thanks to Professor Carlos Graciano, who initiated me in scientific research.

Thanks, of course, to my old folks Blas and María. I don't have enough words to express how much I value the unconditional love and support you have given me through my life. You are the best parents a man could ever dream of. I hope my deeds make you proud.

Thanks, finally, to my dear Bristin. You came into my life like a sudden spring after a long, forgotten winter. You give me joy, strength, courage and wisdom. You make me a better man in ways I never thought I could be.

Introduction

Thin-walled beams can be broadly defined as slender structural elements with distinctive dimensions that are all of different orders of magnitude: their thickness is small when compared with the dimensions of the cross-section, which themselves are small when compared with the element length. This simple geometrical fact, apparently banal in itself, is in fact the source of the many advantages that distinguish thin-walled beams from other structural elements: thin-walled beams are lightweight but can resist significant loads; they can be cheaper to produce, transport and install than more compact beams; they allow for versatility in material and shape, giving more freedom of choice to the structural designer. At the same time, the geometrical particularities of thin-walled beams may make their mechanical behaviour considerably complex: classical beam models often fall short of accurately describing the whole kinematic range of these elements, especially in the case of cold-formed or composite profiles where bending, torsion, cross-section distortion and local effects occur together and in a coupled manner. These complexities translate into a need for modelling and analysis tools that are both highly accurate and computation-

ally cheap. In this sense, the contributions to the modelling and analysis of thin-walled beams can be subdivided in two main categories: one towards an effective three-dimensional "shell" modeling, and the other towards the formulation and development of mono-dimensional beam models with enriched cross-section kinematics. The present work stands within this second kind of approach.

In the first chapter of this work, an overview of the importance of thin-walled beams, their commercial forms, and their manufacturing methods is outlined along with a brief description of some of the most important models used to analyze these elements. Firstly, cold-formed profiles are presented as one of the historically most common application of thin-walled beams. Indeed, the usage of these is ever increasing in the building business and the need to take into account the distortion of their cross section in their analysis is well documented in current standards [1]-[4]. Later on, composite profiles are introduced as a more recent innovation in the field, motivated mainly by the needs of the aeronautical/aerospace industry, but also applied to civil, naval, and turbomachinery construction in the recent decades. After this brief introduction to the subject, some of the most relevant models formulated for thin-walled beams are introduced. The theory of Vlasov [5], the first approach to the modelling of a thin-walled beam, is based on a description of the cross-section warping related to a non-uniform distribution of torsional rotation. A detailed exposition of the Vlasov theory is found in the work of Bleich [6] and Timoshenko [7] with special empha-

sis on stability analysis. From this original model, considerable work has been done over the decades to enhance and extend the Vlasov theory by different methods, such as the incorporation of higher-order parameters in the displacement field. Some significant contributions to the ongoing efforts are those of Kang and Yoo [8], who developed a Vlasov-like model to study large displacement behaviour in curved beams, and the work of Kim [9], Wilson [10], and Stavridis [11] among others who have studied the vibration and stability analysis of thin-walled profiles. However, these formulations have maintained the basic Vlasov hypotheses of the cross-section being rigid in its own plane and of null shear deformability. Regarding the second of these, the work of Capurso [12], [13] extended the model of Vlasov to include shear deformation over the cross-section midline by generalizing the description of warping. More recently, the work of Piovan [14], Gendy and Saleeb [15], and again Kim [16] has revolved around the inclusion of shear deformability on Vlasov-like beam models for vibration and stability analysis. However, beam models based on the kinematics of Vlasov fail to take into account the effects of cross-section distortion and local in-plane deformation of the walls. In this respect, The Generalized Beam Theory (GBT), originally proposed by Schard [17], [18] in the 1980s, is a model that adds to the kinematics of Vlasov the distortion of the cross-section by means of expressing the deformation of the member as the superposition of a series of cross-sectional modes. Following the work of Schardt, many authors have contributed to the improve-

ment of the GBT by extending it beyond its original formulation for open unbranched cross-sections [19]-[21] and by adding nonlinear effects for the analysis of buckling problems [22]-[24]. Moreover, in the spirit of the Kantorovich's semi-variational method, a new approach for the selection of the cross-section deformation modes has been presented in [25]. Recently, the application of the GBT to analyze cold-formed roof systems has been presented in [26]-[28].

As regards the shear deformation, Silvestre and Camotim [29]-[30] were the first to remove the Vlasov constraint of null shear deformation in the GBT. However, their formulation considered constant warping displacement over the wall thickness, which leads to null shear strain between the direction of the beam axis and that orthogonal to the wall midline. This in turn means that classical shear deformable beam theories are not recovered exactly, which limits the attractiveness of the resultant theory. In the second chapter of this work, following the ideas presented in [31],a new formulation of the GBT that coherently accounts for shear deformation is presented. In particular, a modified formulation of the kinematics early proposed by Silvestre and Camotim for shear deformable GBT is devised. The new formulation introduces the shear deformation along the wall thickness direction besides that along the wall midline, so guaranteeing a coherent matching between bending and shear strain components of the beam. According to the new kinematics, a reviewed form of the cross-section analysis procedure is devised, based on a unique modal decomposition for both flexural

and shear modes. Much attention is posed on the mechanical interpretation of the deformation parameters in the modal space. It is shown that, in the modal space, it is possible to clearly distinguish bending deflections from deflections due to shearing strains, and to recover classical beam degrees of freedom and standard beam theories as special cases. The effectiveness of the proposed approach is illustrated on typical benchmark problems.

When it comes to postprocessing, the reconstruction of the three-dimensional stress field from a beam model is a problem seldom studied. The work of Cesnik [32] and more recently Volovoi [33] tackles this problem by means of a variational asymptotic beam-section analysis which allows recovering of a three dimensional stress state in a postprocessing stage, but since it is based in a Vlasov beam model, its accuracy is limited. In the case of GBT, stress recovery has generally been kept at the most basic level of elasto-kinematic relations which, by the very nature of the GBT kinematics, paint an incomplete picture of the stress profiles. Already in Schardt's original work, stress reconstruction was limited to normal stresses in the direction of the axis of the beam by means of a classical constitutive relation. In [34], as a part of a buckling analysis of GBT members with non-standard support conditions, the limitations of the elasto-kinematic approach to stress calculation were put in evidence and the recovery of the sole shear stress component along the section midline from axial stress equilibrium was performed. In Chapter 3 of this thesis, following the stress

recovery procedure recently proposed in [35], a procedure for a posteriori reconstruction of three-dimensional stresses in the finite element analysis of GBT is presented. The reconstruction is based on the enforcement of the pointwise three-dimensional equilibrium equations over the beam, interpreted as an assembly of thick plates, and allows recovering a fully three-dimensional stress profile without the need for corrections to meet the equilibrium boundary conditions on bottom/top wall faces. To improve the approximation of stresses over the finite element, a superconvergent patch-based procedure called Recovery by Compatibility in Patches (RCP) is used. This procedure, originally developed for plates [36]-[43], is here suitably extended to the GBT and permits the reconstruction of a stress profile with an accuracy similar to that of a brick finite element model while carrying a computational cost that is several orders of magnitude lower.

Regardless of the abundant literature on the subject, comparatively little effort has been devoted towards a proper theoretical study of the constitutive relation and its correspondence to the internal constraints of the kinematic model. Given that the GBT essentially considers the cross-section as an assembly of plates, the correct constitutive law to be used for the beam model may not be immediately clear. In the isotropic case, the approach commonly taken in the literature is the adoption of two distinct constitutive laws for the membrane and bending parts of the problem. In the first part of Chapter 4, this issue is addressed and the conventional

approach is presented. On the other hand, in the case of anisotropic thin-walled beams, the Vlasov model was used by Bauld [44] to study fiber-reinforced composite members of open section under different loading conditions. Their model neglected shear deformation, but later efforts by Wu [45], Chandra [46], Kim [47] and others removed this constraint and extended the Vlasov theory to many different types of composites, including laminated profiles. On the GBT front, Silvestre and Camotim [48] were the first to put forward a GBT formulation to account for orthotropic members, studying different cases of lamination and their influence on the GBT equations. Since then, vibration behaviour of arbitrarily loaded lipped channel columns and beams with cross-ply orthotropy has been presented in [49]. The linear and buckling (local and global) behaviours of FRP composite thin-walled members, with special emphasis for the effects of material couplings, have been extensively analysed in [50] and [51]. Regardless of the beam model used, most of the approaches available in the literature rely on satisfying internal kinematic constraints by means of a certain condensation of the constitutive matrix, which poses the problem of the correct choice of condensation and defines very different methods of analysis depending of the material being used: either different membrane and bending constitutive matrices for the isotropic case or a condensed matrix for the orthotropic material. The second part of Chapter 4 addresses this problem by proposing an alternative writing of the constitutive relations. The kinematic constraints are mirrored onto

the stress profile and a single constitutive matrix is obtained which is correct for both the isotropic and orthotropic cases. In the case of a laminated material, an analogous procedure is presented in which the stress profile of the generic layer is assumed so as to satisfy the kinematic constraints of the laminated plate forming the generic wall. Numerical examples are used to show the performance of this approach with both isotropic, orthotropic and laminated materials.

The way in which shear is introduced into the GBT kinematics in Chapter 2 results in a poor description of the membrane shear strain. One way of enriching this description of shear is using a correction factor to adjust for the cross-sectional area that is in fact resistant to shear in a manner analogous to that of the Timoshenko beam. As it is well known, these correction factors may not be trivial to determine, especially in the case of an orthotropic material [52]. The final part of Chapter 4 is a discussion on these shear correction factors and a proposal to determine them in the framework of the GBT. Taking advantage of the recovery procedure presented in the third chapter, the elasto-kinematic shear stress is corrected by comparing its energy contribution to that of the reconstructed component. The correction factor thus obtained is used to improve the GBT solution. The results of this approach are shown in numerical examples.

Chapter 1

An overview of the mechanics of thin-walled members

Abstract

In this chapter, cold-formed and composite profiles, which are the main thin-walled beam products of interest of this work, are presented. A brief description of their use, history, and fabrication methods is outlined along with the peculiarities of these members. Some of the most important analysis tools for the modelling of these members are described, with special attention being paid to beam models. Specifically, the theory of Capurso and the original GBT formulation. The finite strip method is also briefly presented as a numerical option commonly used in this kind of analysis.

In the most elemental texts on structural mechanics, the term "beam" is used to refer to a structural element that can treated as one-dimensional. The dominant dimension in a beam, referred to as its axis, is the only range of variation for deformations and forces that are defined for a certain cross-section normal to the

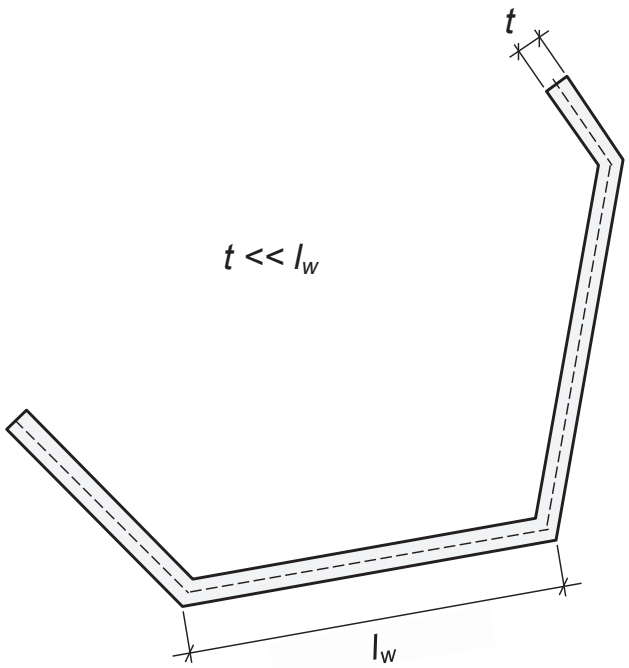

Figure 1.1: Example of a thin-walled cross-section.

axis. Geometrically speaking, this kind of definition points to what is called a beam of "compact" section: a structural member in which all the dimensions of the cross section are similar and in themselves of a smaller order of magnitude than the axial length. Thin-walled beams are a subset of one-dimensional structural elements in which there are three distinctive dimensions instead of two, all of different orders of magnitude. The cross-section is thus understood as a series of segments, with each of them having a dominant dimension in the cross-section plane, as is shown in Fig. 1.1. Each of these segments if referred to as a "wall", thus the wall thickness is small when compared with its length, which itself small compared with the beam's length. This geometrical particularity is the basis for the characteristic behaviour of thin-walled beams, whose thorough description is the purpose of this work.

The use of thin-walled members in construction engineering dates back to the 19th century. Indeed, the first I-beams were manufactured in France in 1849 and the first steel-frame skyscrapers were built in the U.S. in the 1880s. Cold-formed steel specifically, a product widely used today for thin-walled beams, also dates back to the mid-19th century but for a long time the scarce knowledge about its mechanical behaviour made its regular and extensive application in construction impractical. Indeed, even after the first standards for structural steel were adopted in the early 20th century, the geometrical particularities of cold-formed members were such that the construction standards could not be readily applied. For this reason, the first widespread applications of cold-formed profiles in construction date from after the Second World War. However, after such slow beginnings, the usage of cold-formed structural elements has increased at a rapid pace and has extended to many different fields of engineering, not only in civil works, but also in aeronautical, aerospace, and turbomachinery industries. These profiles are in many cases more economical to produce than other structural members with similar performance, and at the same time can weigh considerably less than the alternatives. Additionally, cold-formed profiles provide significantly more flexibility to construction design, since they can be easily worked into many possible shapes, with each particular geometry offering significant differences in strength characteristics. In this work, attention will be focused on two broad categories of thin-walled beams: cold-formed profiles and composite

profiles. Each of these groups has it own manufacturing process, range of applications, and mechanical behaviour, as we shall see below.

1.1 Cold-formed profiles

One of the oldest and most common method of producing thin-walled beams is cold-forming. This term refers to a range of manufacturing processes in which a metal sheet is worked by stamping, rolling, pressing, or bending into a usable structural member. The name derives from the forming process being performed at room temperature, as opposed to hot-rolled members, which are heated before forming. Since pressing or rolling a metal sheet at room temperature is a relatively easy industrial process, cold-formed profiles can be easily prefabricated and mass-produced. It is from this fact that many of the advantages of these profiles derive. Fig. 1.2 shows some of the many forms in which cold-formed profiles can be produced for commercial use.

The first usage of cold-formed profiles can be traced back to the 1850's England, but it was not until the American Iron and Steel Institute (AISI) published the first specification for the design of cold-formed profiles in 1946, based in the work conducted by George Winter at Cornell University, that widespread applications of this technology became conveniently available to engineers. From those initial applications to construction, cold-formed profiles have been increasingly used over time for a variety of purposes such framing in

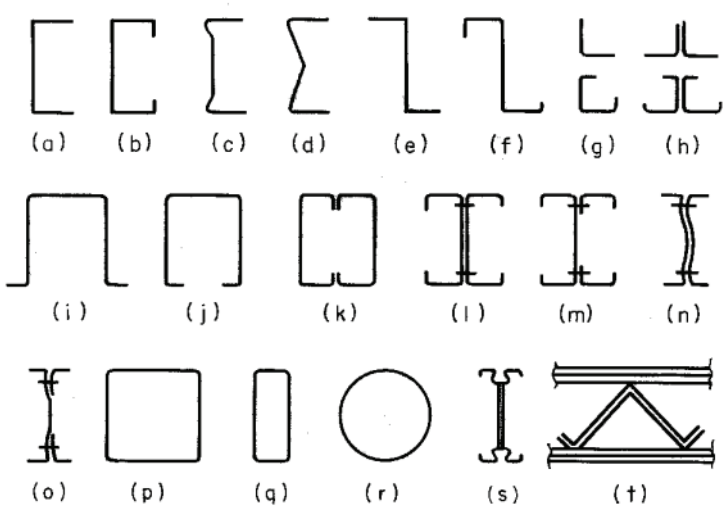

Figure 1.2: Some cold-formed sections.

(a) Building framing using cold-formed profiles

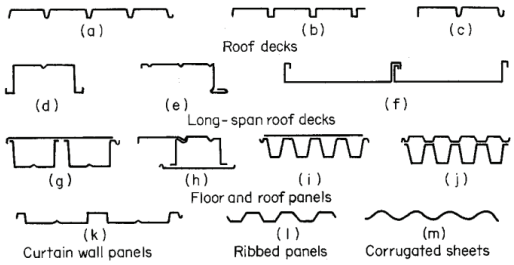

(b) Some types of cold-formed panels

Figure 1.3: Applications of cold-formed structural elements

building construction (Fig. 1.3a), or facesheets for sandwich panels (Fig. 1.3b)

Production process

Cold-formed profiles may be manufactured using two different methods: roll-forming of brake pressing. Roll-forming is a continuous process that shapes a coiled sheet of metal into single profiles. This process is typically performed by means of a series of pairs of rolls

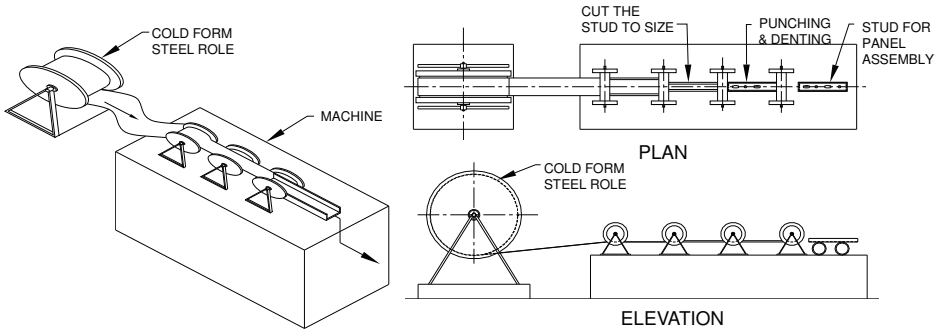

Figure 1.4: Diagram of the roll-forming process.

which rotate in opposite directions drawing the sheet through and slightly changing the shape of the sheet to reach the final configuration by successive deformations. A diagram of he process is shown in Fig. 1.4. Depending on the complexity of the section desired, more or less rolls will be needed in the process, but in general roll-forming is a rapid method of producing standard profiles. Given that the manufacturing of different sections will require different set of rolls, the process is most economically convenient for mass-production.

Brake-pressing is an alternative procedure useful when more complex sections of cold-formed profiles are needed. The section in this case is manufactured by pressing sheets of metal, forming one or two bends at a time. While this method offers more versatility in the sections that can be formed, it is comparatively crude and slow. Additionally, the length of the profile is limited to the width of the pressing machine, which seldom exceeds 6 meters. Since each finished profile results from a single sheet being folded at a time, this method is not as well suited for mass production as cold

rolling. In any case, the choice of method to use will depend on the needs of the engineer, mainly complexity of the section and required quantity.

1.2 Composite profiles

During the rise of the usage of thin-walled beams for structural applications in the 20th century, the vast majority of these elements were made of cold-formed steel or aluminium. Since these are isotropic materials, for a long time there was no real incentive to conduct research in the field of anisotropic thin-walled beams. The Second World War however, brought about the rise of aeronautical engineering, which represented a major inflection point in the history of thin-walled structures. In aeronautics, the combination of strength and stiffness with lightness is a focal point for the design of any particular structure. Along with this basic need, a material that is unlikely to completely break under stress, that is a material in which cracks are less easily spread, is of vital importance. Structural elements in aeronautics would also be exposed to extreme conditions of heat and corrosion, and would be needed to be easily manufactured in very complex shapes. For these tasks, metallic thin-walled profiles were ill-fit, so the solution came in the form of composites.

Composite materials, the macroscopic union of two or more materials to produce a third one with desirable properties present in neither of the constituents alone, are in themselves very old. Ply-

wood, the union of different wood sheets at different angles has been know for millennia. Concrete, made of cement in which a certain granular material is embedded, dates from the times of the Ancient Romans; and reinforced concrete, in which steel and concrete are joined to act as a single unit, has been around since the mid 19th century with the appearance of the skyscraper. However, none of these well known materials could satisfy the needs of the aeronautics industry, which required thin-walled elements. In this context, a common solution offered is the fiber-reinforced composite, which consists of high strength *fibers* embedded in a *matrix* material. Commonly, these fiber-reinforced materials are made in the form of thin layers called *lamina*. A specific profile may then be formed by stacking the layers (each one independently oriented with respect to the resulting profile) to achieve the desired properties. In recent years, this kind of material has progressively seen its production prices drop until a tipping point was reached in which its application to the civil industry became economically feasible, mainly in applications such as offshore structures and chemical plants.

Production process

Generally speaking, producing composites involves mixing the matrix and fiber materials, binding them together by means of heat, or a chemical reaction, into a single unified product. Depending on the materials used, the final shape desired, and the application details, one of the following methods is used:

Hand Laminating and Autoclave These processes consist on depositing successive layers of material on top of each other, either by hand or robotically. Hand laminating is usually achieved using a male pattern from which a female mold is construed. A gel coat is applied to the male pattern and several layers of reinforcement are applied alternating with layers of matrix resin, as shown in Fig. 1.5a. This process is commonly used to make Glass-Fiber-Reinforced-Polymer (GFRP) elements in low-scale production of boats and general prototyping. Autoclave processing, schematically shown in Fig. 1.5b also involves the stacking of successive layers, but in this case the layers are made of both the matrix and fiber material that have been previously combined into a semi-finished form called prepreg. After stacking these layers the resulting laminated profile is placed inside an autoclave, a pressure vessel that binds the element together at high temperatures. The autoclave process is used in the aerospace industry and produces components of a very high quality, but it takes great amounts of time and resources.

Filament Winding and fiber placing Both of these processes similarly revolve around applying reinforcements around a mandrel. In the case of filament winding, fibers are wound over a rotating mandrel (see Fig. 1.6a) following a specific pattern of fiber orientation that gives the finished product its final mechanical properties. In the case of fiber placing, reinforce-

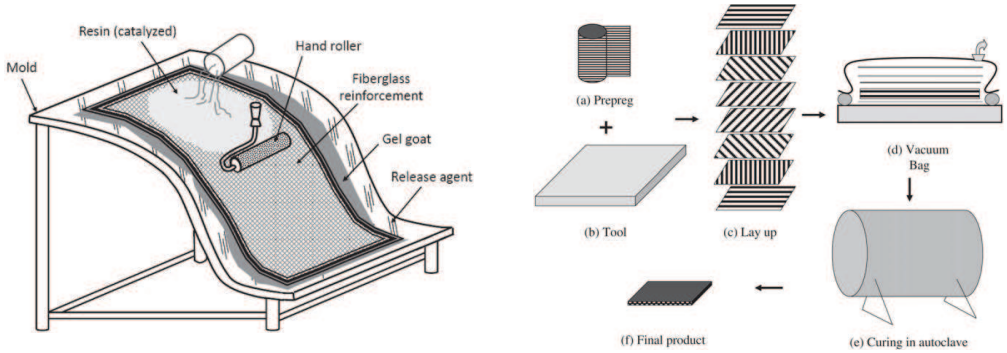

(a) Hand laminating

(b) Autoclave process

Figure 1.5: Schematic view of the hand laminating and autoclave processes

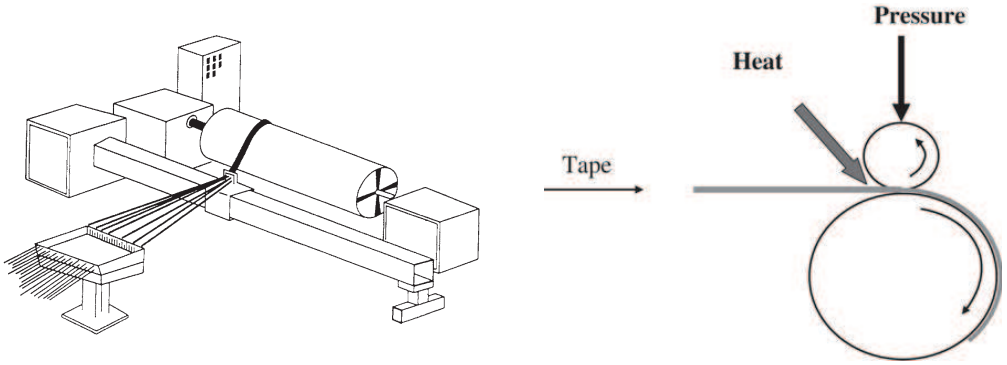

(a) Filament winding

(b) Fiber placing

Figure 1.6: Schematic view of the filament winding and fiber placing processes

ments are applied to the surface of the mandrel in the form of wrapping strips, as shown in Fig. 1.6b, held in place by applying high pressure and temperature. Both of these processes are used to create surfaces of revolution and result in elements that perform very well under high pressures, thus making them ideal for tanks and pipes.

Pultrusion This process is a combination of pulling and extruding (hence its name) and consists of fibers impregnated with resin that are pulled through a stationary heated die (see Fig. 1.7),

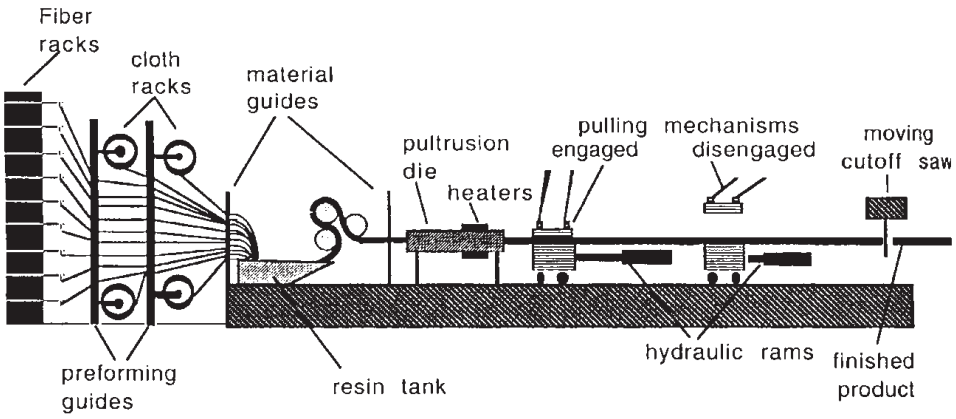

Figure 1.7: Schematic view of the pultrusion process

which solidifies the resin. Upon exiting the die, the structural component is pulled and cut to length in a similar way to cold-rolled metal profiles. This procedure allows the production of composite beams at a low cost and with a high production rate, thus making pultruded beams a good component to use in the construction industry.

Liquid Molding In this family of processes the fibers are packaged into a pre-form having the configuration of the final part. The preform is then placed inside a processing mold and resin is infused at high pressure to wet the fibers and fill any existing cavity, usually catalysts and heat are used to help the process. After the resin has been infused, the part is demolded and ready to be used. This process allows for relatively low cost and high production rates, in a way similar to pultrusion. Fig. 1.8 shows a schematic view of this process.

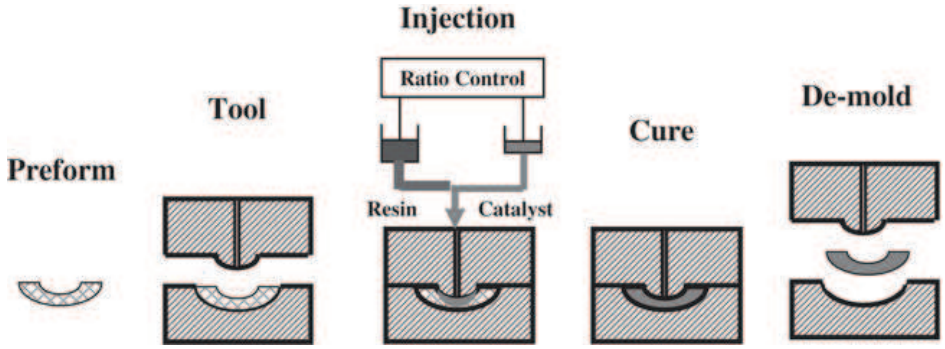

Figure 1.8: Schematic view of the liquid molding process

1.3 Theoretical framework

It is a well known fact that in thin-walled beams torsional loads produce also normal strains and stresses, and longitudinal or transverse loads induce torsion. This coupling of two different sets of kinematics stems of the fact that the cross-section of a thin-walled beam cannot be assumed to remain plane as it would be in compact-section beams, as the cross-section experiences out-of-plane warping in response to torsion. In addition to this, the distortion of the cross-section in its own plane is an aspect that can be critical to structural design depending on the application, as thin-walled cross-sections are essentially folded plates. Moreover, thin-walled profiles are particularly prone to instability phenomena which significantly differ from structural members with compact section. Specifically, thin-walled beams can not only suffer global instability, in which a certain deformation is experienced along the member's longitudinal axis (see Fig. 1.9a) leaving the cross-section undeformed in its own plane, but can also experience distorsional instability characterized by a deformation of the whole cross-section over a certain axial

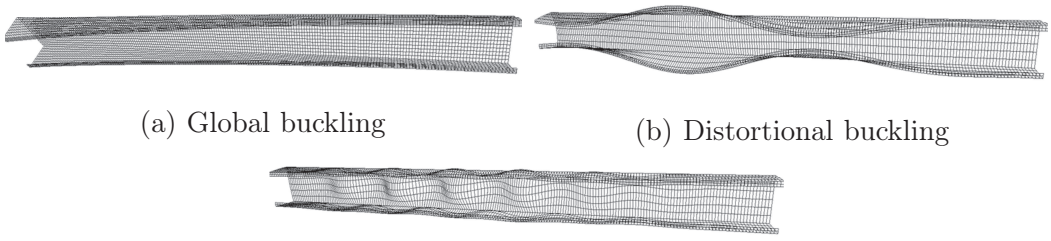

(a) Global buckling

(b) Distortional buckling

(c) Local buckling

Figure 1.9: Buckling modes

length (Fig. 1.9b) and even local instability, in which deformation may be limited to the single walls of the cross-section (Fig. 1.9c).

In light of the particularities explained above, it can be said that even if the manufacturing process of thin-walled profiles is relatively simple, their structural design is far from it. Indeed, any serious attempt to model the mechanics of thin-walled beams must take into account not only cross-section warping, but also shear deformation, cross-section distortion and local effects, while at the same time allowing for the study of many different loading cases and a wide assortment of boundary conditions. The first significant improvement from the classical Euler-Bernoulli beam into the field of thin-walled beams was the work of Vlasov [5] in 1940. The model of Vlasov, also known as the Theory of the Sectorial Area, deals with out-of-plane warping of the cross-section and revolves around a warping function that essentially characterizes the kinematics of non-uniform torsion along the beam axis. The work of Vlasov is still widely used as a standard today for the treatment of thin-walled beams and has been enriched by the efforts of many authors, since the early contributions of Timoshenko and Gere, which described

the stability of thin-walled beams under diverse loading conditions [7] or Murray [53] which applied the theory to standard design practices, to the more recent work on the stability of thin-walled profiles by Wilson et al. [10] and Kim et al [9]. However, the model of Vlasov has several limitations at its core: the cross-section is considered to be perfectly rigid in its own plane, the shear strains in the middle surface of the wall are neglected, and the transverse normal stresses in the walls are ignored along with normal stresses tangent to the midsurface of the wall. These limitations may be more or less relevant depending on the specific case considered, but it is clear that models based on the assumptions of Vlasov are an inherently incomplete description of the mechanics of thin-walled beams.

1.3.1 The theory of Capurso

A first generalization of the well known model of Vlasov is the Capurso Beam Theory. In the 1960s, Michele Capurso [12] introduced a novel model for thin-walled beams based on not just one, but instead a series of warping functions over the cross-section. In his seminal work, Capurso added to the six classical degrees of freedom of a Vlasov beam (axial displacement, displacements and rotations over the two main axes of inertia, and non-uniform torsion) infinite degrees of freedom that describe the many possible shapes in which the cross-section could warp. In essence, this constitutes a *generalization* of the cross-section's degree of freedom concept. If

we consider a generic thin-walled section, such as the one in Fig. 1.10 we can write the displacement field in the x, y, z coordinate system as:

$$d_x(s,z) = u(z) - \varphi_z(z)\,(y(s) - y_C)\,, \tag{1.1}$$

$$d_y(s,z) = v(z) - \varphi_z(z)\,(x(s) - x_C)\,, \tag{1.2}$$

$$d_z(s,z) = w(z) - \varphi_y(z)x(s) + \varphi_x(z)y(s) + \sum_{i=1}^{n} \varphi_i(z)\phi_i(s), \tag{1.3}$$

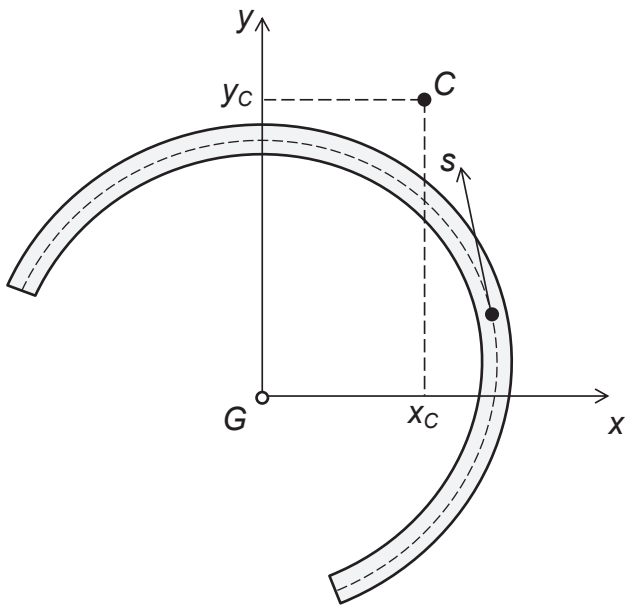

Figure 1.10: Capurso theory: global and local reference systems on a generic thin-walled cross-section.

where d_x, d_y, d_z are the displacements of a generic point on the cross-section in the x, y, z directions, functions $u(z), v(z), w(z)$ are the displacements in the x, y, z directions of the shear center, which is located in the coordinates x_C, y_C, and $\varphi_x, \varphi_y, \varphi_z$ are the rotations of the cross-section around axes x, y, z. The generic $\phi_i(s)$ is a specific warping function, which is weighed by the respective $\varphi_i(z)$.

This description not only contains the kinematic of Vlasov, but also does away with the assumption of null shear strains in the middle surface of the wall.

It is of particular importance to the present work that Capurso developed a *modal* theory, since each new warping function added to the kinematic description is weighed depending on the way the beam is loaded. The appeal of this modal approach will be better understood later on when more sophisticated model are presented, but it should be noticed that this is, to the knowledge of the author, the first instance of a modal description of the mechanics of thin-walled beams beyond the theory of Vlasov.

The model of Capurso remains valid today and in fact has been recently extended to transversely isotropic materials and applied to the analysis of pultruded fiber-reinforced polymer (FRP) thin-walled beams [54][55]. However, as rich as it is, the work of Capurso still lacks some elements that would be desired in a comprehensive model for thin-walled beams. Chief among these missing elements is the cross-section distortion. Without it, in-plane deformations of the cross-section and local phenomena cannot be described, and given the importance of these in the structural performance of thin-walled beams, it is clear that additional effort is needed.

1.3.2 The Generalized Beam Theory

An alternative beam model useful for the analysis of thin-walled beams is the Generalized Beam Theory (GBT) developed by Schardt

[17][18] in the 1980s. The GBT can be viewed as a generalization of the Vlasov theory able to take into account in-plane cross-section deformations while rewriting the beam kinematics in a modal form analogous to that of Capurso. Indeed, the GBT unifies conventional thin-walled beam theories and extends them to include section distortion by treating each particular set of kinematics (bending, torsion, distortion, etc.) as merely a special case of a generalized model.

The fundamental idea of the GBT is to consider a thin-walled beam as an “assembly" of thin plates and to assume the displacement field of the beam as a linear combination of predefined cross-section *deformation modes* (which are known beforehand) multiplied by unknown functions depending on the beam axial coordinate, that can be called *kinematic parameters* or *generalized displacements*. This analytical treatment defines four *fundamental* deformation modes (so called because they must absolutely be included in any GBT formulation) to account for extension, bending about the two principal axes and non-uniform torsion. These modes are also referred to in the literature as “rigid-body modes” because they do not involve any distortion of the cross-section. Additional deformation modes may then be used to include distortion and local effects. This unified writing is not only an elegant way of transition from a beam model to a folded plate problem, but is also very convenient to structural design since all of the classical beam quantities can be recovered directly as special cases of the generalized model.

In the original GBT formulation, the displacement field is defined for the generic i-th wall of the cross-section (see Fig. 1.11) as:

$$d_n(n,s,z) = \boldsymbol{\psi}(s)\mathbf{v}(z), \tag{1.4}$$

$$d_s(n,s,z) = \left[\boldsymbol{\mu}(s) - n\partial_s\boldsymbol{\psi}(s)\right]\mathbf{v}(z), \tag{1.5}$$

$$d_z(n,s,z) = \left[\boldsymbol{\varphi}(s) - n\boldsymbol{\psi}(s)\right]\partial_z\mathbf{v}(z), \tag{1.6}$$

where d_n is the displacement orthogonal to the wall midline, d_s is the displacement tangent to the wall midline, d_z is the displacement in the beam axial direction, $\boldsymbol{\psi}$, $\boldsymbol{\mu}$ and $\boldsymbol{\varphi}$ are row matrices collecting the assumed cross-section deformation modes (depending only on s) and $\mathbf{v}$ is the vector that collects the unknown kinematic parameters (depending only on z). Moreover, ∂_s and ∂_z denote the derivative with respect to the s coordinate and to the z coordinate, respectively. In the following, the term *natural nodes* is used to refer to the vertices of the cross-section midline, while *internal nodes* refers to intermediate points along the wall midline, as shown in Fig. 1.11.

In a similar way to the Capurso theory, the choice of the deformation modes constitutes the core of the GBT. As we shall see shortly, this choice of modes is intrinsically connected to the discretization of the cross-section into natural and internal nodes, since each node considered is the basis for a deformation mode. The procedure by which modes are defined from the cross-section discretization is re-

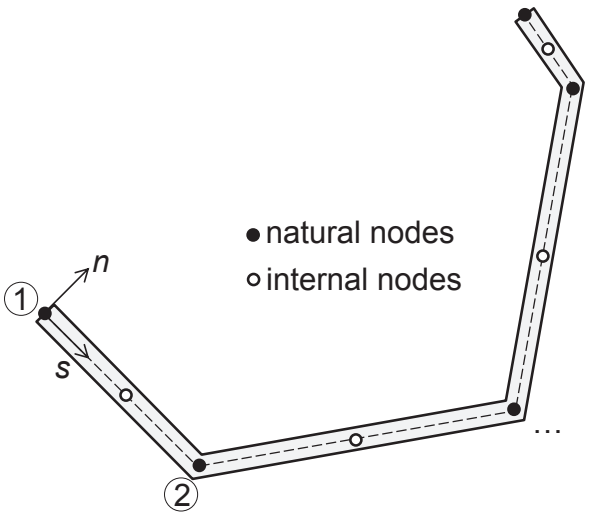

Figure 1.11: GBT: natural and internal nodes in a generic thin-walled cross-section.

ferred to as cross-section analysis and it is in fact a separation of variables, since by performing a cross-section analysis the in-plane kinematics of the cross-section is defined. The original GBT formulation of Schardt relied on the so-called flexural modes, which could be divided in *fundamental flexural modes* and *local flexural modes*.

Fig. 1.12a shows how one *fundamental flexural mode* can be defined for each natural node by assuming along the midline a piecewise linear (linear on each wall) warping function. This warping function has a unit value at the corresponding natural node and is null for all other natural nodes in the cross-section. Analogous functions are defined for the rest of the natural nodes, so the warping description of the cross-section is complete. It is important to note that, while the enrichment of the warping description in this modal way is similar to that of Capurso, the fundamental modes of

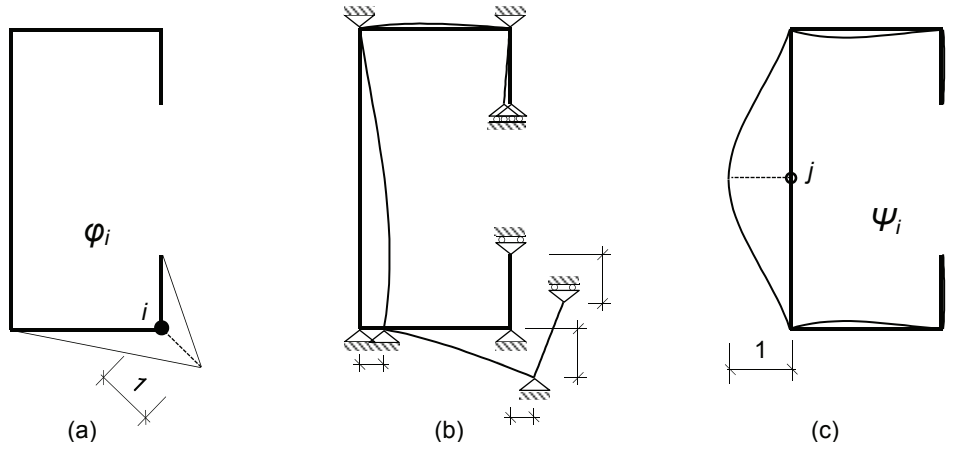

Figure 1.12: GBT: (a) warping in a fundamental flexural mode, (b) in-plane displacements in a fundamental flexural mode, (c) in-plane displacements in a local flexural mode.

the GBT are different in nature, since their warping description is linear. In addition to this, another key aspect of the fundamental modes is the fact that strain γ_{zs} is assumed to be null, thus following the assumption of Vlasov. Later on, we shall see that another version of the GBT can be formulated without recurring to this assumption, but for the time being this conditions implies:

$$\boldsymbol{\varphi}(s) \text{ linear}, \tag{1.7}$$

$$\boldsymbol{\mu}(s) = -\partial_s \boldsymbol{\varphi}(s) \Rightarrow \text{constant}, \tag{1.8}$$

$$\boldsymbol{\psi}(s) \text{ cubic}, \tag{1.9}$$

where the function $\boldsymbol{\mu}$ represents the in-plane displacement of the current natural node in the direction of the midline. Clearly, the relation between $\boldsymbol{\mu}$ and $\boldsymbol{\varphi}$ is the result of Vlasov's assumption. With these displacements completely known, the in-plane displacement transversal to the wall midline, denoted by $\boldsymbol{\psi}$, are easily determined

by considering the cross-section as a planar frame and solving it for $\boldsymbol{\psi}$ with the prescribed values of $\boldsymbol{\mu}$ as end conditions, thus restoring compatibility along the walls subjected to cylindrical bending (see Fig. 1.12b). This procedure is a key feature of the GBT and, after being performed for all the modes, allows to recover the kinematics of a Vlasov beam enriched with $N_n - 4$ distortional modes, being N_n the number of natural nodes.

Local flexural modes can be defined in a similar way. One *local flexural mode* is considered for each internal node by assuming null warping, null shear strain γ_{zs} along the midline of the cross-section and piecewise cubic displacement normal to the wall. Thus, these modes enrich the in-plane kinematic description of the cross-section while not contributing to warping. Functions $\boldsymbol{\psi}$ are determined by assuming unit normal displacement at a certain internal node and zero at the other nodes (see Fig. 1.12c) so their value over each wall is again determined by solving the planar frame of the section with the prescribed conditions, i.e. null $\boldsymbol{\mu}$:

$$\boldsymbol{\varphi}(s) = \boldsymbol{\mu}(s) = \mathbf{0}, \quad \boldsymbol{\psi}(s) \text{ piecewise cubic.} \tag{1.10}$$

While the number of fundamental modes is limited by the geometry of the section (there can be only one per vertex), the number of possible local modes is potentially infinite. By simply refining the discretization of each wall, the description of local phenomena can be enriched as much as needed. This is a significant difference with the models of Vlasov and Capurso, both of which neglect local

effects and distortion.

As said above, the first four fundamental flexural modes correspond to the kinematics of a Vlasov beam, with the rest adding distortion and local effects. This, of course, is not immediately obvious from the way the modes are defined. To make this clear, and indeed to give each mode a distinct physical meaning, it is necessary to transform Eqs. (1.4)-(1.6) through a modal decomposition. In particular, the system can be transformed from its original base to a modal one in which each cross-section deformation mode has a specific meaning. Indeed, it can be shown that, in the modal space, the first four modes correspond to the classical degrees of freedom of a shear-undeformable beam and each additional mode corresponds to section distortion and/or local wall deformation. As an example, in Fig. 1.13 the displacements corresponding to the six fundamental flexural modes of a C-shaped cross-section after such modal decomposition are shown. It can be seen how the classical generalized deformations of a Vlasov beam are recovered, such as axial extension (mode 1), major and minor axis bending (modes 2 and 3), and twisting rotation about the shear centre (mode 4). Modes 5 and 6 are typical GBT higher-order flexural deformations involving section distortion.

1.4 Numerical Modelling

Given the three-dimensional character of the strain field in thin-walled mechanics, a common way to describe these problems is by

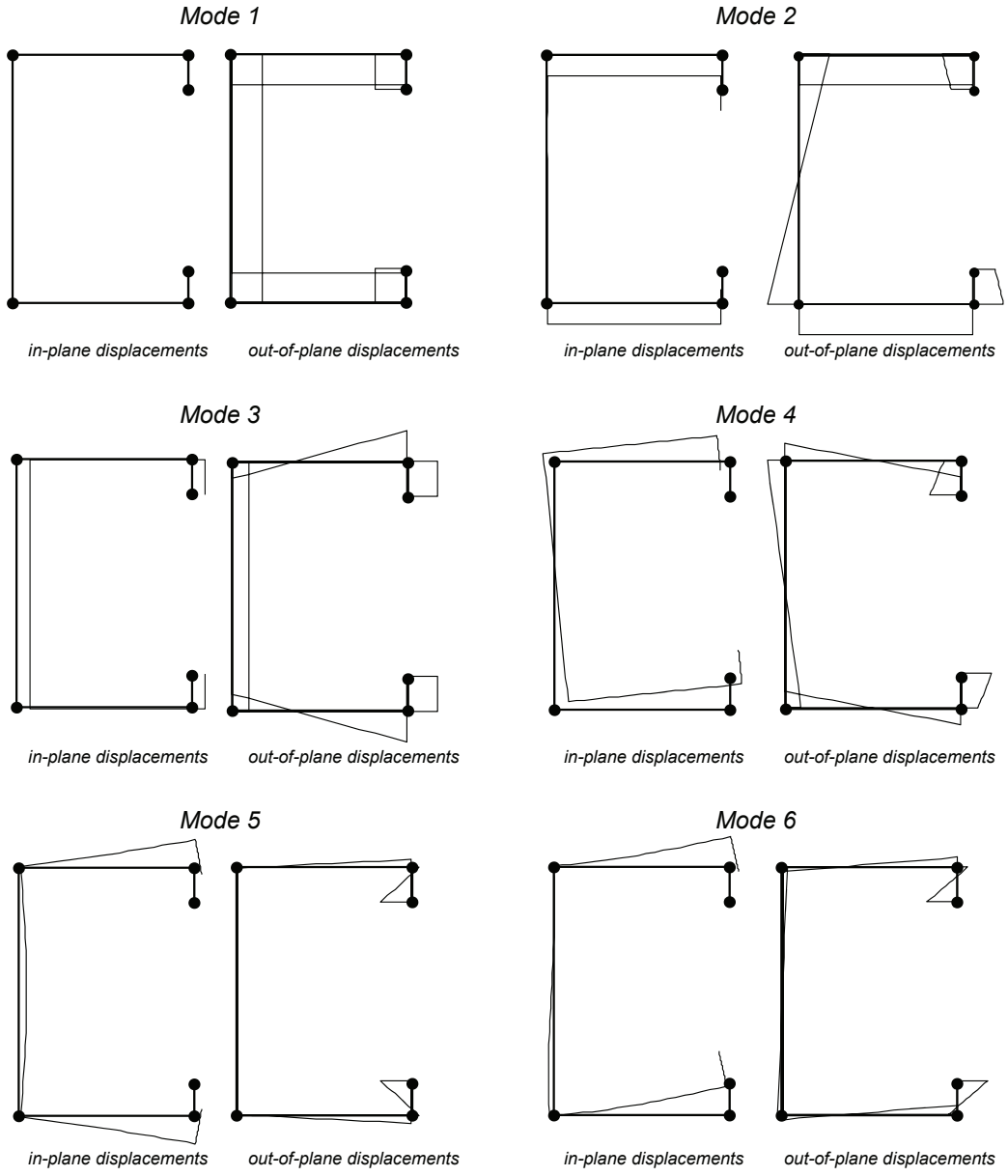

Figure 1.13: C cross-section modelled by GBT: in- and out-of-plane displacements corresponding to the six fundamental flexural modes after modal decomposition.

means of the Finite Element Method (FEM). A thin-walled beam could be modelled as an assembly of plate elements and thus its complete mechanical behaviour could be determined. However, such an approach would carry an important computational cost, since the FEM solution requires discretisation in every dimension of the problem and therefore considerably more unknowns than a beam-based approach. Moreover, a FEM solution is exclusively three-dimensional, which means that classic one-dimensional quantities such as bending moments, normal stress, and shear force (or their kinematic counterparts, like rotations, axial displacement, and shear deflections) cannot be easily identified. This is a significant drawback from the point of view of the structural designer, who needs to use these quantities to follow engineering standards. Enriched beam models, such as that of Capurso or the GBT, are a useful alternative to fully three-dimensional FEM models in this sense. In the following chapters, a numerical implementation of the GBT will be presented as the preferred model for thin-walled beams. However, for the sake of completeness, a numerical approach referred to as the Finite Strip Method (FSM), commonly used to model thin-walled profiles, will be briefly described here. This method is born out of the need to compromise between the kinematic richness of a plate FEM approach and the computational economy of a beam model, and has been proven to give satisfactory results for a variety of problems.

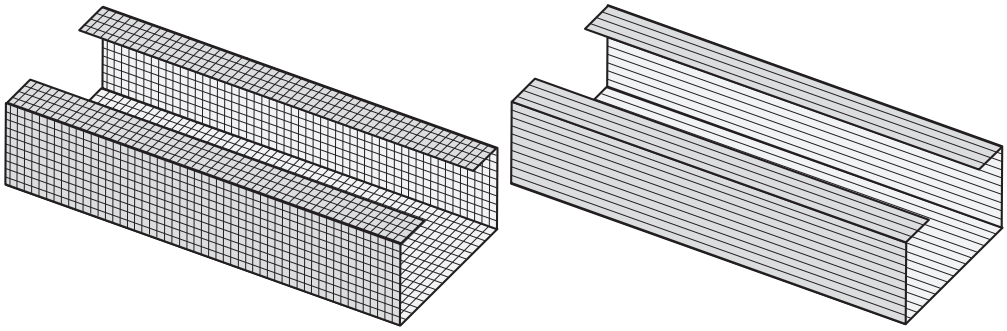

(a) FEM (b) FSM

Figure 1.14: Comparison of the level of discretization used for the same geometry using finite elements and finite strips

1.4.1 The Finite Strip Method

The FSM is a semi-analytical procedure that stands in between the classical Rayleigh-Ritz method and a FEM solution. At its base there is a separation of variables, in a similar way to that of Kantorovich [56], between the axial and cross-sectional directions. From this separation, two different sets of functions can be used to approximate the variables in the corresponding directions.

In the FSM, a beam is divided into longitudinal strips (hence the name of the method) adjacent among themselves, as shown in Fig. 1.14b. Two different sets of approximation functions are then chosen: one along the axial direction and another over the cross-section. Since this sort of discretisation creates significantly less unknowns than a FEM approach (see the equivalent FEM mesh in Fig. 1.14a) the FSM method is able to describe the three-dimensional strains of the problem with reduced computational effort.

Evidently, the accuracy of the FSM method depends on the

choice of the approximation functions. The classical FSM [57]called for using simple polynomials, such as Hermite functions, as shape functions over the cross-section along with continuously differentiable smooth trigonometrical or hyperbolic functions over the axial direction. More recent versions of the method use different functions, such as splines, to overcome the difficulties of the interpolation, but the principle of separation of variables remains. Whatever the shape functions may be, the general form of the displacements can be written as:

$$w(s,z) = \sum_{i=1}^{n} \phi_i(s)\varphi_i(z), \tag{1.11}$$

where $\phi_i(s)$ represents the i-th polynomial shape function over the cross-section. This part of the interpolation must represent a state of constant strain over the cross-section, so as to guarantee convergence as the mesh is refined. The $\varphi_i(z)$ part of the interpolation is the longitudinal series of trigonometrical, hyperbolic or spline functions. This series must evidently satisfy the end conditions imposed on the beam. The choice of these functions is of vital importance in FSM analysis, since no refinement over the strip length is possible. This means that the FSM is susceptible to the specific load and end conditions, with the risk of not being applicable in some cases.

Since each strip is considered to be under a plane stress state and based in the Kirchhoff thin plate theory, the FSM allows to take into account not only the enriched warping description present in the Capurso theory, but also the distortion of the cross-section

and local effects. However, the family of solutions obtained is difficult to classify into meaningful modes, so most current applications of the FSM introduce specific mechanical criteria to separate the displacement field into distinct subspaces. These mechanical criteria, directly motivated by the GBT [58], form the basis of the so-called Constrained Finite Strip Method (cFSM) and generally produce satisfactory results for the stability analysis of thin-walled beams. The cFSM has been successfully used by Schafer [59] to analyze cold-formed steel members and has been used to differentiate global, distortional, and local buckling modes on open cross-section thin-walled beams [60]. However, even when using different longitudinal shape functions, some seemingly insurmountable obstacles remain in the way, mainly:

- Arbitrary boundary conditions are not possible to impose over the member. In particular, longitudinal elastic restraints (much common in cold-formed members applications) are not allowed by the formulation.

- Even when applying the cFSM methodology to identify distinct modes, these don't have a clear mechanical meaning. This means the classical degrees of freedom and stress resultants are not recovered exactly, which thwarts any attempt to use current standards for structural design.

The limitations of the FSM are such that it would be impractical to use for a general study of the mechanics of thin-walled profiles. A

methodology that brought together the versatility of the Capurso theory with the kinematic richness of the FSM is needed. This research work is bent on developing such a methodology based on the GBT.

Chapter 2

A Generalized Beam Theory with shear deformation

Abstract

In this chapter, a GBT formulation that coherently accounts for shear deformation is presented. The new formulation, which preserves the general format of the original GBT for flexural modes, introduces the shear deformation along the wall thickness direction besides that along the wall midline, so guaranteeing a coherent matching between bending and shear strain components of the beam. A reviewed form of the cross-section analysis procedure is devised, based on a unique modal decomposition for both flexural and shear modes. The effectiveness of the proposed approach is illustrated on three benchmark problems.

As shown in Chapter 1, the original formulation of the GBT maintained the Vlasov assumption of null shear deformation of the generic wall. It wasn't until almost two decades later that the work of Silvestre and Camotim [29]-[30] removed this constraint

by adding a new family of *shear modes* to the GBT formulation. These modes are based on the inclusion of non-null warping φ_s in the kinematics together with null in-plane displacement. This leads to the following displacement field (see [49]-[51]):

$$d_n(n,s,z) = \boldsymbol{\psi}(s)\mathbf{v}(z), \tag{2.1}$$

$$d_s(n,s,z) = \left[\boldsymbol{\mu}(s) - n\partial_s\psi(s)\right]\mathbf{v}(z), \tag{2.2}$$

$$d_z(n,s,z) = \left[\boldsymbol{\varphi}(s) - n\boldsymbol{\psi}(s)\right]\partial_z\mathbf{v}(z) + \boldsymbol{\varphi}_s(s)\boldsymbol{\delta}(z), \tag{2.3}$$

where an additional generalized degree of freedom $\boldsymbol{\delta}(z)$ is added to d_z along with a new warping function $\boldsymbol{\varphi}_s(s)$. As has been noted in [51], the above warping kinematics can be recast in the conventional GBT form presented in Chapter 1 by assuming

$$\boldsymbol{\psi}(s) = \boldsymbol{\mu}(s) = \mathbf{0}, \quad \boldsymbol{\varphi}(s) \neq \mathbf{0}. \tag{2.4}$$

In other words, the shear modes introduced in this manner are in fact analogous to the conventional GBT modes with the difference being the imposition of null in-place displacements. However, it is important to notice that these modes can be defined for both natural and internal nodes, which means that $\boldsymbol{\varphi}_s$ can be used to describe a non-linear warping displacement along the wall midline. Indeed, shear modes defined in this manner are formally analogous to those proposed in the theory of Capurso, presented in Chapter 1. Moreover, it is worth noticing that the warping description remains constant along the wall thickness.

Adding shear deformability in the manner presented above clearly removes the Vlasov constraint of null shear strain γ_{zs} along the midline of the cross-section. However, given that the warping description is constant along the wall thickness, shear strain between the direction of the beam axis and the normal to the wall midline γ_{zn} results to be null. In terms of the global beam behaviour, this translates into a lack of coherence between the bending and shear strain components of the beam. This problem is illustrated in Fig. 2.1, where a schematic view of the bending and shear strain components of a beam is shown for the case of a Timoshenko beam and for the conventional GBT model. It becomes clear from this representation that due to the absence of a non-null γ_{zn} the shear strain in a classical shear deformable GBT is inconsistent through the wall thickness with the bending strain component of the beam. This mismatch engenders several theoretical and practical drawbacks:

- An *ad hoc* modal decomposition procedure must be used for shear modes, completely different from the one used for the flexural counterpart.
- There are two generalized strain components associated to each shear mode, instead of a single one as would be reasonable to expect.
- Classical shear deformable beam theories are not recovered exactly.

Indeed, the third point above is a particularly delicate issue,

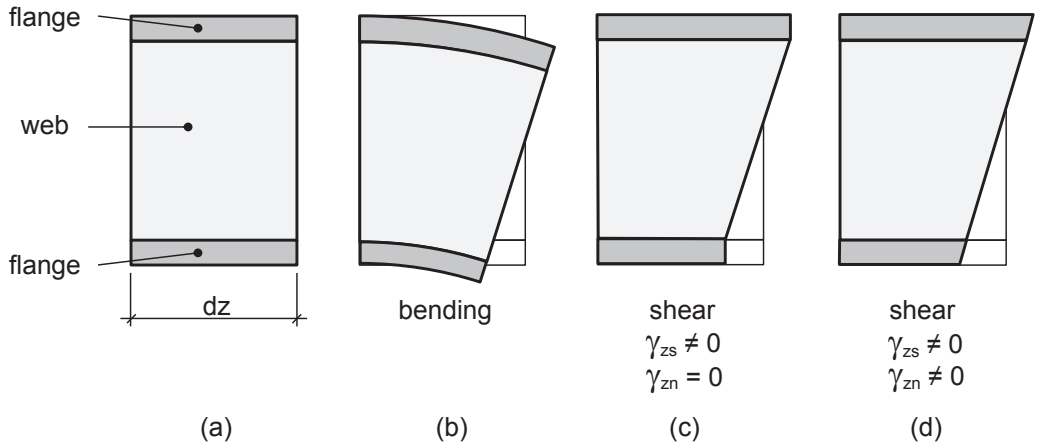

Figure 2.1: Sketch of the main difference between classical shear deformable GBT and the present formulation: (a) undeformed elementary beam, (b) bending strain component, (c) corresponding shear strain component in the classical GBT, (d) corresponding shear strain component in the Timoshenko beam theory and in the present theory.

since one of the main advantages of the GBT is precisely that classical beam theories can be recovered as special cases. The conventional approach to including shear deformability in the GBT is such that, even after modal decomposition, it is not possible to obtain the typical deformation components of classical theories: bending deflections are not clearly distinguishable from deflections due to shearing strains and, in consequence, pure cross-section flexural rotations do not result as natural kinematic parameters. Furthermore, these problems have definite consequences for a GBT numerical implementation: a GBT-based finite element formulated with this theory would not be efficient from the computational point of view and could not be combined with standard elements since the cross-section rotation is not a degree of freedom. For this same

reason, corotational approaches to solve non-linear problems cannot be easily applied in this kind of GBT framework. All of this severely limits the attractiveness of the shear-deformable GBT as has been traditionally presented.

2.1 New kinematics

To properly resolve the problems presented above, a more comprehensive way of introducing shear deformability into the GBT is necessary. In this respect, a new displacement field can be defined for the i-th wall (see Fig. 1.11):

$$d_n(n,s,z) = \boldsymbol{\psi}(s)\mathbf{v}(z), \tag{2.5}$$

$$d_s(n,s,z) = \left[\boldsymbol{\mu}(s) - n\partial_s\boldsymbol{\psi}(s)\right]\mathbf{v}(z), \tag{2.6}$$

$$d_z(n,s,z) = \left[\boldsymbol{\varphi}(s) - n\boldsymbol{\psi}(s)\right]\left[\partial_z\mathbf{v}(z) + \boldsymbol{\delta}(z)\right] + \boldsymbol{\varphi}^h(s)\boldsymbol{\delta}^h(z). \tag{2.7}$$

In line with traditional GBT formulations, the unknown generalized displacements are divided between those related to flexural modes $\mathbf{v}$ and those corresponding to shear modes. In this case, however, there are two distinct parameters related to shear instead of one. The $\boldsymbol{\delta}$ parameter corresponds to basic shear modes, which are in the same number of flexural (both fundamental and local) modes. The second $\boldsymbol{\delta}^h$ parameter corresponds to additional shear modes, which may be used to describe non-linear warping. It is easily seen that if $\boldsymbol{\delta}$ and $\boldsymbol{\delta}^h$ are disregarded then the new displacement field coincides with the conventional one presented in Chapter 1,

thus this new formulation contains the original one as a special case. In this GBT formulation, $\boldsymbol{\delta}$ is the typical term of shear deformable theories, such as the Timoshenko beam theory, in which longitudinal displacement is not defined by the derivative of the transverse displacement $\mathbf{v}$. This term contributes in a different manner from the classical shear deformable GBT shown in Eqs. (2.1)-(2.3), since the term $-n\boldsymbol{\psi}\boldsymbol{\delta}$ is present. Specifically, this formulation allows for a variation of the warping displacement associated to $\boldsymbol{\delta}$ along the wall thickness, in the same way the flexural warping does. The additional $\boldsymbol{\delta}^h$ parameters further enrich the warping description over the cross-section midline (that is over the s coordinate), but these are constant along the wall thickness n. Indeed, these additional shear parameters carry a contribution that is formally analogous to that present in Eqs. (2.1)-(2.3) and in the theory of Capurso.

2.2 Strains and generalized deformations

From the displacement field defined in Eqs. (2.5)-(2.7), strains can be calculated through the point-wise compatibility equations:

$$\begin{aligned}
\varepsilon_{zz}(n,s,z) &= [\boldsymbol{\varphi}(s) - n\boldsymbol{\psi}(s)]\left[\partial_z^2\mathbf{v}(z) + \partial_z\boldsymbol{\delta}(z)\right] + \\
&\quad + \boldsymbol{\varphi}^h(s)\partial_z\boldsymbol{\delta}^h(z), && (2.8)\\
\varepsilon_{ss}(n,s,z) &= \left[\partial_s\boldsymbol{\mu}(s) - n\partial_s^2\boldsymbol{\psi}(s)\right]\mathbf{v}(z), && (2.9)\\
\gamma_{zs}(n,s,z) &= [\boldsymbol{\mu}(s) - 2n\partial_s\boldsymbol{\psi}(s) + \partial_s\boldsymbol{\varphi}(s)]\,\partial_z\mathbf{v}(z) + \\
&\quad + [\partial_s\boldsymbol{\varphi}(s) - n\partial_s\boldsymbol{\psi}(s)]\,\boldsymbol{\delta}(z) +
\end{aligned}$$

$$+\partial_s \boldsymbol{\varphi}^h(s)\boldsymbol{\delta}^h(z), \tag{2.10}$$

$$\gamma_{zn}(s,z) = -\boldsymbol{\psi}(s)\boldsymbol{\delta}(z), \tag{2.11}$$

$$\varepsilon_{nn} = 0 \tag{2.12}$$

$$\gamma_{sn} = 0 \tag{2.13}$$

It is important to note that, differently form the classical shear deformable GBT, the shear strain γ_{zn} is different from zero. As it can be easily realized, the six independent z-fields governing the strain components can be grouped together in a vector $\mathbf{e}$ of *generalized deformation parameters*:

$$\mathbf{e}^{\mathrm{T}} = \left[\begin{array}{cccccc} \mathbf{v}^{\mathrm{T}} & \partial_z \mathbf{v}^{\mathrm{T}} & (\partial_z^2 \mathbf{v} + \partial_z \boldsymbol{\delta})^{\mathrm{T}} & \boldsymbol{\delta}^{\mathrm{T}} & \boldsymbol{\delta}^{h\ \mathrm{T}} & \partial_z \boldsymbol{\delta}^{h\ \mathrm{T}} \end{array} \right]. \tag{2.14}$$

For the sake of convenience, Eqs. (2.8)-(2.11) can be written in a more compact form by introducing vector $\varepsilon = \left[\begin{array}{cccc} \varepsilon_{zz} & \varepsilon_{ss} & \gamma_{zs} & \gamma_{zn} \end{array} \right]^{\mathrm{T}}$, resulting in:

$$\varepsilon(n,s,z) = \mathbf{b}(n,s)\mathbf{e}(z), \tag{2.15}$$

where the modal matrix

$$\mathbf{b}(n,s) = \begin{bmatrix} 0 & 0 & \boldsymbol{\varphi}_j - n\,\boldsymbol{\psi}_j & 0 & 0 & \boldsymbol{\varphi}_j^h \\ -n\,\partial_s^2 \boldsymbol{\psi}_j & 0 & 0 & 0 & 0 & 0 \\ 0 & -2n\partial_s \boldsymbol{\psi}_j & 0 & \partial_s \boldsymbol{\varphi}_j - n\partial_s \boldsymbol{\psi}_j & \partial_s \boldsymbol{\varphi}_j^h & 0 \\ 0 & 0 & 0 & -\boldsymbol{\psi}_j & 0 & 0 \end{bmatrix} \tag{2.16}$$

collects the cross-section deformations for each mode. More clearly, the generalized deformations can be rewritten as

$$\mathbf{e} = \mathbf{D}\mathbf{u}, \tag{2.17}$$

where

$$\mathbf{u} = \begin{bmatrix} \mathbf{v} \\ \boldsymbol{\delta} \\ \boldsymbol{\delta}^h \end{bmatrix}, \qquad \mathbf{D} = \mathbf{I}_m \otimes \mathcal{L}, \qquad \mathcal{L} = \begin{bmatrix} 1 & 0 & 0 \\ \partial_z & 0 & 0 \\ \partial_z^2 & \partial_z & 0 \\ 0 & 1 & 0 \\ 0 & 0 & 1 \\ 0 & 0 & \partial_z \end{bmatrix}, \tag{2.18}$$

In this writing, $\mathbf{I}_m$ is the m-order unit matrix, m is the number of the deformation modes, and symbol $\otimes$ denotes the Kronecker product. The statement in Eq. (2.17) means the differential operator $\mathbf{D}$ can be interpreted as the compatibility operator of the beam model.

Since it will be convenient later on, strains Eqs. (2.8)-(2.11) can be separated into a “membrane" part, not depending on n and denoted by superscript (M), and a “bending" part, proportional to n and denoted by superscript (B), as follows:

$$\varepsilon_{zz}(n,s,z) = \varepsilon_{zz}^{(M)}(s,z) + n\hat{\varepsilon}_{zz}^{(B)}(s,z), \tag{2.19}$$

$$\varepsilon_{ss}(n,s,z) = \varepsilon_{ss}^{(M)}(s,z) + n\hat{\varepsilon}_{ss}^{(B)}(s,z), \tag{2.20}$$

$$\gamma_{zs}(n,s,z) = \gamma_{zs}^{(M)}(s,z) + n\hat{\gamma}_{zs}^{(B)}(s,z), \tag{2.21}$$

$$\gamma_{zn}(s,z) = \gamma_{zn}^{(M)}(s,z), \tag{2.22}$$

where

$$\varepsilon_{zz}^{(M)} = \boldsymbol{\varphi}(s)\left[\partial_z^2\mathbf{v}(z) + \partial_z\boldsymbol{\delta}(z)\right] + \boldsymbol{\varphi}^h(s)\boldsymbol{\delta}^h(z), \tag{2.23}$$

$$\hat{\varepsilon}_{zz}^{(B)} = -\boldsymbol{\psi}(s)\left[\partial_z^2\mathbf{v}(z) + \partial_z\boldsymbol{\delta}(z)\right], \tag{2.24}$$

$$\varepsilon_{ss}^{(M)} = \partial_s\boldsymbol{\mu}(s)\mathbf{v}(z), \tag{2.25}$$

$$\hat{\varepsilon}_{ss}^{(B)} = -\partial_s^2\psi(s)\mathbf{v}(z), \tag{2.26}$$

$$\gamma_{zs}^{(M)} = \left[\boldsymbol{\mu}(s) + \partial_s\varphi(s)\right]\partial_z\mathbf{v}(z) + \partial_s\boldsymbol{\varphi}(s)\boldsymbol{\delta}(z) + \partial_s\boldsymbol{\varphi}^h(s)\boldsymbol{\delta}^h(z), \tag{2.27}$$

$$\hat{\gamma}_{zs}^{(B)} = -2\partial_s\boldsymbol{\psi}(s)\partial_z\mathbf{v}(z) - \partial_s\boldsymbol{\psi}(s)\boldsymbol{\delta}(z) \tag{2.28}$$

$$\tag{2.29}$$

2.3 Generalized stresses

Generalized stresses $\mathbf{s}$ are the dual quantities of the generalized deformations defined in Eq. (2.14) and they can be determined according to the following work equivalence condition:

$$\int_s\int_n \boldsymbol{\sigma}^{\mathrm{T}}\boldsymbol{\varepsilon}\ \mathrm{d}n\ \mathrm{d}s = \mathbf{s}^{\mathrm{T}}\mathbf{e}, \tag{2.30}$$

where $\boldsymbol{\varepsilon}^{\mathrm{T}}$=$[\varepsilon_{zz}\ \varepsilon_{ss}\ \gamma_{zs}\ \gamma_{zn}]^{\mathrm{T}}$ and $\boldsymbol{\sigma}^{\mathrm{T}}$=$[\sigma_{zz}\ \sigma_{ss}\ \tau_{zs}\ \tau_{zn}]^{\mathrm{T}}$. It is important to notice that $\mathbf{e}$ contains cross-section rigid-body motions, so the $\mathbf{s}$ generalized stresses associated to these are meaningless.

Additionally, the equilibrium equations of the beam model can be written by means of the principle of virtual work. That is:

$$\mathbf{D}^*\mathbf{s} = \mathbf{q}, \tag{2.31}$$

with the equilibrium operator:

$$\mathbf{D}^* = \mathbf{I}_m \otimes \mathcal{L}^*, \tag{2.32}$$

being $\mathcal{L}^*$ the differential operator adjoint to $\mathcal{L}$ and $\mathbf{q}$ the vector that collects the generalized loads, work-conjugate of the kinematic parameters $\mathbf{u}$.

2.4 Cross section stiffness matrix

In this chapter, an elastic isotropic material will be considered to write the cross-section stiffness matrix. Later on, a more general treatment of the constitutive relation will be introduced and the expressions obtained below will be generalized to the case of composite materials. However, let us begin with the simplest case of an elastic isotropic material. It may not be evident upon first inspection, but the kinematics defined in Eqs. (2.5)-(2.7) lead to internal constraints that render the beam model overstiff, which is a well know fact reported in the literature. Details on these constraints in the case of the GBT, their consequences, and the way in which they can be satisfied will be given in Chapters 3 and 4. For now, let it suffice to know that some relaxing of the stiffness is needed to balance the effect of internal constraints. The usual way of doing this is an adjustment of the constitutive relation. In this sense, the

membrane-bending separation introduced in the previous section can be exploited by using different constitutive relations for each part:

$$\boldsymbol{\sigma} = \mathbb{C}^{(M)}\boldsymbol{\varepsilon}^{(M)} + \mathbb{C}^{(B)}\boldsymbol{\varepsilon}^{(B)}. \tag{2.33}$$

where

$$\mathbb{C}^{(M)} = \begin{bmatrix} E & 0 & 0 & 0 \\ 0 & E & 0 & 0 \\ 0 & 0 & G & 0 \\ 0 & 0 & 0 & G \end{bmatrix}, \quad \mathbb{C}^{(B)} = \begin{bmatrix} \frac{E}{1-\nu^2} & \frac{\nu E}{1-\nu^2} & 0 & 0 \\ \frac{\nu E}{1-\nu^2} & \frac{E}{1-\nu^2} & 0 & 0 \\ 0 & 0 & G & 0 \\ 0 & 0 & 0 & G \end{bmatrix}, \tag{2.34}$$

being E the Young modulus, ν the Poisson coefficient, and G the shear modulus. Thus, an uncoupled constitutive relation, typical of a beam solution, is assumed for the membrane part of the problem. For the bending part, a coupled constitutive relation is assumed, as is done for plates. From this assumption, the cross-section stiffness matrix $\mathbf{C}$, that is the constitutive relation of the beam model, can be determined by writing a work-equivalence condition:

$$\int_s \int_n \left[\boldsymbol{\varepsilon}^{(M)} + n\hat{\boldsymbol{\varepsilon}}^{(B)}\right]^{\mathrm{T}} \left[\boldsymbol{\sigma}^{(M)} + n\hat{\boldsymbol{\sigma}}^{(B)}\right] \, \mathrm{d}n \, \mathrm{d}s = \mathbf{e}^{\mathrm{T}}\mathbf{C}\mathbf{e}. \tag{2.35}$$

Evaluating the above equation gives us a cross-section stiffness matrix, of the form:

$$\mathbf{C} = \begin{bmatrix} \mathbf{C}_{FF} & \mathbf{C}_{FS} \\ \mathbf{C}_{FS}^{\mathrm{T}} & \mathbf{C}_{SS} \end{bmatrix} = \left[\begin{array}{ccc|ccc} \mathbf{A}_{FF}^{(0)} & \mathbf{0} & \mathbf{G}_{FF} & \mathbf{0} & \mathbf{0} & \mathbf{G}_{FS}^{(0,h2)} \\ \mathbf{0} & \mathbf{A}_{FF}^{(1)} & \mathbf{0} & \mathbf{G}_{FS}^{(1,1)} & \mathbf{G}_{FS}^{(1,h1)} & \mathbf{0} \\ \mathbf{G}_{FF}^{\mathrm{T}} & \mathbf{0} & \mathbf{A}_{FF}^{(2)} & \mathbf{0} & \mathbf{0} & \mathbf{G}_{FS}^{(2,h2)} \\ \hline \mathbf{0} & \mathbf{G}_{FS}^{(1,1)} & \mathbf{0} & \mathbf{A}_{SS}^{(1)} & \mathbf{G}_{SS} & \mathbf{0} \\ \mathbf{0} & \mathbf{G}_{FS}^{(1,h1)} & \mathbf{0} & \mathbf{G}_{SS}^{\mathrm{T}} & \mathbf{A}_{SS}^{(h1)} & \mathbf{0} \\ \mathbf{G}_{FS}^{(0,h2)} & \mathbf{0} & \mathbf{G}_{FS}^{(2,h2)} & \mathbf{0} & \mathbf{0} & \mathbf{A}_{SS}^{(h2)} \end{array}\right] \tag{2.36}$$

The $\mathbf{C}_{FF}$ sub-matrix is exactly the same as the whole cross-section stiffness matrix present in the original GBT and pertains the fundamental flexural modes. On the other hand, $\mathbf{C}_{SS}$ is a new sub-matrix pertaining shear modes as they are defined in the present formulation. The two sub-matrices are coupled by the terms in $\mathbf{C}_{FS}$. The apexes used in the $\mathbf{A}_{ij}^{(\cdot)}$ and $\mathbf{G}_{ij}^{(\cdot)}$ terms of these matrices refer to the differentiation order of the associated generalized deformation parameters. The detailed expression for each of these terms is presented below, where t denotes the thickness of the wall:

$$\begin{aligned} \mathbf{A}_{FF}^{(0)} &= \int_s t\, \mathbb{C}_{22}^{(M)} \partial_s \mu^{\mathrm{T}} \partial_s \mu \, \mathrm{d}s + \\ &\quad \int_s \frac{t^3}{12}\, \mathbb{C}_{22}^{(B)} \partial_s^2 \psi^{\mathrm{T}} \partial_s^2 \psi \, \mathrm{d}s, \end{aligned} \tag{2.37}$$

$$\begin{aligned} \mathbf{A}_{FF}^{(1)} &= \int_s t\, \mathbb{C}_{33}^{(M)} \left(\mu + \partial_s \varphi\right)^{\mathrm{T}} \left(\mu + \partial_s \varphi\right) \, \mathrm{d}s + \\ &\quad + \int_s \frac{t^3}{3}\, \mathbb{C}_{33}^{(B)} \partial_s \psi^{\mathrm{T}} \partial_s \psi \, \mathrm{d}s, \end{aligned} \tag{2.38}$$

$$\mathbf{A}_{FF}^{(2)} = \int_s t\, \mathbb{C}_{11}^{(M)} \varphi^{\mathrm{T}} \varphi \, \mathrm{d}s + \int_s \frac{t^3}{12}\, \mathbb{C}_{11}^{(B)} \psi^{\mathrm{T}} \psi \, \mathrm{d}s, \tag{2.39}$$

$$\mathbf{G}_{FF} = \int_s \frac{t^3}{12}\, \mathbb{C}_{12}^{(B)} \partial_s^2 \psi^{\mathrm{T}} \psi \; \mathrm{d}s, \tag{2.40}$$

$$\mathbf{A}_{SS}^{(1)} = \int_s t\, \mathbb{C}_{33}^{(M)} \partial_s \varphi^{\mathrm{T}} \partial_s \varphi \; \mathrm{d}s + \int_s t\, \mathbb{C}_{44}^{(M)} \psi^{\mathrm{T}} \psi \; \mathrm{d}s + + \int_s \frac{t^3}{12}\, \mathbb{C}_{33}^{(B)} \partial_s \psi^{\mathrm{T}} \partial_s \psi \; \mathrm{d}s, \tag{2.41}$$

$$\mathbf{A}_{SS}^{(h1)} = \int_s t\, \mathbb{C}_{33}^{(M)} \partial_s \varphi^{h\ \mathrm{T}} \partial_s \varphi^h \; \mathrm{d}s, \tag{2.42}$$

$$\mathbf{A}_{SS}^{(h2)} = \int_s t\, \mathbb{C}_{11}^{(M)} \varphi^{h\mathrm{T}} \varphi^h \; \mathrm{d}s, \tag{2.43}$$

$$\mathbf{G}_{SS} = \int_s t\, \mathbb{C}_{33}^{(M)} \partial_s \varphi^{\mathrm{T}} \partial_s \varphi^h \; \mathrm{d}s, \tag{2.44}$$

$$\mathbf{G}_{FS}^{(0,h2)} = \int_s t\, \mathbb{C}_{12}^{(M)} \partial_s \mu^{\mathrm{T}} \varphi^h \; \mathrm{d}s, \tag{2.45}$$

$$\mathbf{G}_{FS}^{(1,1)} = \int_s t\, \mathbb{C}_{33}^{(M)} \left(\mu + \partial_s \varphi\right)^{\mathrm{T}} \partial_s \varphi \; \mathrm{d}s + + \int_s \frac{t^3}{6}\, \mathbb{C}_{33}^{(B)} \partial_s \psi^{\mathrm{T}} \partial_s \psi \; \mathrm{d}s, \tag{2.46}$$

$$\mathbf{G}_{FS}^{(1,h1)} = \int_s t\, \mathbb{C}_{33}^{(M)} \left(\mu + \partial_s \varphi\right)^{\mathrm{T}} \partial_s \varphi^h \; \mathrm{d}s, \tag{2.47}$$

$$\mathbf{G}_{FS}^{(2,h2)} = \int_s t\, \mathbb{C}_{11}^{(M)} \varphi^{\mathrm{T}} \varphi^h \; \mathrm{d}s. \tag{2.48}$$

2.5 Deformation modes

The expressions obtained in the previous sections are all dependant on the functions $\boldsymbol{\varphi}$, $\boldsymbol{\mu}$, $\boldsymbol{\psi}$, and $\boldsymbol{\varphi}^h$. The calculation of these functions, which represent the deformation modes included in the GBT, is the starting point of the cross-section analysis at the heart of the GBT. As has been stated before, each mode is associated with a cross-section node (either natural or internal) and is based on a series of assumptions that depend on the family of modes under consideration, each of which will be described separately below.

2.5.1 Flexural modes

Flexural modes may be either fundamental (associated to a natural node) or local (associated to an internal node) and are governed by the generalized parameters $\mathbf{v}$. As mentioned above, the flexural modes in this formulation are the same as those in the original GBT. In these modes, the cross-section is allowed to deform in its own plane while complying, like a Vlasov beam, with the condition of null strains $\gamma_{zs}^{(M)}$ and $\varepsilon_{ss}^{(M)}$ at all points of the cross-section. The warping function φ is assumed to be piece-wise linear and has a unit value at the considered natural node (see Eqs. (1.7)-(1.9)) and zero in all others, as shown in Fig. 1.12. From this warping description, the imposition of Vlasov's assumption (see Eq. (1.5)) leads to determining the in-plane displacement of the node $\boldsymbol{\mu}$ in the direction of the wall midline as constant over the wall. Functions $\boldsymbol{\psi}$ instead represent the displacement of the node transversal to the wall midline and can be calculated by enforcing compatibility among the walls subject to cylindrical bending. To this end, the cross-section can be considered as a planar frame whose corners (natural nodes) are restrained by pinned supports with displacements prescribed according to $\boldsymbol{\mu}$. This solution is achieved using Euler-Bernoulli plane beams for each wall. A schematic view of these considerations has been shown in Figs. 1.12 a and b. In a similar way, local flexural modes are defined by the assumption 1.10 and the $\boldsymbol{\psi}$ functions, which are the only non-null in this case, are determined again by considering the cross-section as a planar frame. In this case, an

in-plane unit displacement normal to the wall is prescribed at the considered node as shown in Fig. 1.12c. These assumptions simplify some of the expressions for the elements of matrices $\mathbf{C}_{FF}$ and $\mathbf{C}_{FS}$:

$$\mathbf{A}_{FF}^{(0)} = \int_s \frac{t^3}{12}\, \mathbb{C}_{22}^{(B)} \partial_s^2 \boldsymbol{\psi}^{\mathrm{T}} \partial_s^2 \boldsymbol{\psi}\, \mathrm{d}s, \tag{2.49}$$

$$\mathbf{A}_{FF}^{(1)} = \int_s \frac{t^3}{3}\, \mathbb{C}_{33}^{(B)} \partial_s \boldsymbol{\psi}^{\mathrm{T}} \partial_s \boldsymbol{\psi}\, \mathrm{d}s, \tag{2.50}$$

$$\mathbf{G}_{FF} = \int_s \frac{t^3}{12}\, \mathbb{C}_{12}^{(B)} \partial_s^2 \boldsymbol{\psi}^{\mathrm{T}} \boldsymbol{\psi}\, \mathrm{d}s, \tag{2.51}$$

$$\mathbf{G}_{FS}^{(0,h2)} = \mathbf{0}, \qquad \mathbf{G}_{FS}^{(1,h1)} = \mathbf{0}, \tag{2.52}$$

$$\mathbf{G}_{FS}^{(1,1)} = \int_s \frac{t^3}{6}\, \mathbb{C}_{33}^{(B)} \partial_s \boldsymbol{\psi}^{\mathrm{T}} \partial_s \boldsymbol{\psi}\, \mathrm{d}s. \tag{2.53}$$

Hereinafter, the total number of flexural modes (both fundamental and local) is denoted by n_F.

2.5.2 Shear modes

Shear modes may be associated to either natural or internal nodes and are governed by parameters δ and δ^h. As said before, these modes are subdivided into two classes: *basic shear modes* and *additional shear modes*.

- The basic shear modes are ruled by parameters δ and are associated to (fundamental and local) flexural modes, as it can be immediately realized by the assumed kinematics, Eqs. (2.5)-(2.7). Hence, their number is n_F and cross-section functions $\boldsymbol{\varphi}$ and $\boldsymbol{\psi}$ are those assumed for flexural modes. Thus, no other

assumptions are needed. Notice that these modes differ from those proposed in the literature, discussed in Section 2. In particular, coherently with flexural modes, thickness variation is correctly taken into account, differently from Eq. (2.3).

- The additional shear modes are governed by parameters $\boldsymbol{\delta}^h$ and can be introduced to further enrich the sole warping description. Analogously to the choice for $\boldsymbol{\varphi}$, functions $\boldsymbol{\varphi}^h$ can be assumed as piecewise linear functions associated to additional internal nodes, that differ from those used for the basic modes. A hierarchical approach, typical of finite element formulations, can be conveniently adopted to introduce these additional modes. Their number is hereinafter denoted by n_S.

Some remarks

The above assumptions guarantee that flexural and shear modes are independent from each other apart from one “dependence" case. In fact, there is a flexural mode which engenders the same kinematics of a basic shear mode and corresponds to

$$\boldsymbol{\varphi}(s) \text{ constant}, \tag{2.54}$$

$$\mu(s) = -\partial_s \boldsymbol{\varphi}(s) \Rightarrow \text{null} \ , \tag{2.55}$$

$$\boldsymbol{\psi}(s) \text{ null} \ . \tag{2.56}$$

The above choice complies with conditions (1.7)-(1.9) and leads to null displacements in the plane of the cross-sections and con-

stant axial displacement (constant warping). On the other hand, each flexural mode has an associated basic shear mode yielding the same axial displacement field and null displacements in the plane of the cross-section. Therefore, it can be immediately realized that the displacement field coming from the flexural mode conforming with conditions (2.54)-(2.56) can be also reproduced by basic shear modes. According to this, there is one $\boldsymbol{\delta}$-parameter that is redundant.

2.6 Cross section analysis

Once the shape functions $\boldsymbol{\psi}(s)$, $\boldsymbol{\mu}(s)$ and $\boldsymbol{\varphi}(s)$ are selected, the cross-section stiffness matrix $\mathbf{C}$ can be computed as discussed in Section 2.4. In the general case, matrix $\mathbf{C}$ will show a pattern such as that presented in Fig. 2.2a for the case of a section with $n_F = n_S = 6$. The pattern of each of the macro-blocks is that given in Eq. (2.36) together with Eqs. (2.37)-(2.53). In general, the various matrices composing the cross-stiffness matrix $\mathbf{C}$ are full, which determines high coupling among the generalized deformation parameters and, hence, in the final governing equations. In addition to this, the mechanical meaning of the generalized deformation parameters is not at all obvious and, in particular, the classical parameters of standard beam theories cannot be clearly distinguished. For this reason, a modal transformation is needed to gain a partial uncoupling of the generalized deformation parameters and, more importantly, to identify their mechanical meaning. The new basis

in which the problem will be expressed is called plainly *modal base* and the transformation used is referred to as *modal decomposition*. Hereinafter, whenever a generic matrix/vector "$\cdot$" is expressed in the modal space, the symbol "$\hat{\cdot}$" is used.

2.6.1 Modal decomposition of flexural modes

In a manner analogous to that of the original GBT formulation, the modal decomposition procedure starts from the solution of the following eigenvalue problem:

$$\left(\mathbf{A}_{FF}^{(0)} - \lambda_i \mathbf{A}_{FF}^{(2)}\right) \mathbf{\Lambda}_i = \mathbf{0}. \tag{2.57}$$

where it should be noted that $\mathbf{A}_{FF}^{(2)}$ is positive-definite. As well known from the literature on GBT, the first four resulting eigenvalues are null ($\lambda_i = 0,\ i = 1, ..., 4$) and these correspond to rigid-body motions of the cross-section. The rest of the eigenvalues are positive ($\lambda_i > 0,\ i = 5, ..., n_F$) and correspond to flexural deformation (distortion) modes of the cross-section. Correspondingly, the matrix $\mathbf{\Lambda}$ collecting the eigenvectors can be split as follows:

$$\mathbf{\Lambda} = \left[\begin{array}{cc} \mathbf{\Lambda}_R & \mathbf{\Lambda}_F \end{array} \right], \tag{2.58}$$

where $\mathbf{\Lambda}_R$ is the $(n_F \times 4)$ block collecting the eigenvectors related to rigid-body motions. Indeed, $\mathbf{\Lambda}_R$ collects a generic linear combination of the typical four rigid-body motions of the cross-section, that are the axial displacement, the two flexural rotations about the principal axes of inertia and the twisting rotation about the

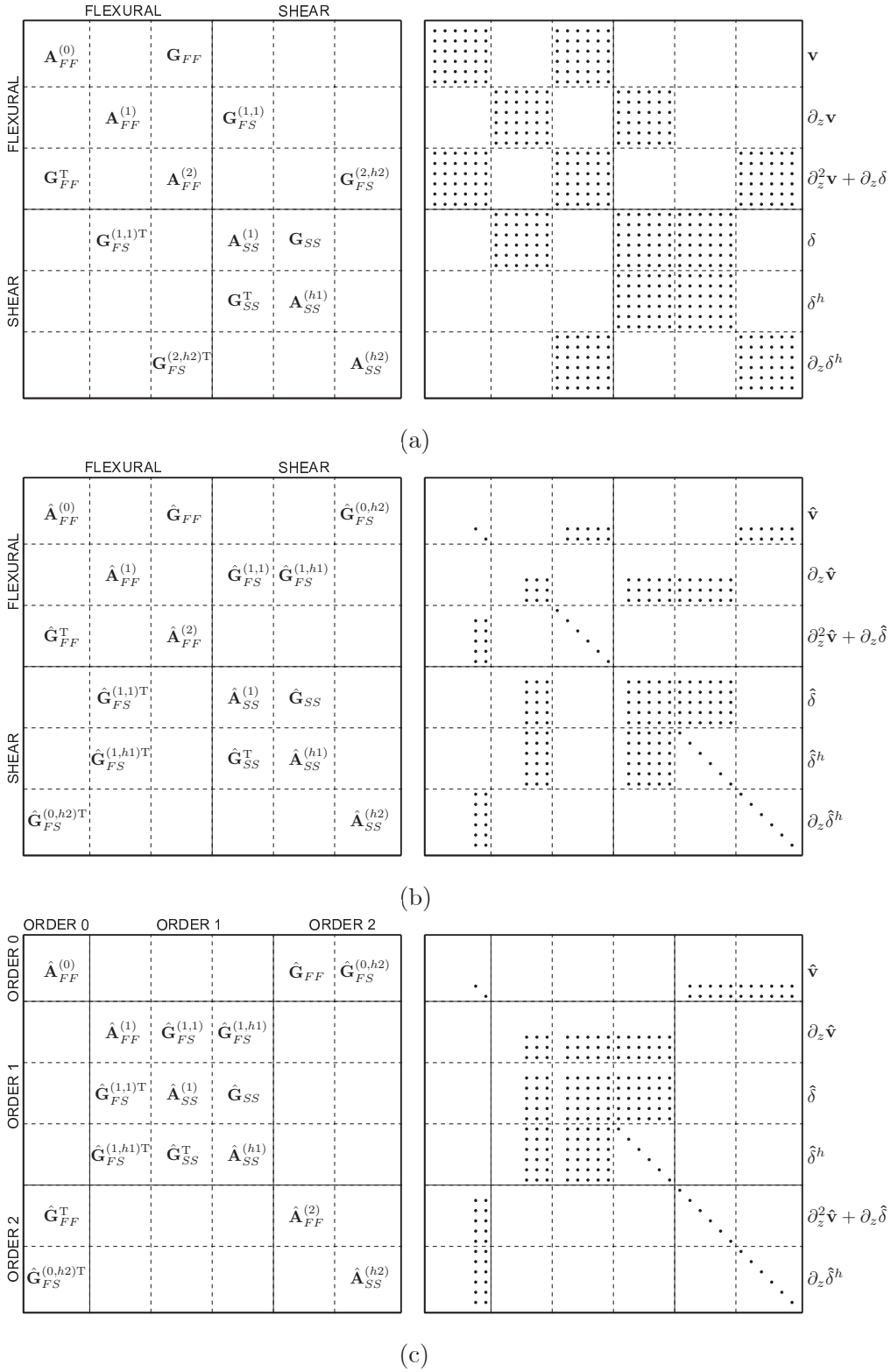

Figure 2.2: Pattern of the cross-section stiffness matrix for $n_F = n_S = 6$: (a) in the natural space, (b) in the modal space, (c) in the modal space after reordering.

shear centre. However, a clear separation between these four modes is crucial to recover the classical contributions of well-known beam theories as special cases of the GBT. In this respect, a simple procedure to automatically separate the typical four rigid-body motions starting from $\mathbf{\Lambda}_R$ is given in the next section.

Evidently, the modal decomposition procedure applies as well to the generalized displacements. In accordance to the original GBT, the generalized displacements $\mathbf{v}$ are related to the modal ones $\hat{\mathbf{v}}$ by the following relationship:

$$\mathbf{v}(z) = \mathbf{\Lambda}\hat{\mathbf{v}}(z). \tag{2.59}$$

2.6.2 Rigid-body modes

As said above, it is necessary to separate the four rigid-body motions of the cross-section to obtain the axial displacement, the two rotations about the principal axes of inertia and the torsional rotation about the shear center. This is of great importance if the GBT is to be used by any engineer for structural design, since the classical beam quantities are at the base of any standard. The procedure adopted in this work differs from the procedure usually adopted in the literature, since it is based only on terms derived within the outlined framework, without any need to resort to additional information coming from geometrically nonlinear contributions.

Once $\mathbf{\Lambda}_R$ is computed through Eq. (2.57), the separation of the classical beam modes starts by projecting matrices $\mathbf{A}_{FF}^{(1)}$ and $\mathbf{A}_{FF}^{(2)}$ into the space spanned by the rigid-body modes:

$$\mathbf{\Lambda}_R^{\mathrm{T}}\mathbf{A}_{FF}^{(1)}\mathbf{\Lambda}_R = \mathbf{R}_{FF}^{(1)}, \tag{2.60}$$

$$\mathbf{\Lambda}_R^{\mathrm{T}}\mathbf{A}_{FF}^{(2)}\mathbf{\Lambda}_R = \mathbf{R}_{FF}^{(2)}. \tag{2.61}$$

The resultant (4×4) matrices $\mathbf{R}_{FF}^{(1)}$ and $\mathbf{R}_{FF}^{(2)}$ are used to set up the following eigenvalue problem:

$$(\mathbf{R}_{FF}^{(1)} - \lambda_i \mathbf{R}_{FF}^{(2)})\boldsymbol{\rho}_i = \mathbf{0}, \tag{2.62}$$

whose solution yields: $\lambda_i = 0,\ i = 1, .., 3;\ \lambda_4 > 0$. The eigenvector $\boldsymbol{\rho}_4$ associated to the non-null eigenvalue λ_4 is the twisting about the shear centre. In fact, this is the only rigid-body motion of the cross-section with a non-null rigidity associated to parameters $\partial\mathbf{v}$ and, hence, to matrix $\mathbf{A}_{FF}^{(1)}$ or, equivalently, to its projection $\mathbf{R}_{FF}^{(1)}$. We can then define the (4×3) matrix $\boldsymbol{\rho}$ by collecting the remaining three eigenvectors related to null eigenvalues. In order to distinguish these three contributions, the following matrix is defined:

$$\mathbf{Q} = \frac{1}{l}\int_s \left(\boldsymbol{\psi}^{\mathrm{T}}\boldsymbol{\psi} + \boldsymbol{\mu}^{\mathrm{T}}\boldsymbol{\mu}\right)\ \mathrm{d}s, \tag{2.63}$$

where l is the cross-section midline lenght, and matrices $\mathbf{A}_{FF}^{(2)}$ and $\mathbf{Q}$ are projected into the reduced space spanned by the remaining three cross-section rigid-body modes:

$$\left(\mathbf{\Lambda}_R\boldsymbol{\rho}\right)^{\mathrm{T}}\mathbf{A}_{FF}^{(2)}\left(\mathbf{\Lambda}_R\boldsymbol{\rho}\right) = \tilde{\mathbf{R}}_{FF}^{(2)}, \tag{2.64}$$

$$\left(\mathbf{\Lambda}_R\boldsymbol{\rho}\right)^{\mathrm{T}}\mathbf{Q}\left(\mathbf{\Lambda}_R\boldsymbol{\rho}\right) = \tilde{\mathbf{Q}}. \tag{2.65}$$

Then, the resultant (3×3) matrices $\tilde{\mathbf{R}}^{(2)}_{FF}$ and $\tilde{\mathbf{Q}}$ are used in turn to set up another eigenvalue problem:

$$(\tilde{\mathbf{Q}} - \lambda_i \tilde{\mathbf{R}}^{(2)}_{FF})\tilde{\boldsymbol{\rho}}_i = \mathbf{0}, \tag{2.66}$$

whose solution yields: $\lambda_1 = 0$ and $\lambda_2, \lambda_3 > 0$. The eigenvector associated to the null eigenvalue λ_1 is the rigid-body axial translation and the others are the two rigid-body rotations about the two principal axes of inertia of the cross-section.

Hence, the final modal matrix is given by

$$\hat{\mathbf{\Lambda}}_R = \mathbf{\Lambda}_R \begin{bmatrix} \boldsymbol{\rho}\tilde{\boldsymbol{\rho}} & \boldsymbol{\rho}_4 \end{bmatrix}. \tag{2.67}$$

As a last step, matrix $\hat{\mathbf{\Lambda}}_R$ should be normalized such that the cross-section rigid-body modes are of unit amplitude.

2.6.3 Modal decomposition of basic shear modes

On the other hand, the modal decomposition of shear modes is achieved by the following transformation:

$$\begin{bmatrix} \boldsymbol{\delta}(z) \\ \boldsymbol{\delta}^h(z) \end{bmatrix} = \begin{bmatrix} \mathbf{\Lambda} & \mathbf{\Gamma}_F \\ \mathbf{0} & \mathbf{\Gamma}_S \end{bmatrix} \begin{bmatrix} \hat{\boldsymbol{\delta}}(z) \\ \hat{\boldsymbol{\delta}}^h(z) \end{bmatrix}, \tag{2.68}$$

where it is important to notice that $\mathbf{\Lambda}$ is the same matrix used in Eq. (2.59) for the flexural modes. Instead, matrices $\mathbf{\Gamma}_F$ and $\mathbf{\Gamma}_S$ are defined according to the following conditions:

- matrices $\mathbf{A}^{(h1)}_{SS}$ and $\mathbf{A}^{(h2)}_{SS}$ should be diagonal in the modal

space,

$$\left(\mathbf{A}_{SS}^{(h1)} - \lambda_i \mathbf{A}_{SS}^{(h2)}\right) \boldsymbol{\Gamma}_S = \mathbf{0}, \tag{2.69}$$

- matrix $\mathbf{G}_{FS}^{(2,h2)}$ should be null in the modal space,

$$\boldsymbol{\Lambda}^{\mathrm{T}} \left(\mathbf{A}_{FF}^{(2)} \boldsymbol{\Gamma}_F + \mathbf{G}_{FS}^{(2,h2)} \boldsymbol{\Gamma}_S\right) = \mathbf{0}. \tag{2.70}$$

Note that both $\mathbf{A}_{SS}^{(h2)}$ and $\mathbf{A}_{FF}^{(2)}$ are positive-definite. It is worth to remark that the modal decomposition of basic shear modes is identical to that of flexural modes (it is operated by the same matrix $\boldsymbol{\Lambda}$). This is a distinctive feature of the present formulation and guarantees that the out-of-plane modal displacements of the two classes perfectly match, as would be desirable.

2.6.4 Modal decomposition of additional shear modes

The modal decomposition of additional shear modes is somewhat different from that of basic shear modes and requires the computation of matrices $\boldsymbol{\Gamma}_F$ and $\boldsymbol{\Gamma}_S$. The computation of these matrices, so as to comply with conditions (2.69) and (2.70), starts by evaluating the solution $\mathbf{Y}$ of the following linear algebraic system

$$\left(\boldsymbol{\Lambda}^{\mathrm{T}} \mathbf{A}_{FF}^{(2)}\right) \mathbf{Y} = -\boldsymbol{\Lambda}^{\mathrm{T}} \mathbf{G}_{FS}^{(2,h2)}, \tag{2.71}$$

and then computing the matrices

$$\mathbf{R}_{SS}^{(h1)} = \mathbf{J}^{\mathrm{T}} \mathbf{A}_{SS}^{(h1)} \mathbf{J}, \tag{2.72}$$

$$\mathbf{R}_{SS}^{(h2)} = \mathbf{J}^{\mathrm{T}} \mathbf{A}_{SS}^{(h2)} \mathbf{J}, \tag{2.73}$$

where the $(n_F + n_S) \times n_S$ matrix $\mathbf{J}$ is defined as

$$\mathbf{J} = \begin{bmatrix} \mathbf{Y} \\ \mathbf{I} \end{bmatrix}, \tag{2.74}$$

and $\mathbf{I}$ is the identity matrix of order n_S.

Once this first step is done, the following eigenvalue problem is solved

$$\left(\mathbf{R}_{SS}^{(h1)} - \lambda_i \mathbf{R}_{SS}^{(h2)}\right) \boldsymbol{\Omega}_i = \mathbf{0}, \tag{2.75}$$

being $\mathbf{R}_{SS}^{(h2)}$ positive-definite.

Finally, $\boldsymbol{\Gamma}_F$ and $\boldsymbol{\Gamma}_S$ are obtained as:

$$\begin{bmatrix} \boldsymbol{\Gamma}_F \\ \boldsymbol{\Gamma}_S \end{bmatrix} = \mathbf{J}\boldsymbol{\Omega} = \begin{bmatrix} \mathbf{Y}\boldsymbol{\Omega} \\ \boldsymbol{\Omega} \end{bmatrix}, \tag{2.76}$$

where $\boldsymbol{\Omega}$ is the matrix collecting eigenvalues $\boldsymbol{\Omega}_i$.

2.7 Cross-section stiffness matrix and generalized strain parameters in the modal space

As desired, transformations (2.59) and (2.68) permit to express the beam kinematics in terms of modal parameters. In this respect, Fig. 2.2b shows the pattern of the cross-section stiffness matrix in the modal space, $\hat{\mathbf{C}}$. For illustrative purposes, the case with $n_F = n_S = 6$ is considered. Analogously to what already observed for matrix $\mathbf{C}$ of Fig. 2.2a, the right-upper (3×3) macro-block $\hat{\mathbf{C}}_{FF}$ is related to the flexural behavior typical of the original GBT, the

left-lower (3×3) macro-block $\hat{\mathbf{C}}_{SS}$ is related to the shear deformability as introduced in the present formulation, and, finally, the off-diagonal (3×3) macro-block $\hat{\mathbf{C}}_{FS}$ couples flexural and shear deformation. Comparing Figs. 2.2a and b highlights the almost diagonal structure of matrix $\hat{\mathbf{C}}$ and, hence, the relevant uncoupling obtained passing to the modal space. This is even more clear by rearranging the cross-section stiffness matrix according to a different ordering of the deformation parameters, as shown in Fig. 2.2c. This new order is based on physical arguments as discussed in the following. In particular, inspecting carefully matrix $\hat{\mathbf{C}}$ and Figs. 2.2b and c the following remarks can be done.

1. In all, matrix $\hat{\mathbf{C}}$ has 8 null rows and columns: 7 in the flexural part and 1 in the shear part. The relevant deformation components are indeed cross-section rigid-body displacements, since no strain energy is associated to them. All the other deformation parameters are actually associated to non-null strain energy and can be referred to as *generalized strains*.

2. Flexural modes are those of the original GBT; as a consequence, $\hat{\mathbf{C}}_{FF}$ is exactly the same of original GBT and the corresponding generalized deformation parameters inherit the same mechanical meaning. Specifically, $\hat{v}_1$ is the primitive of the axial displacement, $\hat{v}_2$ and $\hat{v}_3$ are the rigid-body translations of the cross-section in the directions of its principal inertia axes, and $\hat{v}_4$ is the twisting rotation about the shear

center. As expected, the 4 rows and columns associated to these parameters are null. The remaining rows and columns pertaining to $\hat{\mathbf{v}}$ are non-null and the relevant strain parameters – i.e. $\hat{v}_i,\ i = 5, ..., n_F$ – govern the in-plane deformation of the cross-section. Moving on to the terms associated to $\partial\hat{\mathbf{v}}$, the first 3 rows and columns are null, as expected, because $\partial\hat{v}_1$, $\partial\hat{v}_2$ and $\partial\hat{v}_3$ are, respectively, the rigid-body axial translation and the two rigid-body out-of-plane rotations of the cross-section about its principal inertia axes in the absence of shear deformation. Notice that in the absence of shear deformation, the out-of-plane rotations actually coincide with the derivatives of transverse displacements. The remaining rows and columns pertaining to $\partial\hat{\mathbf{v}}$ are non-null. In particular, $\partial\hat{v}_4$ is the rate of twist and $\partial\hat{v}_i,\ i = 5, ..., n_F$ are generalized strains corresponding to higher-order deformations due to section distortion.

3. Parameter $\hat{\bar{\delta}}_1$ corresponds to a rigid-body axial translation. As discussed in Section 2.5.2, it is redundant, since the associated displacement field is already present in the flexural part, governed by parameter $\partial\hat{v}_1$. For this reason, it can be disregarded.

4. Each basic shear mode is characterized by the same warping displacement of a flexural mode with null in-plane displacements. Based on this observation, it can be immediately realized that parameters $\hat{\bar{\delta}}_2$ and $\hat{\bar{\delta}}_3$ (associated to the derivatives of

transverse displacements $\partial\hat{v}_2$ and $\partial\hat{v}_3$) are the shear deflections of the classical Timoshenko beam theory, $\hat{\delta}_4$ (associated to the rate of twist $\partial\hat{v}_4$) is the shear deformation due to warping torsion, and $\hat{\delta}_i,\ i = 5, ..., n_F$ can be interpreted as higher-order shear strain components. Note that parameter $\hat{\delta}_4$ is present neither in the De Saint Venant theory nor in the Vlasov one, while it is present in the theory of Capurso. Moreover, $\hat{\mathbf{A}}_{SS}^{(1)}$ is, in general, a non diagonal matrix since the modal parameters refer to the principal axes for bending (that are the principal axes of inertia of the cross-section) that, as well known, do not necessarily coincide with the principal axes of the shearing forces. For illustrative purpose, a very simple example is given in Fig. 2.3, to make clear such correspondence.

5. Based on the previous remarks, the strain parameters $\left(\partial^2\hat{v}_i + \partial\hat{\delta}_i\right)$ can be interpreted as generalized curvatures. In particular, $\left(\partial\hat{v}_2 + \hat{\delta}_2\right)$ and $\left(\partial\hat{v}_3 + \hat{\delta}_3\right)$ are the rigid-body cross-section rotations about the principal inertia axes, given by the sum of the bending deflection and shear deflection. Hence, $\left(\partial^2\hat{v}_2 + \partial\hat{\delta}_2\right)$ and $\left(\partial^2\hat{v}_3 + \partial\hat{\delta}_3\right)$ are the bending curvatures. Parameter $\left(\partial^2\hat{v}_4 + \partial\hat{\delta}_4\right)$ is the twisting curvature due to non-uniform warping. The remaining parameters, $\left(\partial^2\hat{v}_i + \partial\hat{\delta}_i\right),\ i = 5, ..., n_F$, can be interpreted as higher-order curvatures associated to section distortion. As regards the first parameter, it corresponds to axial deformation, since $\partial\hat{v}_1$ is the rigid-body cross-section axial displacement and $\hat{\delta}_1$ has been disregarded. On the other

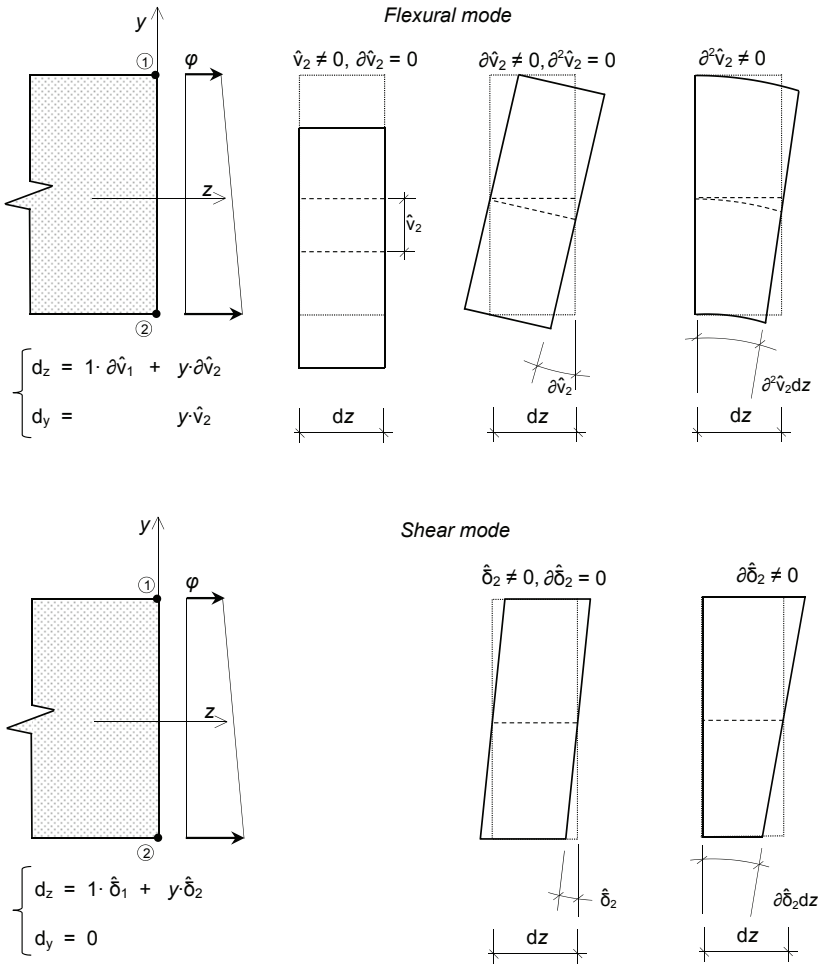

Figure 2.3: Schematic view of the effect of a flexural mode and of the associated shear mode on a two-nodes cross-section.

hand, as expected, matrix $\hat{\mathbf{A}}_{FF}^{(2)}$ turns out to be diagonal and in the first four positions we find exactly the stiffness moduli of the classical beam: the axial stiffness, the two bending stiffness and the warping stiffness.

6. Generalized curvatures are coupled with in-plane cross-section deformation through matrix $\hat{\mathbf{G}}_{FF}$, while there is no coupling with strain parameters $\partial\hat{v}_i$ and $\hat{\delta}_i$.

7. Basic shear parameters $\hat{\delta}_i$ are coupled with flexural strain parameters $\partial\hat{v}_i$ through matrix $\hat{\mathbf{G}}_{FS}^{(1,1)}$.

8. Additional shear strain parameters $\hat{\delta}_i^h$ are coupled only with basic shear strain parameters $\hat{\delta}_i$ and the rate of in-plane strain parameters $\partial\hat{v}_i$.

9. As it can be easily realized, adding or eliminating shear modes does not modify the flexural contributions.

The above remarks on the physical meaning of the various deformation parameters in the modal space are summarized in Table 1. Additionally, The complete list of the generalized stress parameters is also given in Table 1. It should be noted that the stress resultants typical of classical theories are obtained in correspondence to the standard beam strain parameters. In addition, non standard stress parameters corresponding to self-equilibrated stress distributions over the cross-section are obtained as counterparts of non standard strain parameters. In particular, higher-order warping

moments and shearing forces are conjugate of generalized curvatures and shearing strain parameters and in-plane auto-forces and auto-couples are conjugate of in-plane and rate of in-plane strain parameters.

2.8 A GBT-based finite element

The GBT formulation proposed in this chapter can be implemented into a compatible finite element. This would allow to numerically evaluate the validity of the formulation when compared to other modelling approaches. In this sense, a generic beam can be modelled as a series of non-overlapping finite elements in which the generalized displacements are expressed by:

$$\mathbf{u}(z) = \mathbf{N}(z)\mathbf{q}, \tag{2.77}$$

where $\mathbf{q}$ is the vector of nodal parameters and $\mathbf{N}$ is the matrix collecting the interpolation functions. In this implementation, $\mathbf{v}$-parameters are approximated by cubic Hermitian functions, with C^1-continuity at nodes, while $\boldsymbol{\delta}$-parameters are approximated by quadratic polynomials with C^0-continuity at nodes.

From these initial assumptions, the principle of virtual work allows to determine, for any element, the relation between nodal displacements $\mathbf{q}$ and equivalent nodal loads $\mathbf{g}$:

$$\mathbf{K}\mathbf{q} = \mathbf{g} \tag{2.78}$$

Table 1
Generalized deformation and generalized stress parameters in the modal space.

Cross-section rigid body displacements		Generalized strain parameters		Generalized stress parameters	
		$\partial^2\hat{v}_1$	axial strain	N	axial force
$\hat{v}_2,\ \hat{v}_3$	transverse displacements of shear center along principal inertia axes	$(\partial^2\hat{v}_2+\partial\hat{\delta}_2)$ $(\partial^2\hat{v}_3+\partial\hat{\delta}_3)$	bending curvatures about principal inertia axes	M_x M_y	bending moments
$\hat{v}_4$	twist about shear center				
$\partial\hat{v}_1$	axial displacement	$(\partial^2\hat{v}_4+\partial\hat{\delta}_4)$	torsional curvature due to non-uniform warping	B	bimoment
$(\partial\hat{v}_2+\hat{\delta}_2)$ $(\partial\hat{v}_3+\hat{\delta}_3)$	rotations about principal inertia axes	$\hat{\delta}_2,\ \hat{\delta}_3$	transverse shear strains	$V_x,\ V_y$	shearing forces
$\hat{v}_1,\ \hat{\delta}_1$	no physical meaning (disregarded)	$\hat{\delta}_4$	torsional shear strain	T_ω	warping torsion
		$\partial\hat{v}_4$	rate of twist	T_{SV}	De Saint Venant torsion
		$i\geq 5$			
		$\hat{v}_i$	in-plane shear parameters	S_i	in-plane auto-forces
		$\partial\hat{v}_i$	rate of in-plane shear parameters	T_i	in-plane auto-couples
		$(\partial^2\hat{v}_i+\partial\hat{\delta}_i)$	higher-order curvatures	M_i	higher-order warping moments
		$\hat{\delta}_i$	higher-order shearing strains	V_i	higher-order shearing forces
		$\hat{\delta}_i^h$	(additional) higher-order shearing strains	V_i^h	(additional) higher-order shearing forces
		$\partial\hat{\delta}_i^h$	(additional) higher-order shear curvatures	M_i^h	(additional) higher-order warping moments

where $\mathbf{K}$ is the stiffness matrix of the element, which is defined as:

$$\mathbf{K} = \int_0^{L_e} (\mathbf{DN})^{\mathrm{T}} \mathbf{C} (\mathbf{DN}) \, \mathrm{d}z \tag{2.79}$$

with $\mathbf{C}$ being the cross-section stiffness matrix, $\mathbf{D}$ the differential operator introduced in Eq. (2.18), and L_e the length of the finite element. From this point, the conventional procedure of assembly and imposition of boundary conditions can be followed as done with standard beam finite elements.

2.9 Some examples

Some examples are presented in this section to illustrate the effectiveness of the proposed GBT formulation. Specifically, the importance of section distortion, shear deformability and local effects will be shown.

2.9.1 Test 1: C-section cantilever beam under torsion

A cantilever C-profile is subjected to a torsional moment T applied at the free end, as shown in Fig. 2.4. Following the original example proposed by Capurso [13], the dimensions of the element are: $b =$ 3.5 m, $h = 5$ m, $t = 20$ cm and $L = 18$ m, the applied torsional moment is $T = 1000$ kNm and the material is concrete.

This test is used to illustrate the predictive capability of shear modes. Only the four fundamental flexural modes are considered for the flexural part, so that the cross-section remains rigid in its own

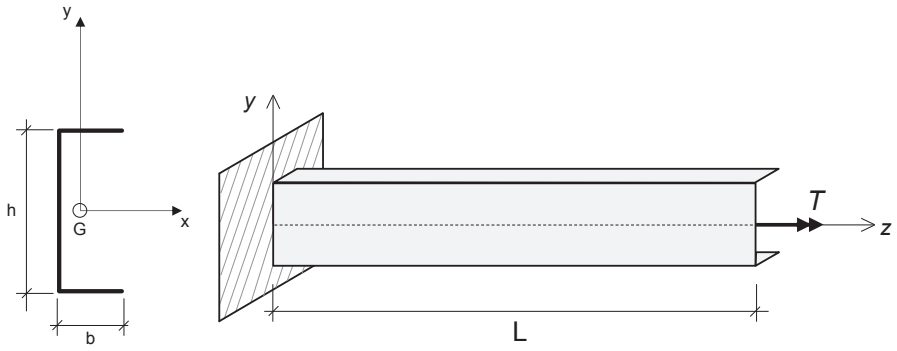

Figure 2.4: C-section cantilever beam under torsion.

plane. The predicted torsional rotations at various points along the beam axis are given in Table 2 and compared with those obtained based on Vlasov and Capurso theories. Indeed, Capurso values can be taken as reference values for shear modes improvement (with undeformable cross-section). It has been verified that the results are not affected by error due to the z-discretization. As it can be noted, even using only the basic shear modes very good results are obtained. Accuracy is further increased by adding one internal node for each wall and the relevant shear modes ($n_S = 3$). As expected, adding more internal nodes the solution converges to the Capurso one.

2.9.2 Test 2: Z-section cantilever beam under transversal load

As a second test, a Z-section cantilever beam with a transversal distributed load applied at the end of the web is considered, see Fig. 2.5. The material is steel and the dimensions are: $b = 40$ mm,

Table 2
C-section cantilever beam - Torsional rotation expressed in milliradians.

z/L	Present formulation		Capurso	Vlasov
	$n_F = 4,\ n_S = 0$	$n_F = 4,\ n_S = 3$		
1/6	1.88	1.91	1.93	1.63
1/3	6.59	6.66	6.69	6.11
1/2	13.54	13.64	13.68	12.84
2/3	22.15	22.28	22.33	21.25
5/6	31.85	32.01	32.07	30.75
1	42.10	42.29	42.36	40.81

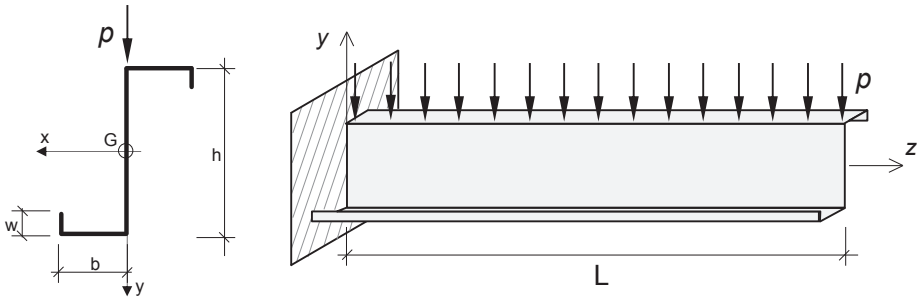

Figure 2.5: Z-section cantilever beam under transversal load.

$h = 120$ mm, $w = 15$ mm, $t = 1.5$ mm, $L = 500$ mm.

This test is used to illustrate the predictive capability of both shear and flexural modes. The six fundamental flexural modes together with the associated shear modes are considered. The results obtained with the present formulation with and without shear modes − denoted respectively by "GBT w S modes" and "GBT wo S modes" − are compared with those obtained with a 3D shear deformable shell model and with the Vlasov theory. The finite element meshes are chosen such that the discretization error is negligible. Fig. 2.6 shows the y-displacement of node 4, normalized by

the factor $\frac{pL^4}{EI}$. The y-displacement of node 4 is not influenced by the cross-section in-plane deformation and the difference between the 3D and Vlasov results is due to the shear deformation. As it can be noted, the present formulation predicts essentially the same results of the 3D model when shear modes are used. On the other hand, the y-displacement of node 2, shown in Fig. 2.7 normalized by the factor $\frac{pL^4}{EI}$, is influenced by both the shear deformation and the cross-section in-plane deformation. In particular, the difference between the results of the present formulation with and without shear modes allows to evaluate the effect of the shear deformation. Moreover, the difference with respect to the Vlasov theory permits to evaluate the influence of the cross-section in-plane deformation. Also in this case, the results of the present formulation with shear modes are in very good agreement with those predicted by the 3D model.

2.9.3 Test 3: C-section fixed-fixed beam under a transversal load.

For the sake of completeness, an additional test will be presented focusing not so much on the influence of shear deformation, but instead on the effect of the local modes. In this third and final test a C-section fixed-fixed beam with a transversal surface load applied over the web, as shown in Fig. 2.8. In this case the material is also steel and the dimensions are $h = 16cm$, $b = 10cm$, $w = 4cm$, $t = 0.3cm$, $L = 200cm$ and $p = 1N/cm^2$.

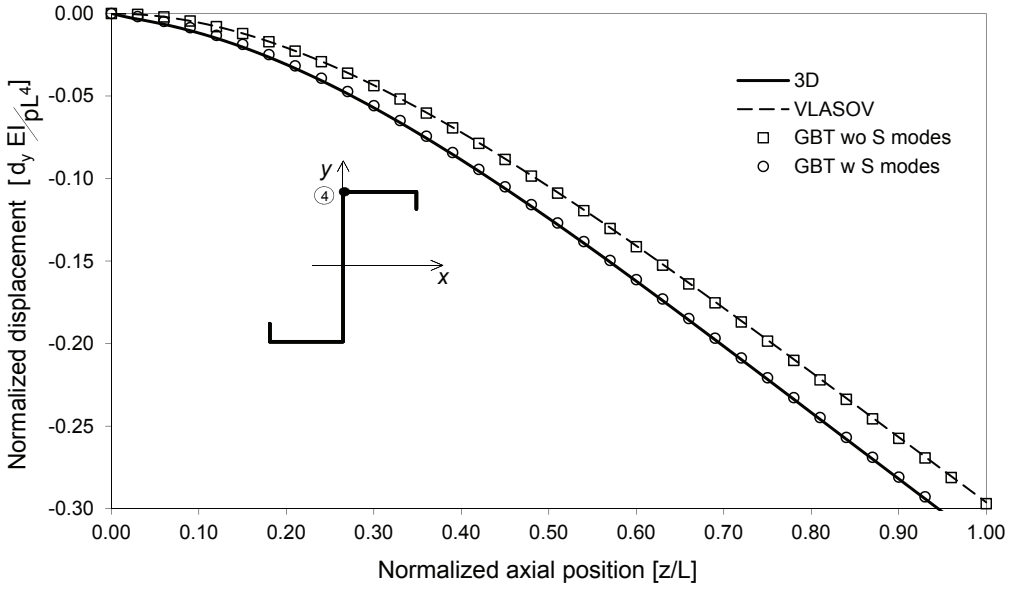

Figure 2.6: Z-section cantilever beam: y-displacement of node 4.

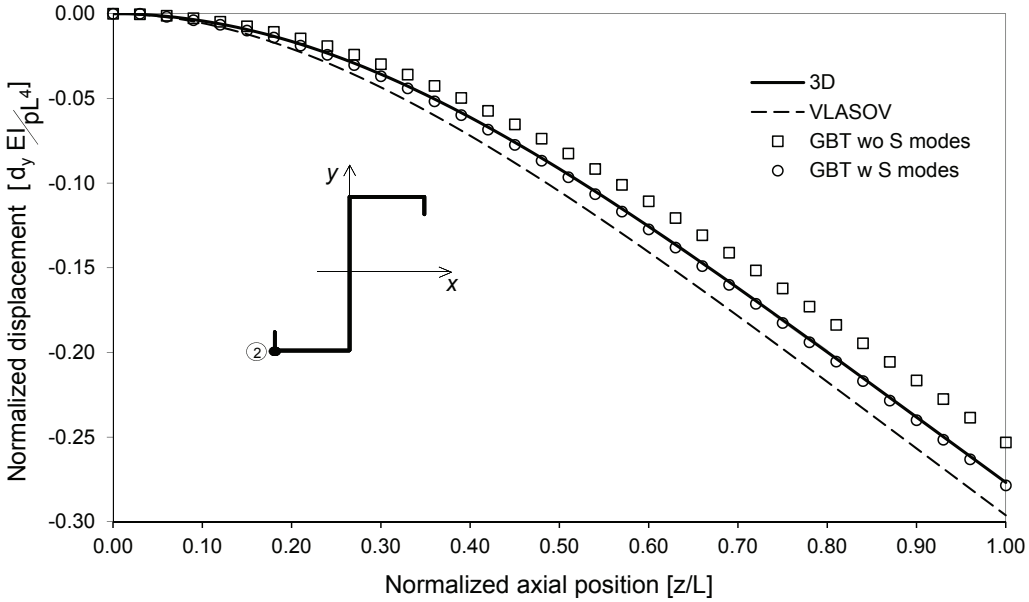

Figure 2.7: Z-section cantilever beam: y-displacement of node 2.

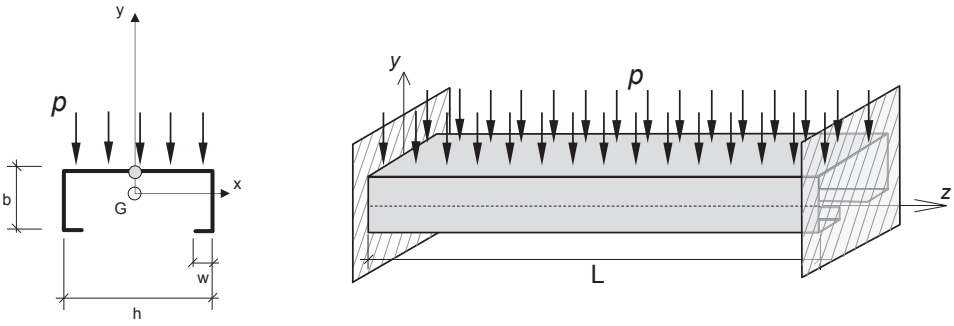

Figure 2.8: C-section fixed-fixed beam under transversal load.

This final test shows the influence of local flexural modes. One local flexural mode per wall is considered in addition to the six fundamental flexural modes, along with shear deformability. The results obtained in this manner are denoted as "GBT w local modes". These results are compared with those obtained by considering only the six fundamental modes with shear deformability, referred in this test as "GBT wo local modes". As a benchmark, a 3D shear deformable shell model is used. Fig. 2.9 shows the y-displacement of the midpoint of the web normalized by the factor $\frac{phL^4}{EI}$. In this case, the y-displacement of the point of interest is considerably influenced by local deformation of the cross-section. It can be seen that the sole consideration of fundamental flexural modes with shear deformability is not enough to recover the in-plane deformation of the web in this example. The inclusion of local flexural modes instead results in good agreement with the y-displacement predicted by the 3D shell model.

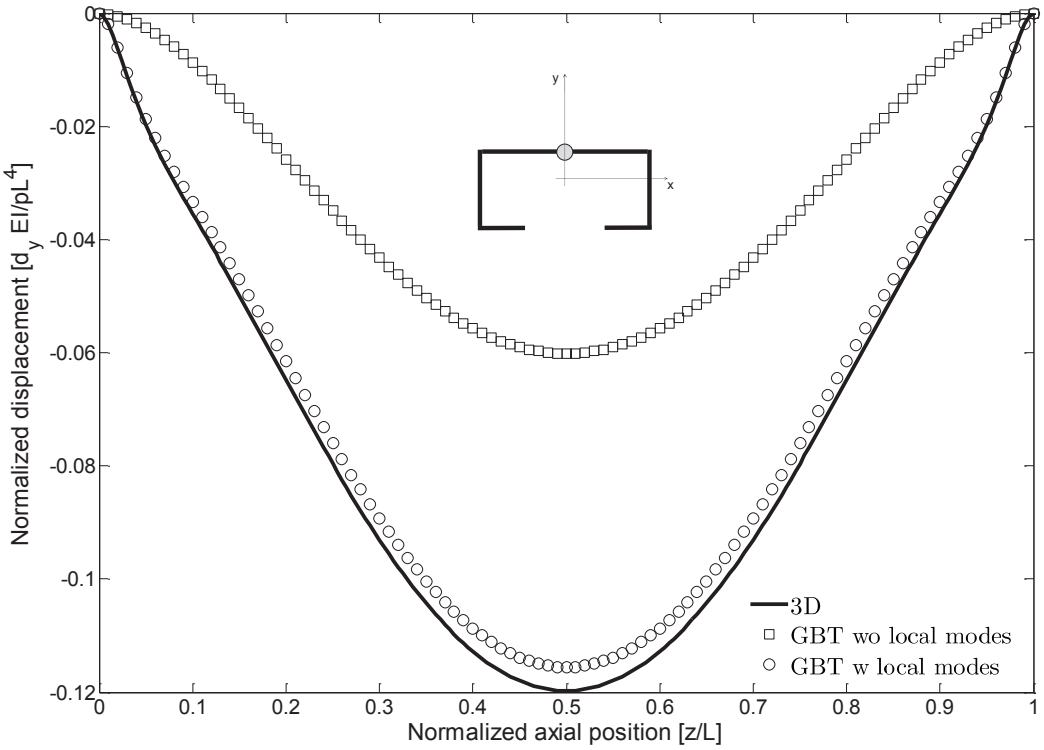

Figure 2.9: C-section fixed-fixed beam: y-displacement of the web midpoint.

Chapter 3

Stress reconstruction in the framework of the GBT

Abstract

In this chapter, a procedure for a posteriori reconstruction of three-dimensional stresses in the finite element analysis of Generalized Beam Theory members is presented. The reconstruction is based on the enforcement of the point-wise three-dimensional equilibrium equations over the beam, interpreted as an assembly of thick plates, and on the use of the Recovery by Compatibility in Patches procedure. No corrections to meet the equilibrium boundary conditions on bottom/top wall faces are needed. Numerical results show that the proposed approach allows to effectively recover local stress profiles which match those of three-dimensional solid finite element models.

The GBT model studied in the previous chapters is essentially the representation of a three-dimensional body on whose displacements some kinematic assumptions are made in order to restrict the class of admissible deformations to those peculiar of a mono-

dimensional beam model. While the modal nature of the GBT indeed allows describing essentially three-dimensional phenomena like cross-section distortion and local effects, the fact remains that the GBT is one-dimensional. For this reason, the kinematic assumptions at the base of the GBT play the role of an internal constraint imposed on the parent three-dimensional body to derive the corresponding mono-dimensional beam model. In the case of displacements, this internal constraint may be resolved by properly adjusting the constitutive law, as explained in Chapter 2. However, when postprocessing those displacements to obtain the three-dimensional stress field, the solution to the problem of the internal constraint is not as simple. Indeed, in presence of internal constraints, the stress field decomposes into the sum of an active and a reactive part. The active part is related to the strains by means of a constitutive equation while the reactive part is given the role of maintaining the constraints. In other words, only the active part of the stress field does work over the prescribed deformations. The reactive part instead is essentially a series of reactions to the internal constraints of the beam model.

As it can be easily realized, when the three-dimensional beam-like body is mapped into the mono-dimensional beam model, only active stresses come into play. As a consequence, only the active part of stresses is constitutively determined by the solution of the beam problem. However, it is obvious that the reactive stresses can be useful to approximate the three-dimensional stress field, so a

procedure to recover these stresses is necessary if the constitutively determined active stress field is to be improved with the aim of obtaining a truly three-dimensional solution.

In the GBT literature, the stress recovery problem outlined above has seldom been addressed. The original work of Schardt limited stress recovery to normal stresses in the direction of the axis of the beam by means of a classic constitutive relation. In [34], as a part of a buckling analysis of GBT members with non-standard support conditions, the limitations of the elasto-kinematic approach to stress calculation were put in evidence and the recovery of the sole shear stress component along the section midline from axial stress equilibrium was performed. With the intention of addressing these issues, the reactive part of the stress field can be recovered by enforcing the three-dimensional equilibrium conditions, so healing the equilibrium injuries inevitably introduced by the kinematical assumptions. Such is the approach that will be presented in the following.

3.1 Reconstruction of the three-dimensional stresses

The procedure proposed herein to recover stresses is based on satisfying three-dimensional equilibrium. Evidently, this can only be done a posteriori since the active part of the stress field is needed in order to enforce the equilibrium equations and reconstruct the fully three-dimensional stress field. With this in mind, we can write the three-dimensional equilibrium equations as:

$$\partial_z \sigma_{zz} + \partial_s \tau_{zs} + \partial_n \tau_{zn} + b_z = 0, \tag{3.1}$$

$$\partial_z \tau_{zs} + \partial_s \sigma_{ss} + \partial_n \tau_{sn} + b_s = 0, \tag{3.2}$$

$$\partial_z \tau_{zn} + \partial_s \tau_{sn} + \partial_n \sigma_{nn} + b_n = 0, \tag{3.3}$$

where ∂_s, ∂_z, and ∂_n denote the derivatives with respect to the s, z, n coordinates, and the terms b_z, b_s and b_n denote the bulk loads.

Based on the reasoning exposed at the beginning of this chapter, let us recall here the stress field introduced in Chapter 2 and write each stress component explicitly. In addition to the membrane-bending separation, we shall divide each stress component into the active part, related to the strains by a constitutive relation and denoted with the superscript A, and the reactive part, denoted with the superscript R, as follows:

$$\sigma_{zz} = \sigma_{zz}^{(M)A} + n\hat{\sigma}_{zz}^{(B)A}, \tag{3.4}$$

$$\sigma_{ss} = \sigma_{ss}^{(M)R} + n\hat{\sigma}_{ss}^{(B)A}, \tag{3.5}$$

$$\tau_{zs} = \tau_{zs}^{(M)R} + n\hat{\tau}_{zs}^{(B)A}, \tag{3.6}$$

$$\tau_{sn} = \tau_{sn}^{R}, \tag{3.7}$$

$$\tau_{zn} = \tau_{zn}^{R}, \tag{3.8}$$

$$\sigma_{nn} = \sigma_{nn}^{R}. \tag{3.9}$$

The choice between active and reactive parts is based on the internal constraints of the GBT model. In particular, in the case

of σ_{zz}, in line with the GBT spirit that interprets the thin-walled beam as an assembly of plates, both membrane and bending components are deemed active, as in standard plate theories. As regards σ_{ss}, given that for all the mode families considered in this work the modal function $\boldsymbol{\mu}$ is constant over s, the membrane component $\varepsilon_{ss}^{(M)}$ given by Eq. (2.9) is null. for this reason $\sigma_{ss}^{(M)}$ is considered to be reactive. Analogously, shear stress τ_{zs} has a reactive membrane part related to the constraint of constant $\gamma_{zs}^{(M)}$ shown in Eq. (2.10) (indeed, $\gamma_{zs}^{(M)}$ is null if no shear modes are considered). Finally, the transverse shear stresses τ_{zn} and τ_{sn} are assumed to be completely reactive given that their correspondent strains are, respectively, constant on the wall thickness and null. These last two stresses are indeed the transverse shear stresses in the plate forming the generic wall, so they can be reconstructed assuming a parabolic distribution (illustrated in Fig. 3.1a) over the wall thickness in agreement with plate theories that allow for transverse shear deformability:

$$\tau_{zn}^{R} = g(n)\tilde{\tau}_{zn}, \tag{3.10}$$

$$\tau_{sn}^{R} = g(n)\tilde{\tau}_{sn}, \tag{3.11}$$

where $\tilde{\tau}_{zn}$ and $\tilde{\tau}_{sn}$ are unknown parameters and $g(n)$ denotes the parabolic function, shown in Fig. 3.1a, which is assumed to have unit area and zero value at $n = \pm t/2$, being t the thickness of the wall.

In addition to the assumptions above, the effect of external sur-

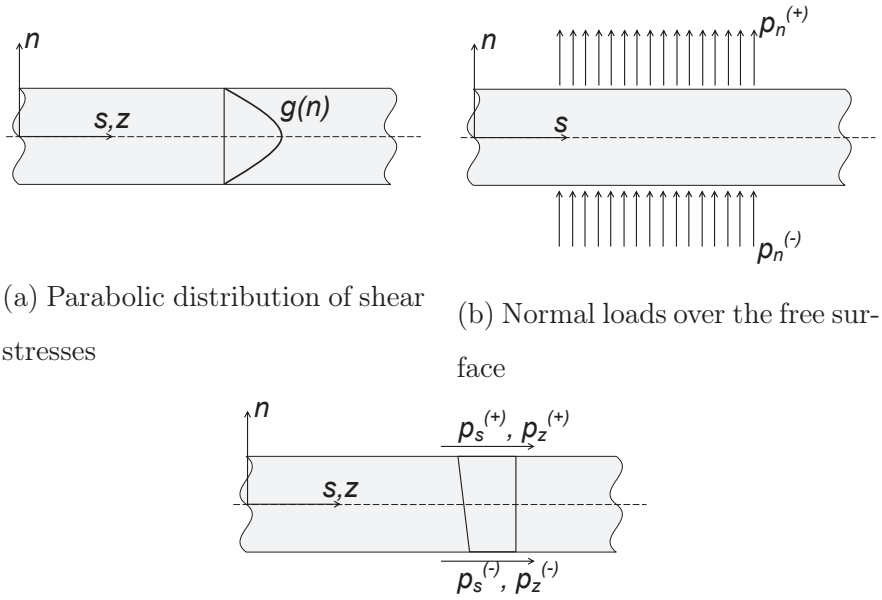

(a) Parabolic distribution of shear stresses

(b) Normal loads over the free surface

(c) Tangent loads over the free surface

Figure 3.1: Different assumptions made over the generic wall

face loads must be taken into account if equilibrium is to be enforced. In this sense, let us consider some distributed forces $p_n^{(+)}$ and $p_n^{(-)}$ on the top and bottom surfaces of the generic wall in the n direction, each identified with the superscript $(+)$ or $(-)$ according to the sign of n on said surfaces, as illustrated in Fig. 3.1b. Given that during the cross-section analysis the wall rotations are obtained by considering the cross-section as a planar frame (an explanation of this procedure is given in Chapter 1), $p_n^{(+)}$ and $p_n^{(-)}$ will be translated into their equivalent nodal forces as is done normally when using beam finite elements. If the in-plane bending moment generated by these forces over the generic wall is to be recovered (thus satisfying equilibrium conditions) then Eq. (3.5) must be enriched by adding a term such as:

$$\sigma_{ss}^{p} = n\,\beta\left(p_n^{(+)} + p_n^{(-)}\right)\left(\frac{s^2 - l_w\,s}{2}\right), \tag{3.12}$$

where l_w is the generic wall length and the substitution $\beta = \mathrm{d}^2 g(n)/\mathrm{d}n^2$ has been made. In a similar way, loads in the s and z directions on the top and bottom faces can be considered to have a linear distribution over the wall thickness, as shown in Fig. 3.1c. These loads can be used to enrich the assumption on the transverse shear stresses τ_{sn} and τ_{zn} so as to guarantee the fulfilment of the equilibrium boundary conditions on the top and bottom faces of the wall. This results in the following corrective terms:

$$\begin{aligned}\tau_{sn}^{p} =& g(n)\,\left(p_n^{(+)} + p_n^{(-)}\right)\left(\frac{l_w}{2} - s\right) + p_s^{(+)}\left(\frac{n}{t} + \frac{1}{2}\right) + \\ &+ p_s^{(-)}\left(\frac{n}{t} - \frac{1}{2}\right),\end{aligned} \tag{3.13}$$

$$\tau_{zn}^{p} = p_z^{(+)}\left(\frac{n}{t} + \frac{1}{2}\right) + p_z^{(-)}\left(\frac{n}{t} - \frac{1}{2}\right). \tag{3.14}$$

It should be noted that in the corrections above, uniform surface loads have been assumed for simplicity.

Integration of the equilibrium equations

Once all the relevant assumptions have been made, the reconstruction procedure starts by substituting Eqs. (3.4), (3.6), (3.8), (3.10) and (3.14) in Eq. (3.1). Taking into account only the membrane contributions in the resultant equation leads to:

$$\partial_z \sigma_{zz}^{(M)A} + \partial_s \tau_{zs}^{(M)R} + b_z^{(M)} + \frac{p_z^{(+)} + p_z^{(-)}}{t} = 0, \tag{3.15}$$

which then can be solved for the first unknown stress component, $\tau_{zs}^{(M)R}$:

$$\tau_{zs}^{(M)R} = -\int_0^s \left(b_z^{(M)} + \partial_z \sigma_{zz}^{(M)A} + \frac{p_z^{(+)} + p_z^{(-)}}{t} \right) \mathrm{d}s. \tag{3.16}$$

On the other hand, taking into account only the bending contributions in Eq. (3.1) gives:

$$\partial_z \sigma_{zz}^{(B)A} + \partial_s \tau_{zs}^{(B)A} + \beta \hat{\tau}_{zn} + b_z^{(B)} = 0, \tag{3.17}$$

and this allows to determine $\tilde{\tau}_{zn}$:

$$\tilde{\tau}_{zn} = -\frac{1}{\beta} \left(\hat{b}_z^{(B)} + \partial_s \hat{\tau}_{zs}^{(B)A} + \partial_z \hat{\sigma}_{zz}^{(B)A} \right). \tag{3.18}$$

In a similar way, substituting Eqs. (3.5), (3.6), (3.7), (3.11), (3.12) and (3.13) in Eq. (3.2) and taking into account separately the membrane contribution leads to:

$$\partial_z \tau_{zs}^{(M)R} + \partial_s \sigma_{ss}^{(M)R} + b_s^{(M)} + \frac{p_s^{(+)} + p_s^{(-)}}{t} = 0, \tag{3.19}$$

hence the expression for the recovered $\sigma_{ss}^{(M)R}$:

$$\sigma_{ss}^{(M)R} = -\int_0^s \left(b_s^{(M)} + \partial_z \tau_{zs}^{(M)R} + \frac{p_s^{(+)} + p_s^{(-)}}{t} \right) \mathrm{d}s. \tag{3.20}$$

On the other hand, the bending part of Eq. (3.2) is:

$$\partial_z \tau_{zs}^{(B)A} + \partial_z \sigma_{ss}^{(B)A} + \beta \hat{\tau}_{sn} + b_s^{(B)} = 0, \tag{3.21}$$

thus allowing to determine another reactive stress component:

$$\tilde{\tau}_{sn} = -\frac{1}{\beta}\left(\hat{b}_s^{(B)} + \partial_z \hat{\tau}_{zs}^{(B)A} + \partial_s \hat{\sigma}_{ss}^{(B)A}\right). \tag{3.22}$$

Finally, once the transverse shear stresses are known, substituting Eqs. (3.10), (3.11), (3.13) and (3.14) in Eq. (3.3) and integrating in n, it is possible to reconstruct the transverse normal stress profile:

$$\sigma_{nn}^{R} = -p_n^{(-)} - \int_{-t/2}^{n} g(n)\left(\partial_z \tilde{\tau}_{zn} + \partial_s \tilde{\tau}_{sn} - p_n^{(+)} - p_n^{(-)}\right) \mathrm{d}n. \tag{3.23}$$

It can be easily verified that the reconstructed stress profile σ_{nn}^{R} automatically meets the boundary condition on the top and bottom faces of the wall ($n = \pm t/2$).

Integration constants

In order to use Eqs. (3.16) and (3.20) in the reconstruction procedure, it is necessary to determine the proper integration constants that give the value of the desired stress component at the starting point ($s = 0$) of each internal wall. Figure 3.2 shows the free body diagram of an arbitrary natural node between two consecutive walls, i and $i+1$, forming an angle θ. Starting from there, the balance of forces in the z-direction gives:

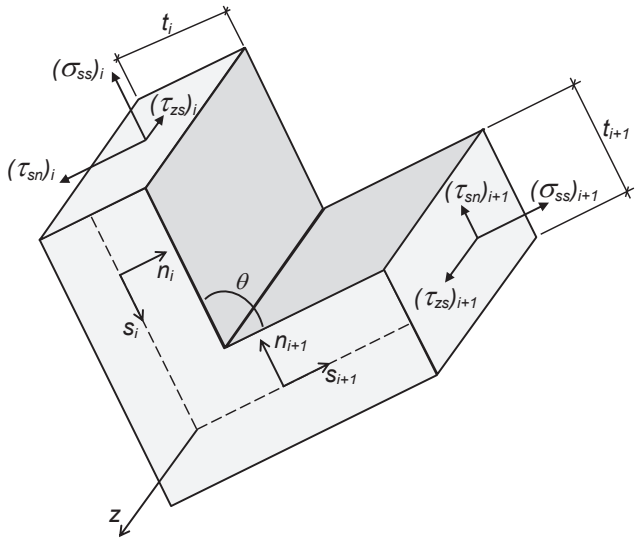

Figure 3.2: Free body diagram of an arbitrary natural node.

$$\left(\tau_{zs}^{(M)R}\right)_{i+1} = \left(\tau_{zs}^{(M)R}\right)_i \frac{t_{i+1}}{t_i}. \tag{3.24}$$

Analogously, the balance of forces in the s_{i+1} direction gives:

$$\left(\sigma_{ss}^{(M)R}\right)_{i+1} = -\left(\sigma_{ss}^{(M)R}\right)_i \frac{t_i}{t_{i+1}}\cos\theta + \frac{1}{t_{i+1}}\int_{-t_i/2}^{t_i/2}(\tau_{sn})_i \sin\theta \, \mathrm{d}n. \tag{3.25}$$

Eqs. (3.24) and (3.25) are used together with Eqs. (3.16) and (3.20) to perform the reconstruction of $\tau_{zs}^{(M)R}$ and $\sigma_{ss}^{(M)R}$ along the entire section midline.

It is worth to note that the reconstruction does not need any correcting procedure to accommodate boundary equilibrium conditions on the bottom/top faces of the walls, since this task is performed by adding the corrections introduced in Eqs. (3.12), (3.13), and (3.14). This significantly simplifies the procedure. However, it can be easily seen, in Eqs.(3.16) and (3.20), that the reconstruction is performed using the first- and second-order derivatives of

the active stress components and, hence, of the generalized stresses of the beam, so that their accuracy is crucial in order to guarantee the accuracy of the whole reconstruction strategy. Indeed, in the framework of a finite element analysis, neither a precise evaluation nor the convergence of these quantities is guaranteed if standard finite elements are used to evaluate the generalized stress fields. In order to overcome this limitation, it is possible to suitably post-process the generalized stresses obtained from the finite element analysis before using them in the reconstruction process.

3.2 Recovery of the generalized stresses

Although easy from the theoretical point of view, the approach proposed above needs as input first and second-order derivatives of the beam generalized stresses, which are usually characterized by lack of accuracy if standard finite elements are used. To improve the accuracy of the first- and second-order derivatives of the generalized stresses, the Recovery by Compatibility in Patches (RCP) procedure can be used. This procedure has been shown to provide an excellent basis for stress recovery, error estimation and adaptivity both in plane and plate problems [36]-[43]. The main idea of the RCP is to recover stresses by minimizing the complementary energy associated to a patch of elements, among an assumed set of self-equilibrated stress fields. The patch is considered as a separate domain on whose boundary the displacements coming from the finite element analysis are prescribed. The minimization of the

complementary energy associated to the patch yields the following local compatibility condition:

$$\int_{\Omega_p} \delta\mathbf{s}^{r^T} \left(\mathbf{e}^r - \mathbf{e}^h\right) \mathrm{d}z = 0 \qquad \forall\, \delta\mathbf{s}^r \mid \mathbf{D}^*\delta\mathbf{s}^r = \mathbf{0}, \tag{3.26}$$

where Ω_p is the patch domain, $\mathbf{s}^r$ is the recovered generalized stress vector, $\mathbf{e}^r$ is the vector of generalized deformations related to $\mathbf{s}^r$ via constitutive equations and $\mathbf{e}^h$ is the generalized deformation vector resulting from the finite element solution. To apply the RCP, a new approximation for the generalized stresses over the patch is introduced:

$$\mathbf{s}^r = \mathbf{P}^r\,\alpha + \mathbf{s}^p, \tag{3.27}$$

where $\mathbf{P}^r$ is a matrix of self-equilibrated generalized stress modes (i.e. $\mathbf{D}^*\mathbf{P}^r = \mathbf{0}$ in Ω_p), α is a vector of unknown parameters and $\mathbf{s}^p$ is a particular solution of the beam equilibrium equations depending only on external loads. Substituting Eq. (3.27) into Eq. (3.26) leads to a system of linear algebraic equations, whose solution permits to determine α and, consequently allows to calculate the recovered stress field over the patch. Here, motivated by [42] and in order to ensure accuracy of second-order derivatives of reconstructed generalized stresses, a five-element patch is used (see Fig. 3.3) and a double recovery is performed. In this approach, firstly a RCP recovery of the generalized stresses is performed and, then, the generalized strains related to the recovered stresses are evaluated and used in a second RCP recovery. Naturally, in order to be able to evaluate the second-order derivatives of the recovered

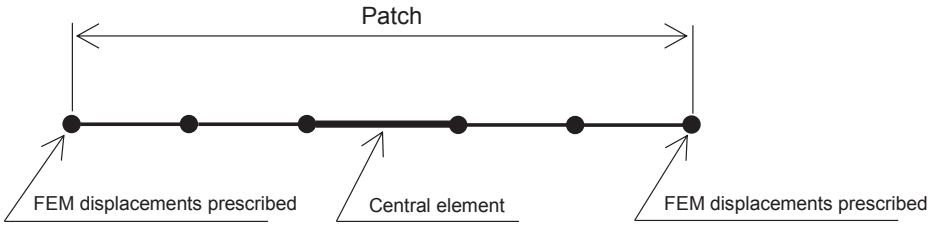

Figure 3.3: Element patch used in the RCP recovery.

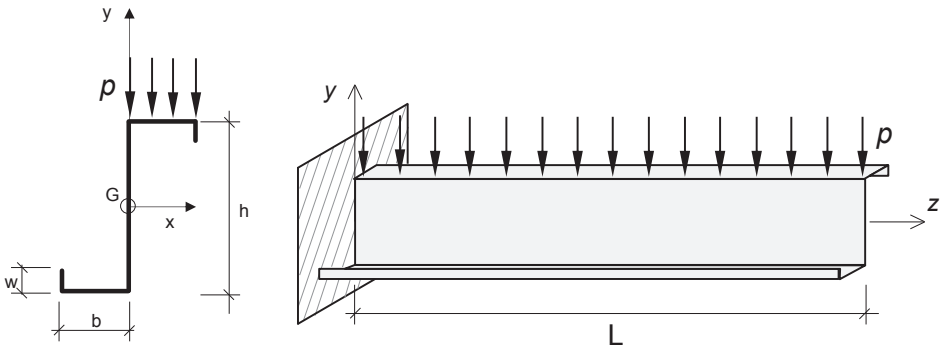

Figure 3.4: Z-section cantilever beam.

quantities, it is necessary to use at least a quadratic polynomial approximating function in the matrix $\mathbf{P}^r$.

3.3 Some examples

To test the performance of the procedure, a Z-section cantilever beam with a uniform transversal surface load $p_n^{(+)} = -0.025\, N/mm^2$ applied over the upper flange is considered, as shown in Fig. 3.4. The material is steel and the dimensions are: $b = 40\, mm$, $h = 120\, mm$, $w = 15\, mm$, $t = 1.8\, mm$, $L = 1200\, mm$.

The GBT solution has been obtained using a GBT-based finite element code implemented as described in Chapter 2. For this test, the six fundamental flexural modes associated to the six natural nodes of the section are considered along with shear modes.

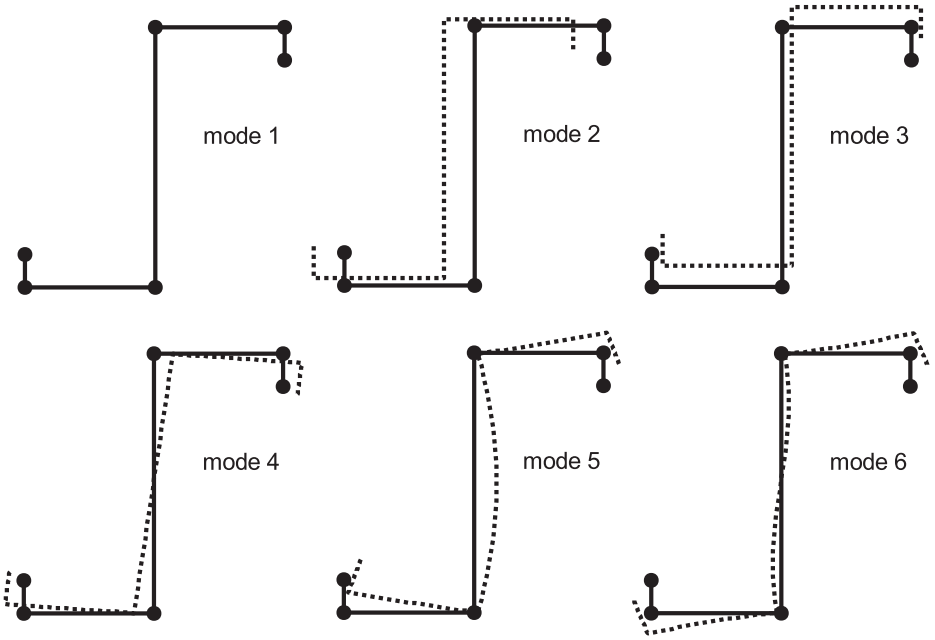

Figure 3.5: Z-section cantilever beam: in-plane displacements associated to fundamental flexural modes (shear modes have null in-plane displacements).

Figs. 3.5 and 3.6 show, respectively, the in-plane and the out-of-plane displacements associated to the modes considered. Moreover, the $\mathbf{v}$-parameters are approximated by cubic hermitian functions while the δ-parameters are approximated by quadratic polynomials. The finite element mesh is chosen such that the discretization error is negligible. In the proposed stress reconstruction procedure, a complete cubic polynomial approximation depending on 31 α-parameters has been used for the RCP-recovered stress resultants. For comparison, the above problem has been also solved using 8-node brick finite elements on a very fine mesh of about $2 \cdot 10^6$ finite elements.

In the following, the three-dimensional stress distributions obtained from the GBT solution using the proposed recovery proce-

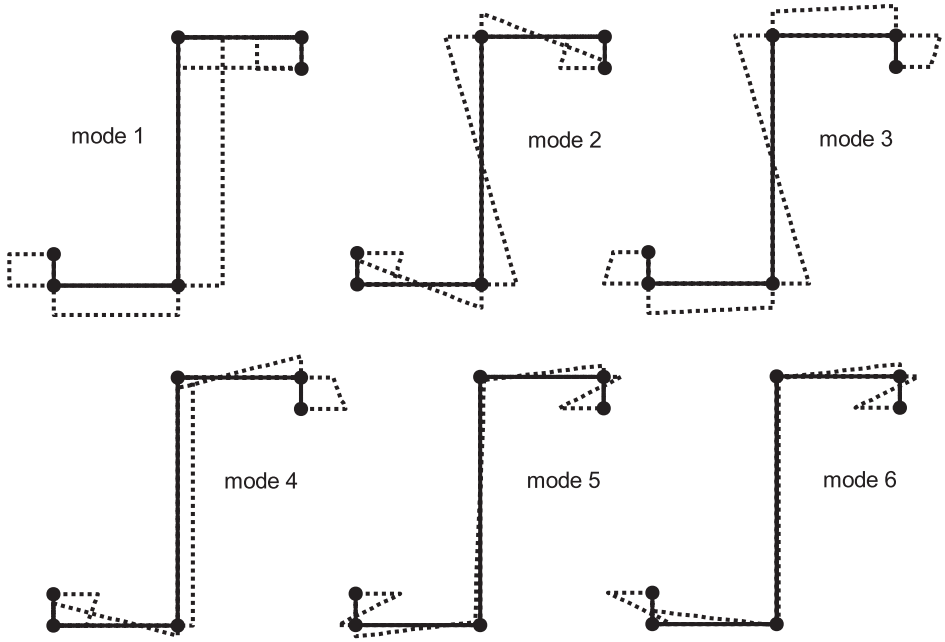

Figure 3.6: Z-section cantilever beam: out-of-plane displacements associated to fundamental flexural modes and shear modes.

dure are compared with those predicted by the three-dimensional finite element model. Moreover, for completeness, also the stress distributions obtained from the GBT solution via the elasto-kinematic relations are reported.

Fig. 3.7 shows the distribution of σ_{zz} along the midline (note that the bending part is zero on the section midline) of the cross-sections at $z/L = 0.5$ and $z/L = 0.75$. In the reconstruction procedure, σ_{zz} is assumed to be completely active, hence the results obtained via the elasto-kinematic relations and with the present procedure coincide and only one of them is reported. As can be seen, the results obtained with the GBT model correspond accurately with those of the three-dimensional solution. It is important to notice this component of stress is the only one traditionally con-

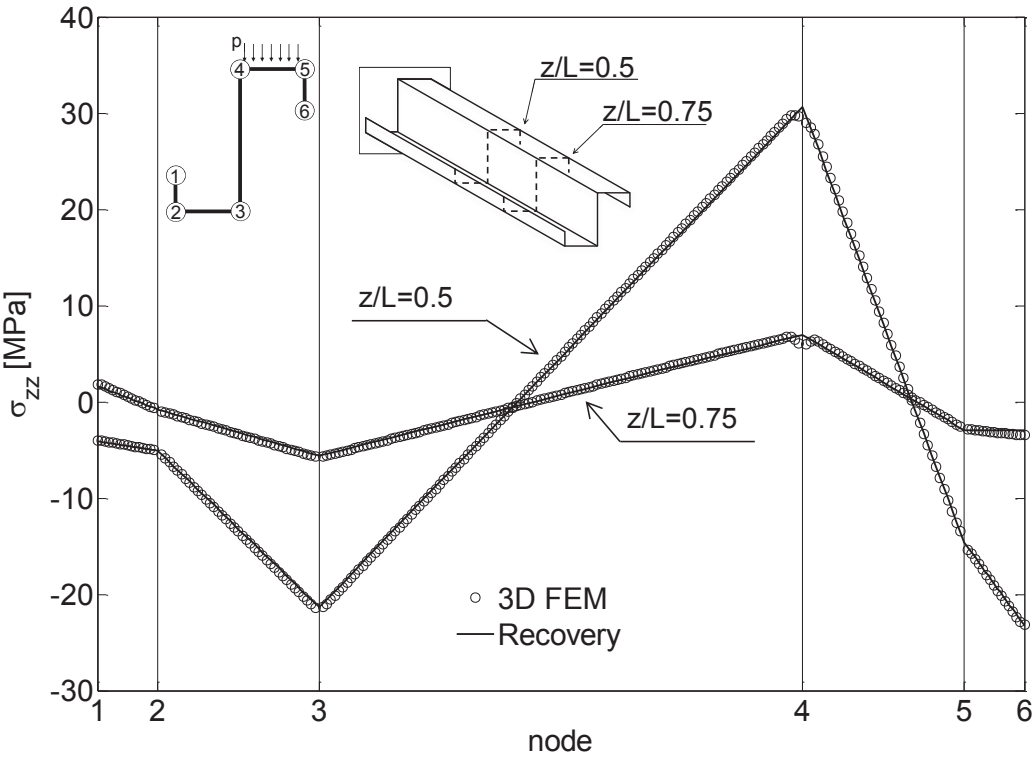

Figure 3.7: Normal stress σ_{zz} along the section midline at $z/L = 0.5$ and $z/L = 0.75$.

sidered in GBT formulations.

The distribution of the normal stress σ_{ss} over the section midline is shown in Fig. 3.8. Also in this case, a very good agreement between the distribution obtained via the proposed procedure and that of the three-dimensional finite element model can be observed. In this case there is no elasto-kinematic distribution to compare, since the internal constraints render this component null.

The distribution of the shear stress τ_{zs} along the section midline is shown in Fig. 3.9. It can be seen that the elasto-kinematic distribution, constant on each wall as expected, lacks accuracy whereas that obtained with the reconstruction procedure matches very well the three-dimensional one.

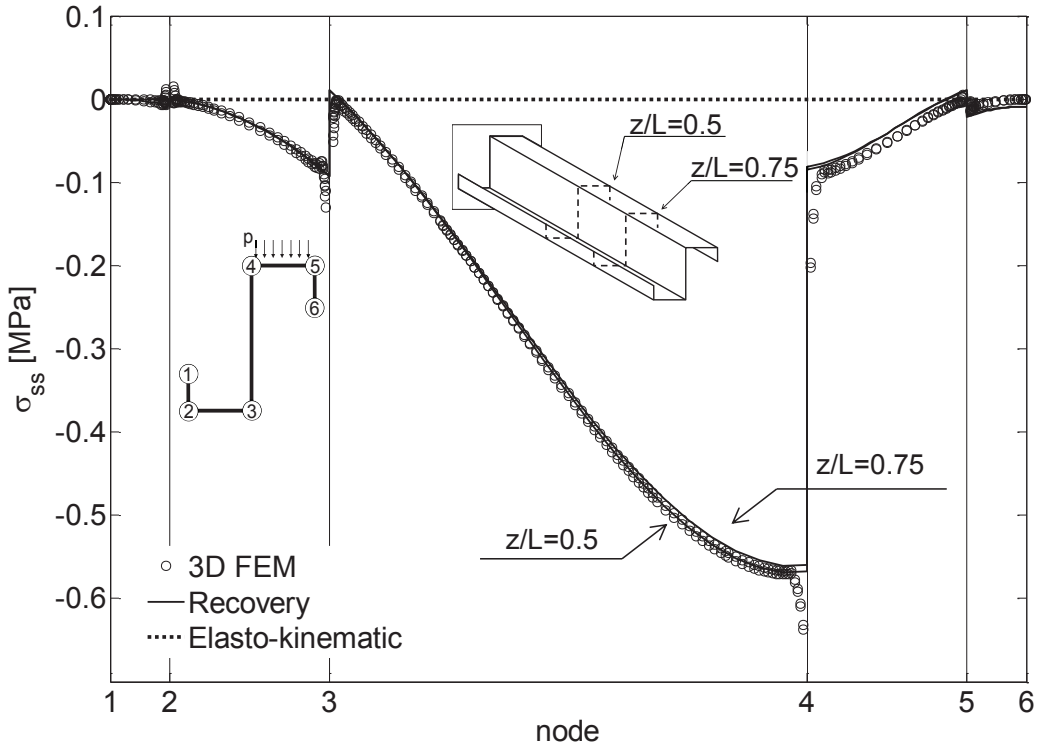

Figure 3.8: Normal stress σ_{ss} along the section midline at $z/L = 0.5$ and $z/L = 0.75$.

Fig. 3.10 shows the distribution of the σ_{zz} stress component over the $z/L = 0.5$, but this time results are obtained outside of the midline. In particular, the coordinate $n = t/4$ is chosen here to illustrate the recovery of the bending part of the stress profile. As with the corresponding membrane part, this stress component is completely active, so the elasto-kinematic solution coincides with the proposed procedure and with the three-dimensional model.

In the case of σ_{ss}, the stress distribution over the cross-section is showed in Fig. 3.11. In this case, the elasto-kinematic solution is not null, but still lacks accuracy with respect to the proposed procedure. Specifically, the boundary condition over Wall 4 is not completely recovered, since the elasto-kinematic solution implies a

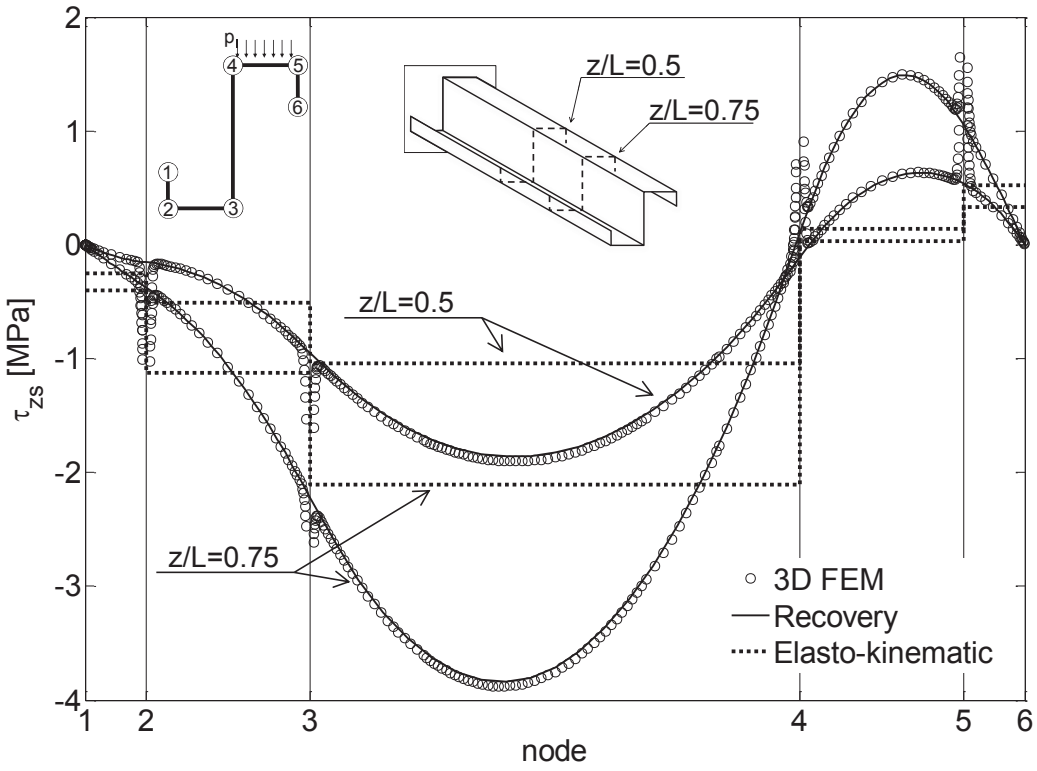

Figure 3.9: Shear stress τ_{zs} along the section midline at $z/L = 0.5$ and $z/L = 0.75$.

substitution of the distributed load over the wall by it's equivalent nodal loads. Such approximations are not present in the recovered procedure.

The distribution of the τ_{zs} along the s coordinate for $z/L = 0.5$ and $n = t/4$ is shown in Fig. 3.11. The very good agreement between the distributions obtained with the recovery procedure and that of the solid finite element model can be noted also in this case.

Figure 3.13 shows the distributions of the shear stress τ_{sn} over the section midline. Here, the capability of the proposed procedure to recover stresses including the boundary conditions over the free surfaces is even more patent, as the shear force over Wall 4 is cor-

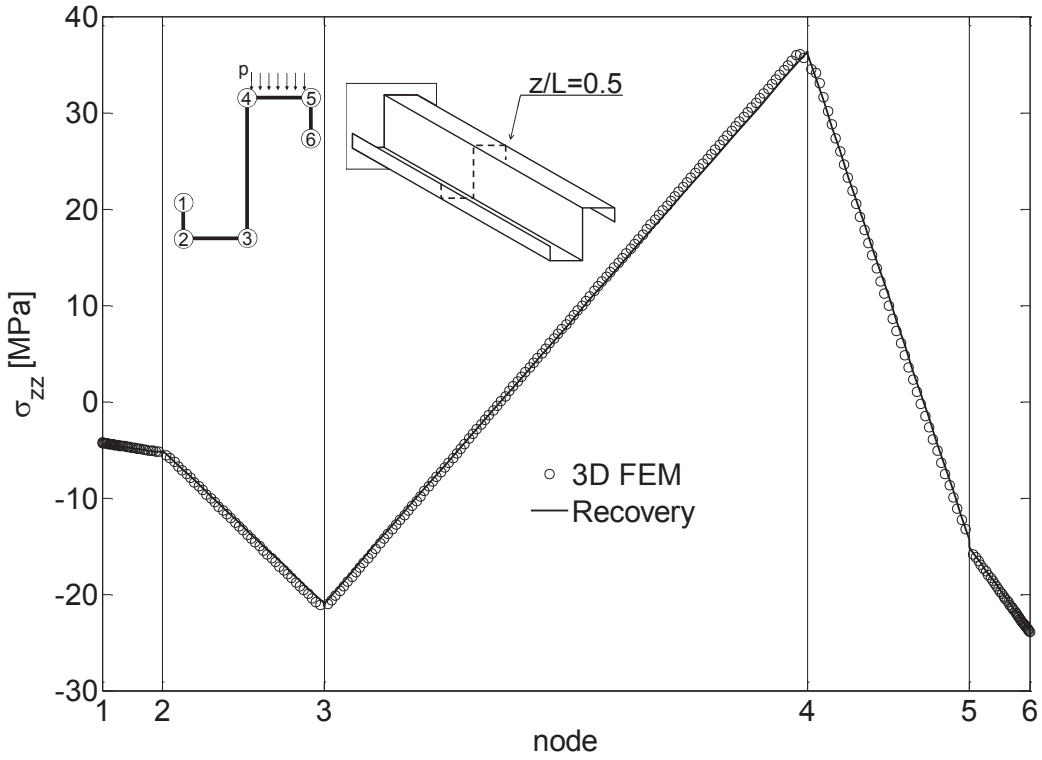

Figure 3.10: Normal stress σ_{zz} along the section at $z/L = 0.5$ and $n = t/4$.

rectly obtained. The corresponding elasto-kinematic component is, as expected, null.

Fig. 3.14 shows the distribution along the beam length of τ_{zn} evaluated at the midpoint of the upper flange for $n = 0$. This axial distribution was chosen in lieu of one over the cross-section not only because this is the actual plane where this stress component acts, but also to show how the solution obtained with the elasto-kinematic approach noticeably differs from that of the three-dimensional solution, while the reconstruction procedure closely follows it.

Further insight into the distributions of τ_{sn} and τ_{zn} is given by Fig. 3.15, which shows the profiles of these shear stresses along the

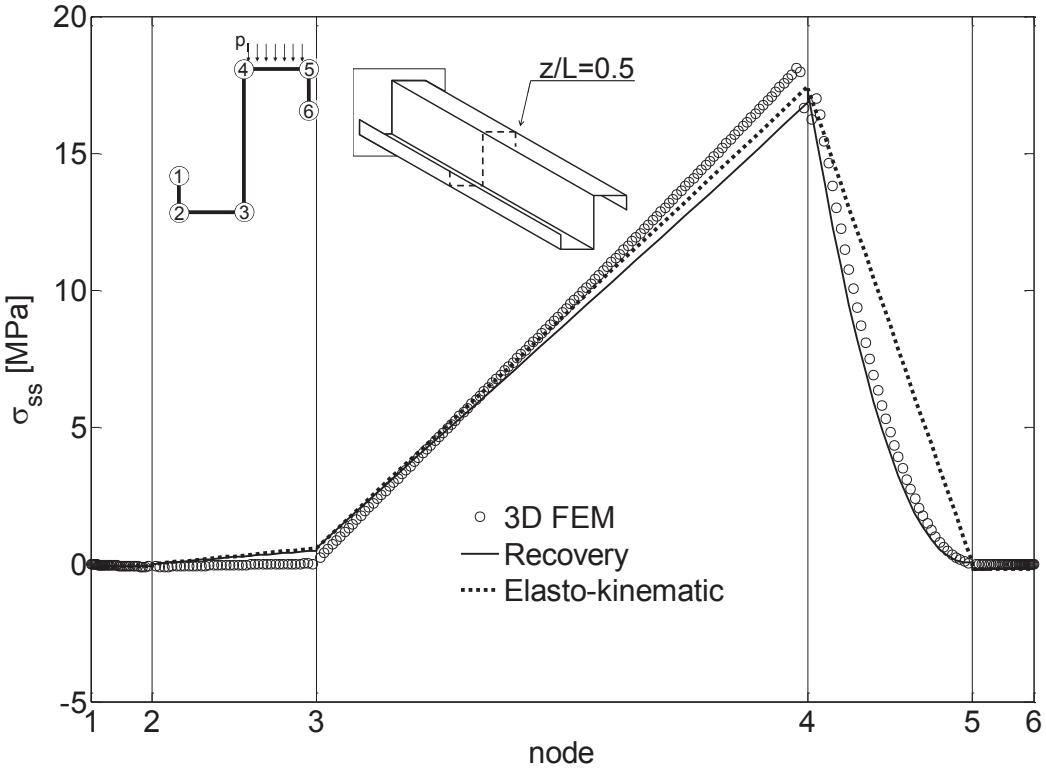

Figure 3.11: Normal stress σ_{ss} along the section at $z/L = 0.5$ and $n = t/4$.

wall thickness, at the midpoint of both the web and each flange. In particular, full circle markers at the extremes highlight the stress values imposed by the boundary conditions. The elasto-kinematic solution in the case of τ_{sn} is null whereas for τ_{zn} it is not reported since it would be outside of the scale presented, as can be easily realized by inspecting Fig. 3.14. In all the cases, the stress distributions obtained with the reconstruction procedure fit well those of the three-dimensional finite element model. Additionally, in all cases the recovered stress distributions satisfy the boundary conditions on the bottom and top faces of the walls.

Finally, Fig. 3.16 shows the profile of σ_{nn} along the thickness of the wall at the midpoint of the upper flange for $z/L = 0.5$. It can be

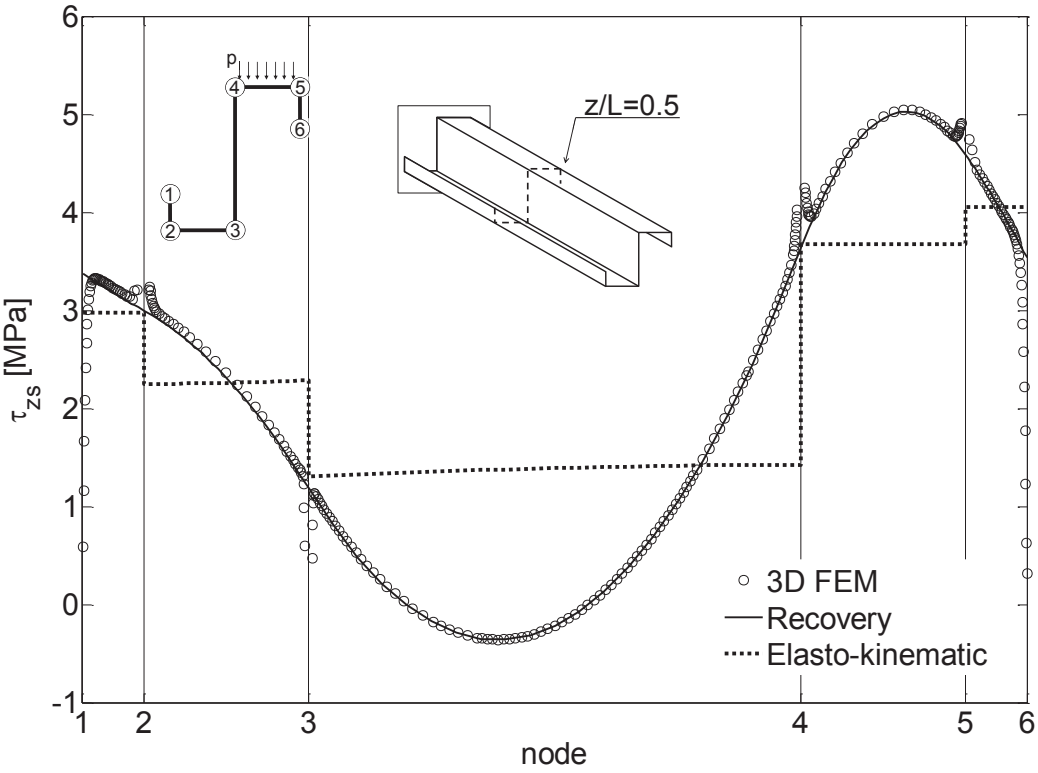

Figure 3.12: Shear stress τ_{zs} along the section $z/L = 0.5$ and $n = t/4$.

seen that the profile predicted by the recovery procedure matches the one of the three-dimensional finite element model, while the elasto-kinematic approach gives a null result. It is also worth noticing that the boundary condition at the top face of the wall is met exactly.

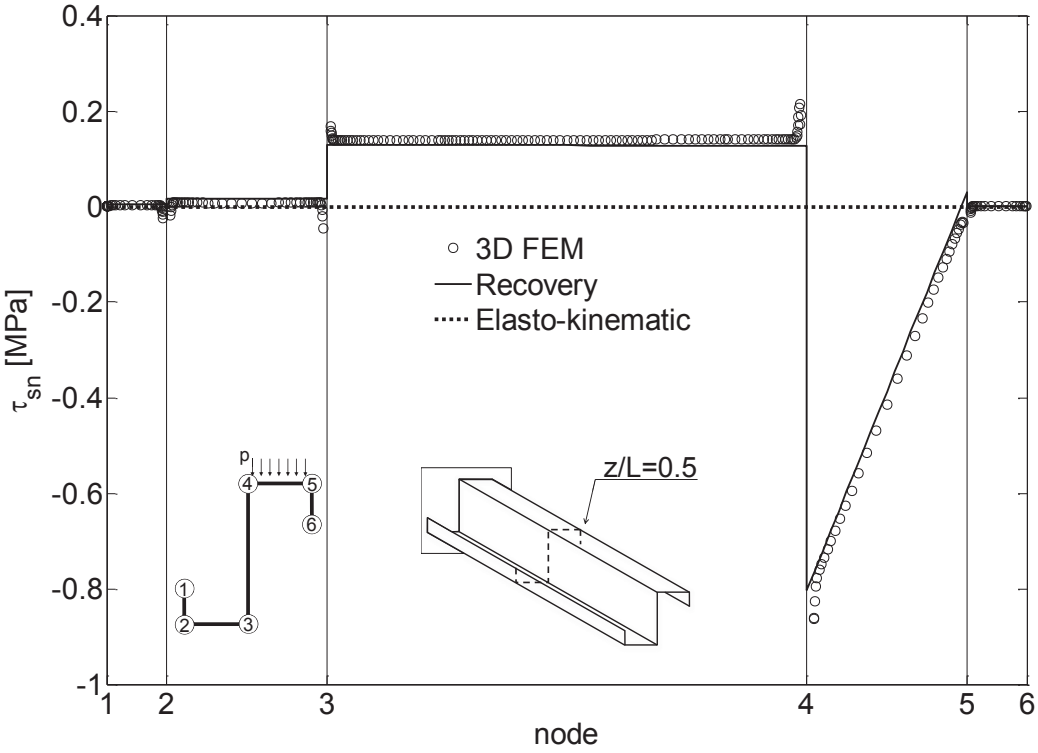

Figure 3.13: Shear stress τ_{sn} along the section midline at $z/L = 0.5$.

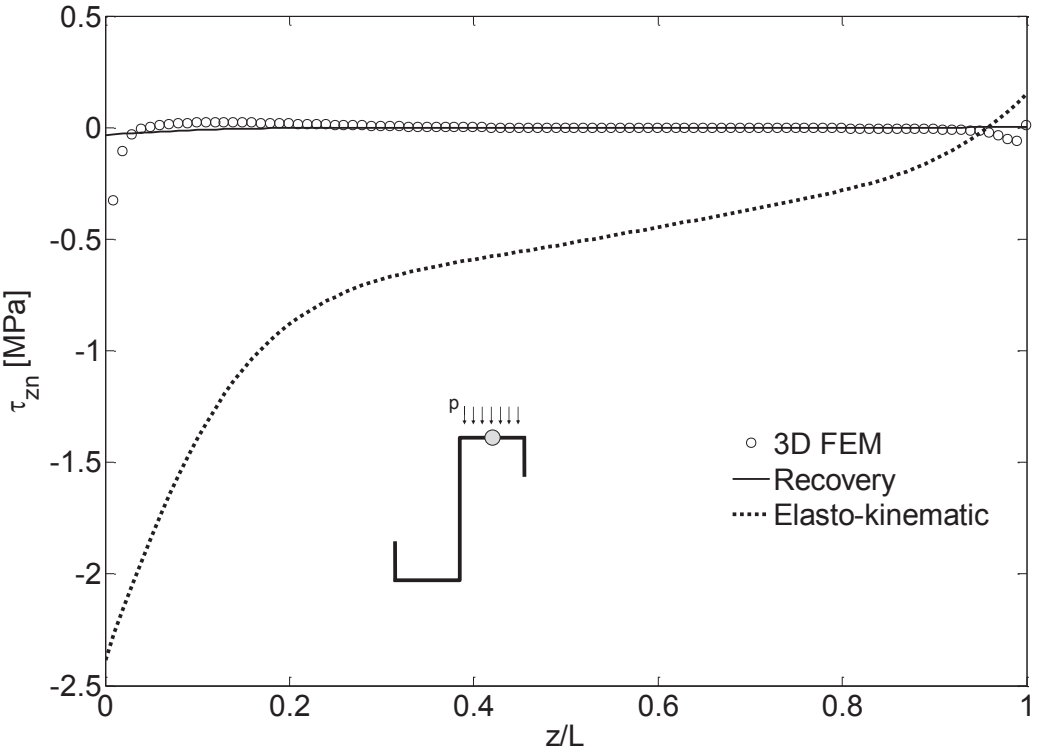

Figure 3.14: Shear stress τ_{sn} along the midpoint of wall 4.

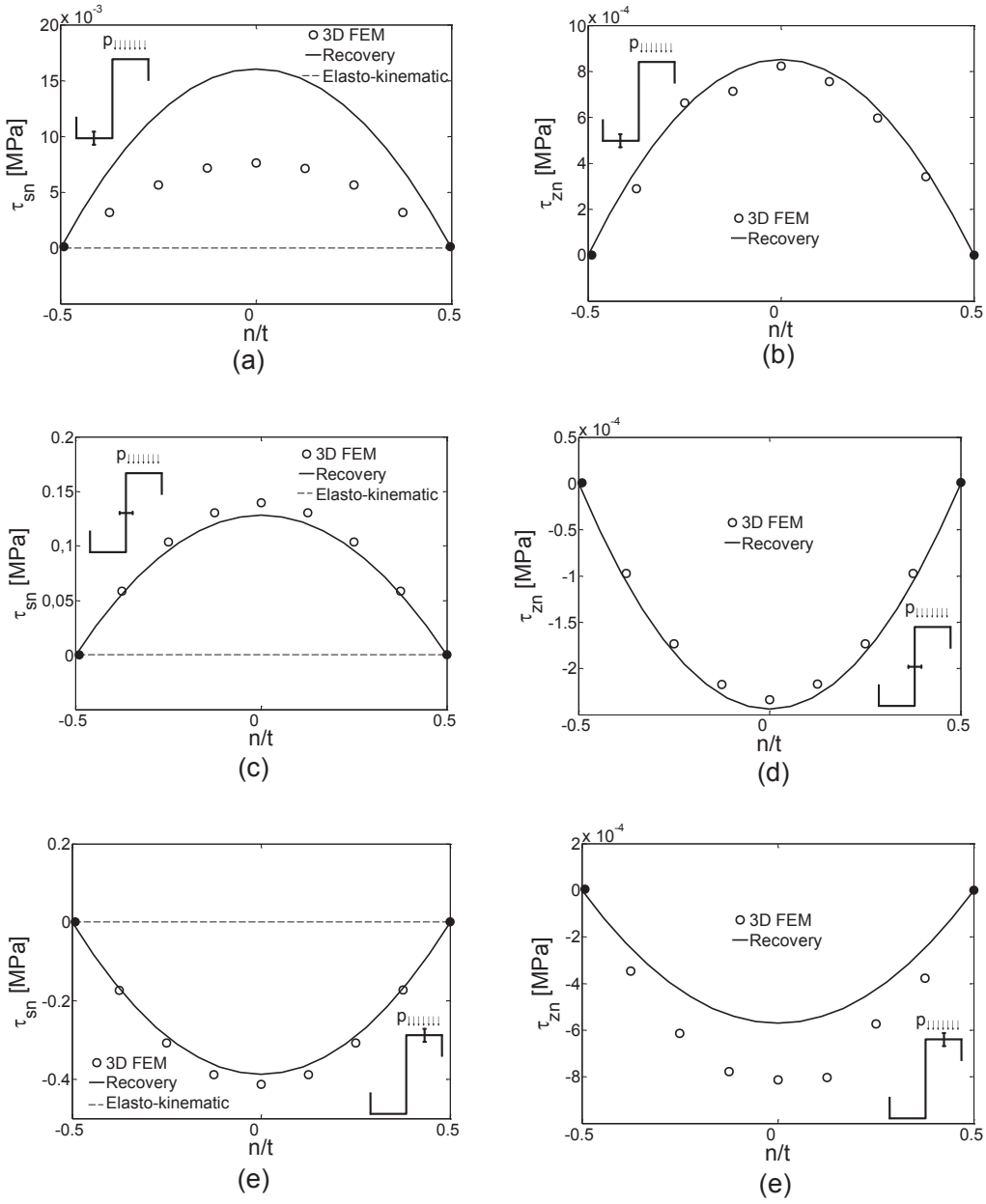

Figure 3.15: Shear stresses along the wall thickness for $z/L = 0.5$: (a) τ_{sn} at midpoint of the lower flange; (b) τ_{zn} at midpoint of the lower flange; (c) τ_{sn} at midpoint of the web; (d) τ_{zn} at midpoint of the web; (e) τ_{sn} at midpoint of the upper flange; (f) τ_{zn} at midpoint of the upper flange.

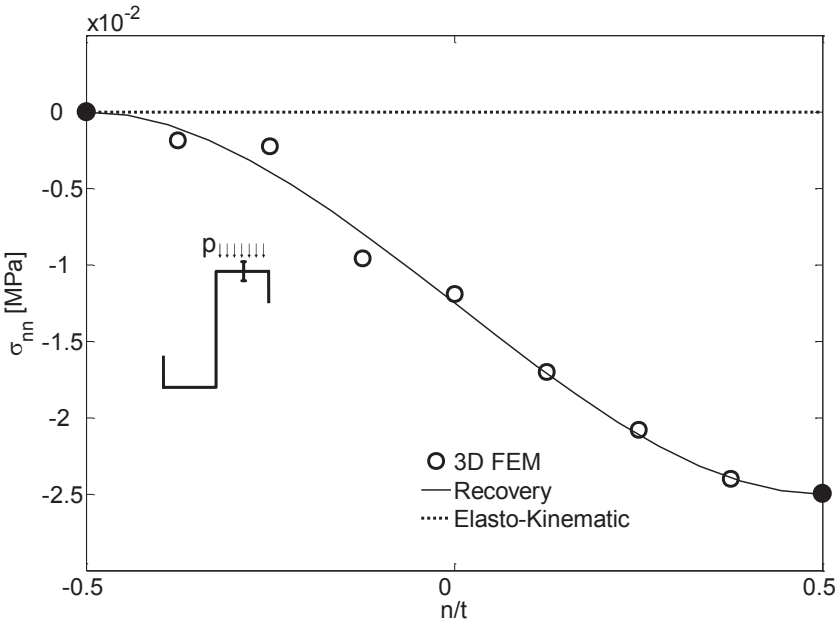

Figure 3.16: Normal stress σ_{nn} along the wall thickness at the midpoint of the upper flange for $z/L = 0.5$.

Chapter 4

Constitutive relations: from the isotropic to the composite beam

Abstract

In this chapter, some issues related to the treatment of the constitutive relation within the GBT are addressed. Firstly, the conventional adoption of separate membrane and bending constitutive laws is recalled. Later, a different approach commonly used in the literature for the orthotropic case is outlined. To bridge the gap between the two, a new approach is proposed based on a specific assumption on the stress field. For the case of laminated materials, an analogous approach is presented, based on a stress assumption over the generic orthotropic layer. Finally, further improvement to the constitutive law is introduced by means of shear corrections factors. Several numerical examples are presented to test the validity of the proposed approaches.

4.1 The constitutive relation in the conventional GBT

In the GBT literature, a recurring point is that of the constitutive relation of the beam model. Given that the GBT essentially considers the cross-section as an assembly of plates, the correct constitutive law to be used for the beam model may not be immediately clear. This issue becomes even more delicate if one is to depart from considering isotropic materials to model composite beams. In this section, an outline of the current approaches to the constitutive relation of the GBT is presented.

4.1.1 The isotropic beam

As was explained in Chapter 2, the internal constraints inherent to the GBT model render it overstiff, which is true for any compatibility-based beam model. The usual solution to this problem is an adjustment of the constitutive equations by introducing a separation of the strains in two different contributions: one "membrane" part, which is constant over the wall thickness and is relevant to the cross-section midline and one "bending" part proportional to the thickness coordinate n:

$$\varepsilon_{zz}(n,s,z) = \varepsilon_{zz}^{(M)}(s,z) + n\hat{\varepsilon}_{zz}^{(B)}(s,z), \tag{4.1}$$

$$\varepsilon_{ss}(n,s,z) = \varepsilon_{ss}^{(M)}(s,z) + n\hat{\varepsilon}_{ss}^{(B)}(s,z), \tag{4.2}$$

$$\gamma_{zs}(n,s,z) = \gamma_{zs}^{(M)}(s,z) + n\hat{\gamma}_{zs}^{(B)}(s,z), \tag{4.3}$$

$$\gamma_{zn}(s,z) = \gamma_{zn}^{(M)}(s,z). \tag{4.4}$$

with the expressions for each strain component introduced in Chapter 2 recalled below for the reader's convenience:

$$\varepsilon_{zz}^{(M)} = \boldsymbol{\varphi}(s)\left[\partial_z^2\mathbf{v}(z) + \partial_z\boldsymbol{\delta}(z)\right] + \boldsymbol{\varphi}^h(s)\boldsymbol{\delta}^h(z), \tag{4.5}$$

$$\hat{\varepsilon}_{zz}^{(B)} = -\boldsymbol{\psi}(s)\left[\partial_z^2\mathbf{v}(z) + \partial_z\boldsymbol{\delta}(z)\right], \tag{4.6}$$

$$\varepsilon_{ss}^{(M)} = \partial_s\boldsymbol{\mu}(s)\mathbf{v}(z), \tag{4.7}$$

$$\hat{\varepsilon}_{ss}^{(B)} = -\partial_s^2\boldsymbol{\psi}(s)\mathbf{v}(z), \tag{4.8}$$

$$\begin{aligned}\gamma_{zs}^{(M)} &= \left[\boldsymbol{\mu}(s) + \partial_s\boldsymbol{\varphi}(s)\right]\partial_z\mathbf{v}(z) + \partial_s\boldsymbol{\varphi}(s)\boldsymbol{\delta}(z) + \\ &\quad + \partial_s\boldsymbol{\varphi}^h(s)\boldsymbol{\delta}^h(z),\end{aligned} \tag{4.9}$$

$$\hat{\gamma}_{zs}^{(B)} = -2\partial_s\boldsymbol{\psi}(s)\partial_z\mathbf{v}(z) - \partial_s\boldsymbol{\psi}(s)\boldsymbol{\delta}(z), \tag{4.10}$$

$$\gamma_{zn}^{(M)} = -\boldsymbol{\psi}(s)\boldsymbol{\delta}(z). \tag{4.11}$$

This separation allows to write a constitutive relation of the form:

$$\boldsymbol{\sigma} = \mathbb{C}^{(M)}\boldsymbol{\varepsilon}^{(M)} + \mathbb{C}^{(B)}\boldsymbol{\varepsilon}^{(B)}, \tag{4.12}$$

where $\boldsymbol{\varepsilon}^{(M)\mathrm{T}}=[\varepsilon_{zz}^{(M)}\ \varepsilon_{ss}^{(M)}\ \gamma_{zs}^{(M)}\ \gamma_{zn}^{(M)}]$ and $\hat{\boldsymbol{\varepsilon}}^{(B)\mathrm{T}}=[\hat{\varepsilon}_{zz}^{(B)}\ \hat{\varepsilon}_{ss}^{(B)}\ \hat{\gamma}_{zs}^{(B)}\ 0]$. The constitutive matrices $\mathbb{C}^{(M)}$ and $\mathbb{C}^{(B)}$ can then be chosen specifically to resolve the overstiffness problem of the model. In particular, the following assumption is made:

$$\mathbb{C}^{(M)} = \begin{bmatrix} E & 0 & 0 & 0 \\ 0 & E & 0 & 0 \\ 0 & 0 & G & 0 \\ 0 & 0 & 0 & G \end{bmatrix}, \quad \mathbb{C}^{(B)} = \begin{bmatrix} \frac{E}{1-\nu^2} & \frac{\nu E}{1-\nu^2} & 0 & 0 \\ \frac{\nu E}{1-\nu^2} & \frac{E}{1-\nu^2} & 0 & 0 \\ 0 & 0 & G & 0 \\ 0 & 0 & 0 & G \end{bmatrix} \tag{4.13}$$

where E is the Young modulus, ν the Poisson coefficient, and G the shear modulus. Using this constitutive relation, the cross-section stiffness matrix $\mathbf{C}$ can be obtained by means of the following work-equivalence condition:

$$\int_s \int_n \left[\boldsymbol{\varepsilon}^{(M)} + \boldsymbol{\varepsilon}^{(B)}\right]^{\mathrm{T}} \Big[\mathbb{C}^{(M)}\boldsymbol{\varepsilon}^{(M)} + \mathbb{C}^{(B)}\boldsymbol{\varepsilon}^{(B)}\Big] \, \mathrm{d}n \, \mathrm{d}s = \mathbf{e}^{\mathrm{T}}\mathbf{C}\mathbf{e}, \tag{4.14}$$

where the individual terms of $\mathbf{C}$ can be written as:

$$\mathbf{C}_{jk} = \int_s t \; \mathbf{b}_j^{(M)\mathrm{T}} \mathbb{C}^{(M)} \mathbf{b}_k^{(M)} \, \mathrm{d}s + \int_s \frac{t^3}{12} \; \mathbf{b}_j^{(B)\mathrm{T}} \mathbb{C}^{(B)} \mathbf{b}_k^{(B)} \, \mathrm{d}s, \tag{4.15}$$

being $\mathbf{b}_j$ the modal matrix, recalled here for the sake of clarity:

$$\mathbf{b}_j = \begin{bmatrix} 0 & 0 & \boldsymbol{\varphi}_j - n\,\boldsymbol{\psi}_j & 0 & 0 & \boldsymbol{\varphi}_j^h \\ -n\,\partial_s^2\boldsymbol{\psi}_j & 0 & 0 & 0 & 0 & 0 \\ 0 & -2n\partial_s\boldsymbol{\psi}_j & 0 & \partial_s\boldsymbol{\varphi}_j - n\partial_s\boldsymbol{\psi}_j & \partial_s\boldsymbol{\varphi}_j^h & 0 \\ 0 & 0 & 0 & -\boldsymbol{\psi}_j & 0 & 0 \end{bmatrix}. \tag{4.16}$$

4.1.2 The composite beam

While it is easy to realize the GBT, in principle, has no limitations on the material to be considered, the usage of a non-isotropic material carries significant changes to the constitutive relation. In this section, the conventional GBT constitutive relation will be presented for a generic orthotropic material and later the extension will be made to the composite case.

Orthotropic material

Let us consider the generic cross-section as an assembly of orthotropic plates as the one shown in Fig. 4.1. Two reference systems are defined: the n, s, z reference will be referred to as the "local" one since it is related to the plate, that is the generic wall. A second x_1, x_2, x_3 system will instead be called the "material" reference system since it is the one in which the fibers of the material are oriented. The material reference system is rotated with respect to the local system by an angle θ, as shown in Fig. 4.1. It should be noted that the normal directions n and x_3 are coincident.

The generic orthotropic plate is considered to have a constitutive law of the form:

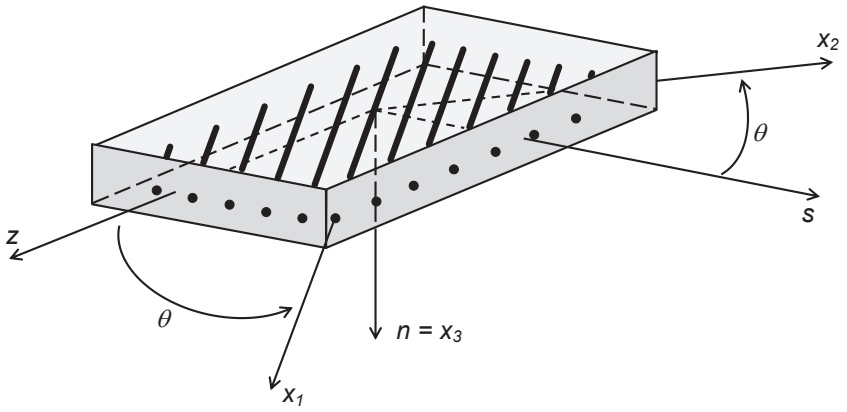

Figure 4.1: Orthotropic plate: material (x_1, x_2, x_3) and local (n, s, z) reference systems.

$$\begin{bmatrix} \sigma_{11} \\ \sigma_{22} \\ \sigma_{33} \\ \tau_{23} \\ \tau_{13} \\ \tau_{12} \end{bmatrix} = \begin{bmatrix} C_{11} & C_{12} & C_{13} & 0 & 0 & 0 \\ C_{12} & C_{22} & C_{23} & 0 & 0 & 0 \\ C_{13} & C_{23} & C_{33} & 0 & 0 & 0 \\ 0 & 0 & 0 & C_{44} & 0 & 0 \\ 0 & 0 & 0 & 0 & C_{55} & 0 \\ 0 & 0 & 0 & 0 & 0 & C_{66} \end{bmatrix} \begin{bmatrix} \varepsilon_{11} \\ \varepsilon_{22} \\ \varepsilon_{33} \\ \gamma_{23} \\ \gamma_{13} \\ \gamma_{12} \end{bmatrix}. \quad (4.17)$$

Since this constitutive law is written in the material reference system, which is arbitrarily rotated by an angle θ around the normal axis with respect to the local reference system, a tensor transformation is required to express all material properties in the local system. This tensor transformation is of the form:

$$\mathbb{C}_P = \mathbf{T}\,\mathbb{C}_M\mathbf{T}^T, \quad (4.18)$$

where $\mathbb{C}_M$ is the material constitutive matrix defined in Eq. (4.17),

$\mathbb{C}_P$ is the constitutive matrix in the local reference system, and $\mathbf{T}$ is a transformation matrix of the form:

$$\mathbf{T} = \begin{bmatrix} cos^2(\theta) & sin^2(\theta) & 0 & 0 & 0 & -2\,cos(\theta)\,sin(\theta) \\ sin^2(\theta) & cos^2(\theta) & 0 & 0 & 0 & 2\,cos(\theta)\,sin(\theta) \\ 0 & 0 & 1 & 0 & 0 & 0 \\ 0 & 0 & 0 & cos(\theta) & sin(\theta) & 0 \\ 0 & 0 & 0 & -sin(\theta) & cos(\theta) & 0 \\ cos(\theta)\,sin(\theta) & -cos(\theta)\,sin(\theta) & 0 & 0 & 0 & cos^2(\theta) - sin^2(\theta) \end{bmatrix}. \quad (4.19)$$

Applying the tensor transformation, we can write the constitutive law in the local reference system:

$$\boldsymbol{\sigma} = \mathbb{C}_P \boldsymbol{\varepsilon}, \quad (4.20)$$

or, more explicitly:

$$\begin{bmatrix} \sigma_{zz} \\ \sigma_{ss} \\ \sigma_{nn} \\ \tau_{sn} \\ \tau_{zn} \\ \tau_{zs} \end{bmatrix} = \begin{bmatrix} \bar{C}_{11} & \bar{C}_{12} & \bar{C}_{13} & 0 & 0 & \bar{C}_{16} \\ \bar{C}_{12} & \bar{C}_{22} & \bar{C}_{23} & 0 & 0 & \bar{C}_{26} \\ \bar{C}_{13} & \bar{C}_{23} & \bar{C}_{33} & 0 & 0 & \bar{C}_{36} \\ 0 & 0 & 0 & \bar{C}_{44} & \bar{C}_{45} & 0 \\ 0 & 0 & 0 & \bar{C}_{45} & \bar{C}_{55} & 0 \\ \bar{C}_{16} & \bar{C}_{26} & \bar{C}_{36} & 0 & 0 & \bar{C}_{66} \end{bmatrix} \begin{bmatrix} \varepsilon_{zz} \\ \varepsilon_{ss} \\ \varepsilon_{nn} \\ \gamma_{sn} \\ \gamma_{zn} \\ \gamma_{zs} \end{bmatrix}. \quad (4.21)$$

Given that in the GBT formulation presented in this work the strains ε_{nn} and γ_{sn} are null, we can reduce the $\mathbb{C}_P$ matrix by eliminating the rows and columns corresponding to null strain and stress components. This results in a reduced constitutive law:

$$\boldsymbol{\sigma} = \tilde{\mathbb{C}}_P \boldsymbol{\varepsilon}, \quad (4.22)$$

where vectors $\boldsymbol{\sigma}$ and $\boldsymbol{\varepsilon}$ are now of dimension [4x1] since two components have been dismissed. The reduced constitutive law has the form:

$$\begin{bmatrix} \sigma_{zz} \\ \sigma_{ss} \\ \tau_{zs} \\ \tau_{zn} \end{bmatrix} = \begin{bmatrix} \tilde{C}_{11} & \tilde{C}_{12} & \tilde{C}_{13} & 0 \\ \tilde{C}_{12} & \tilde{C}_{22} & \tilde{C}_{23} & 0 \\ \tilde{C}_{13} & \tilde{C}_{23} & \tilde{C}_{33} & 0 \\ 0 & 0 & 0 & \tilde{C}_{44} \end{bmatrix} \begin{bmatrix} \varepsilon_{zz} \\ \varepsilon_{ss} \\ \gamma_{zs} \\ \gamma_{zn} \end{bmatrix}. \tag{4.23}$$

In this reduced constitutive law, the positions of the shear stress components have been reorganized for the reader's convenience, thus the substitutions $\tilde{C}_{13} = \bar{C}_{16}$, $\tilde{C}_{23} = \bar{C}_{26}$, $\tilde{C}_{33} = \bar{C}_{66}$, and $\tilde{C}_{44} = \bar{C}_{55}$ have been made.

Once the constitutive law for the generic wall has been defined, the cross-section stiffness matrix for the GBT can be written by means of the work-equivalence condition:

$$\int_s \int_n \boldsymbol{\varepsilon}^{\mathrm{T}} \tilde{\mathbb{C}}_P \boldsymbol{\varepsilon} \, \mathrm{d}n \, \mathrm{d}s = \mathbf{e}^{\mathrm{T}} \mathbf{C} \mathbf{e}. \tag{4.24}$$

It is important to note here that matrix $\tilde{\mathbb{C}}_P$ has been obtained from a generic orthotropic constitutive law, without any sort of separation, in contrast to the membrane-bending approach used in the isotropic case. Given the new couplings present in $\tilde{\mathbb{C}}_P$, the resulting $\mathbf{C}$ matrix will be generally full, so a change in notation is convenient to simplify the writing. The new $\mathbf{C}$ matrix will have the form:

$$\mathbf{C} = \left[\begin{array}{ccc|ccc} \mathbf{C}_{11} & \mathbf{C}_{12} & \mathbf{C}_{13} & \mathbf{C}_{14} & \mathbf{C}_{15} & \mathbf{C}_{16} \\ \mathbf{C}_{12}^T & \mathbf{C}_{22} & \mathbf{C}_{23} & \mathbf{C}_{24} & \mathbf{C}_{25} & \mathbf{C}_{26} \\ \mathbf{C}_{13}^T & \mathbf{C}_{23}^T & \mathbf{C}_{33} & \mathbf{C}_{34} & \mathbf{C}_{35} & \mathbf{C}_{36} \\ \hline \mathbf{C}_{14}^T & \mathbf{C}_{24}^T & \mathbf{C}_{34}^T & \mathbf{C}_{44} & \mathbf{C}_{45} & \mathbf{C}_{46} \\ \mathbf{C}_{15}^T & \mathbf{C}_{25}^T & \mathbf{C}_{35}^T & \mathbf{C}_{45}^T & \mathbf{C}_{55} & \mathbf{C}_{56} \\ \mathbf{C}_{16}^T & \mathbf{C}_{26}^T & \mathbf{C}_{36}^T & \mathbf{C}_{46}^T & \mathbf{C}_{56}^T & \mathbf{C}_{66} \end{array}\right] \tag{4.25}$$

with:

$$\mathbf{C}_{jk} = \int_s \int_n \mathbf{b}_j^T \tilde{\mathbb{C}}_P \, \mathbf{b}_k \; \mathrm{d}n \, \mathrm{d}s. \tag{4.26}$$

At first sight, it would seem that the matrix above should be equal to the $\mathbf{C}$ matrix of an isotropic beam defined in (4.14) if the proper material constants were used. However, since the cross-section stiffness matrix for the isotropic case was written from two different constitutive laws ($\mathbb{C}^{(M)}$ for the membrane part and $\mathbb{C}^{(B)}$ for the bending part) instead of just one, this is not true. In any case, as discussed in Chapter 2, the $\mathbf{C}$ matrix can be divided into four sub-matrices: the upper-left block corresponds to flexural modes and is analogous to the cross-section stiffness matrix of the original GBT, the lower-right block pertains the shear modes as introduced in Chapter 2, and the other two blocks couple the flexural and shear parts. The specific expressions for each of the $\mathbf{C}_{jk}$ sub-matrices are given below:

$$\mathbf{C}_{11} \;=\; \int_s D_{22} \partial_s^2 \boldsymbol{\psi}_j \, \partial_s^2 \boldsymbol{\psi}_k \, \mathrm{d}s, \tag{4.27}$$

$$\mathbf{C}_{12} = 2\int_s D_{23}\partial_s^2\boldsymbol{\psi}_j\,\partial_s\boldsymbol{\psi}_k\,\mathrm{d}s, \tag{4.28}$$

$$\mathbf{C}_{13} = -\int_s B_{12}\boldsymbol{\varphi}_k\,\partial_s^2\boldsymbol{\psi}_j\,\mathrm{d}s + \int_s D_{12}\partial_s^2\boldsymbol{\psi}_j\,\boldsymbol{\psi}_k\,\mathrm{d}s, \tag{4.29}$$

$$\mathbf{C}_{14} = -\int_s B_{23}\partial_s^2\boldsymbol{\psi}_j\,\partial_s\boldsymbol{\varphi}_k\,\mathrm{d}s + \int_s D_{23}\partial_s^2\boldsymbol{\psi}_j\,\partial_s\boldsymbol{\psi}_k\,\mathrm{d}s, \tag{4.30}$$

$$\mathbf{C}_{15} = -\int_s B_{23}\partial_s\boldsymbol{\varphi}_k^h\,\partial_s^2\boldsymbol{\psi}_j\,\mathrm{d}s, \tag{4.31}$$

$$\mathbf{C}_{16} = -\int_s B_{12}\boldsymbol{\varphi}_k^h\,\partial_s^2\boldsymbol{\psi}_j\,\mathrm{d}s, \tag{4.32}$$

$$\mathbf{C}_{22} = 4\int_s D_{33}\partial_s\boldsymbol{\psi}_j\,\partial_s\boldsymbol{\psi}_k\,\mathrm{d}s, \tag{4.33}$$

$$\mathbf{C}_{23} = -2\int_s B_{13}\boldsymbol{\varphi}_k\,\partial_s\boldsymbol{\psi}_j\,\mathrm{d}s + 2\int_s D_{13}\partial_s\boldsymbol{\psi}_j\,\boldsymbol{\psi}_k\,\mathrm{d}s, \tag{4.34}$$

$$\mathbf{C}_{24} = -2\int_s B_{33}\partial_s\boldsymbol{\varphi}_k\,\partial_s\boldsymbol{\psi}_j\,\mathrm{d}s + 2\int_s D_{33}\partial_s\boldsymbol{\psi}_j\,\partial_s\boldsymbol{\psi}_k\,\mathrm{d}s, \tag{4.35}$$

$$\mathbf{C}_{25} = -2\int_s B_{33}\partial_s\boldsymbol{\varphi}_k^h\,\partial_s\boldsymbol{\psi}_j\,\mathrm{d}s, \tag{4.36}$$

$$\mathbf{C}_{26} = -2\int_s B_{13}\boldsymbol{\varphi}_k^h\,\partial_s\boldsymbol{\psi}_j\,\mathrm{d}s, \tag{4.37}$$

$$\begin{aligned}\mathbf{C}_{33} = {} & \int_s A_{11}\boldsymbol{\varphi}_j\boldsymbol{\varphi}_k\,\mathrm{d}s - \int_s B_{11}\left(\boldsymbol{\varphi}_j\,\boldsymbol{\psi}_k + \boldsymbol{\varphi}_k\,\boldsymbol{\psi}_j\right)\,\mathrm{d}s + \\ & + \int_s D_{11}\boldsymbol{\psi}_j\,\boldsymbol{\psi}_k\,\mathrm{d}s,\end{aligned} \tag{4.38}$$

$$\begin{aligned}\mathbf{C}_{34} = {} & \int_s A_{13}\boldsymbol{\varphi}_j\partial_s\boldsymbol{\varphi}_k\,\mathrm{d}s - \int_s B_{13}\left(\boldsymbol{\varphi}_j\,\partial_s\boldsymbol{\psi}_k + \boldsymbol{\partial_s\varphi}_k\,\boldsymbol{\psi}_j\right)\,\mathrm{d}s + \\ & + \int_s D_{13}\boldsymbol{\psi}_j\,\partial_s\boldsymbol{\psi}_k\,\mathrm{d}s,\end{aligned} \tag{4.39}$$

$$\mathbf{C}_{35} = \int_s A_{13}\boldsymbol{\varphi}_j\partial_s\boldsymbol{\varphi}_k^h\,\mathrm{d}s - \int_s B_{13}\partial_s\boldsymbol{\varphi}_k^h\,\boldsymbol{\psi}_j\,\mathrm{d}s, \tag{4.40}$$

$$\mathbf{C}_{36} = \int_s A_{11}\boldsymbol{\varphi}_j\boldsymbol{\varphi}_k^h\,\mathrm{d}s - \int_s B_{11}\boldsymbol{\varphi}_k^h\,\boldsymbol{\psi}_j\,\mathrm{d}s, \tag{4.41}$$

$$\begin{aligned}\mathbf{C}_{44} = {} & \int_s A_{44}\boldsymbol{\psi}_j\boldsymbol{\psi}_k\,\mathrm{d}s + \int_s A_{33}\partial_s\boldsymbol{\varphi}_j\partial_s\boldsymbol{\varphi}_k\,\mathrm{d}s + \\ & - \int_s B_{33}\left(\partial_s\boldsymbol{\varphi}_j\,\partial_s\boldsymbol{\psi}_k + \partial_s\boldsymbol{\varphi}_k\,\partial_s\boldsymbol{\psi}_j\right)\,\mathrm{d}s +\end{aligned}$$

$$+ \int_s D_{33} \partial_s \boldsymbol{\psi}_j \, \partial_s \boldsymbol{\psi}_k \, \mathrm{d}s, \tag{4.42}$$

$$\mathbf{C}_{45} = \int_s A_{33} \partial_s \boldsymbol{\varphi}_j \partial_s \boldsymbol{\varphi}_k^h \, \mathrm{d}s - \int_s B_{33} \partial_s \boldsymbol{\varphi}_k^h \, \partial_s \boldsymbol{\psi}_j \, \mathrm{d}s, \tag{4.43}$$

$$\mathbf{C}_{46} = \int_s A_{13} \partial_s \boldsymbol{\varphi}_j \boldsymbol{\varphi}_k^h \, \mathrm{d}s - \int_s B_{13} \boldsymbol{\varphi}_k^h \, \partial_s \boldsymbol{\psi}_j \, \mathrm{d}s, \tag{4.44}$$

$$\mathbf{C}_{55} = \int_s A_{33} \partial_s \boldsymbol{\varphi}_j^h \partial_s \boldsymbol{\varphi}_k^h \, \mathrm{d}s, \tag{4.45}$$

$$\mathbf{C}_{56} = \int_s A_{13} \partial_s \boldsymbol{\varphi}_j^h \boldsymbol{\varphi}_k^h \, \mathrm{d}s, \tag{4.46}$$

$$\mathbf{C}_{66} = \int_s A_{11} \boldsymbol{\varphi}_j^h \boldsymbol{\varphi}_k^h \, \mathrm{d}s. \tag{4.47}$$

In the expressions above, the following substitutions have been made:

$$A_{jk} = \int_{-t/2}^{t/2} \tilde{\mathbb{C}}_{P\,jk} \, \mathrm{d}n, \tag{4.48}$$

$$B_{jk} = \int_{-t/2}^{t/2} n \, \tilde{\mathbb{C}}_{P\,jk} \, \mathrm{d}n, \tag{4.49}$$

$$D_{jk} = \int_{-t/2}^{t/2} n^2 \, \tilde{\mathbb{C}}_{P\,jk} \, \mathrm{d}n, \tag{4.50}$$

where A_{jk}, B_{jk}, and D_{jk} are, respectively, membrane, membrane-bending, and bending plate stiffness terms. It should be noted that, since the generic plate is homogeneous, B_{jk} is generally zero and there is no coupling between membrane and bending stiffness. At this point, the internal constraints of the model should be addressed. In the GBT, the membrane transverse extension $\varepsilon_{ss}^{(M)}$ is null for the mode families present in this work. This constraint, along with the Poisson effect, results in transverse extension locking and is a cause of the overstiffness of the model. For this reason,

it is crucial to correct the membrane stiffness values A_{jk}. This can be done in two ways:

Approach A Is the most commonly used in the GBT literature. It consists of modifying $\tilde{\mathbb{C}}_P$ by neglecting the coupling between $\varepsilon_{zz}^{(M)}$ and $\varepsilon_{zz}^{(M)}$ when calculating the membrane stiffness components A_{jk}, while using the complete $\tilde{\mathbb{C}}_P$ to calculate B_{jk} and D_{jk}. This is the essence of the membrane-bending separation that is used in the isotropic case. This approach, however, has been found (see [48] and [51]) to lead to non-satisfactory results in the case of orthotropic beams.

Approach B Was first employed in the GBT in [51] and has been also applied to Vlasov-like beam models (see [61]-[63]) and assumes that the membrane transversal extensions $\varepsilon_{ss}^{(M)}$ are free, which corresponds to adopting plate constitutive relations associated with a null normal stress resultant in the transverse direction. This leads to corrected plate stiffness components, as will be shown in the following.

To follow Approach B, we can write the constitutive relation of the plate forming the generic wall in the form (see [64]):

$$\left[\begin{array}{c} \mathbf{n} \\ \hline \mathbf{m} \end{array}\right] = \left[\begin{array}{c|c} \mathbf{A} & \mathbf{0} \\ \hline \mathbf{0} & \mathbf{D} \end{array}\right] \left[\begin{array}{c} \boldsymbol{\lambda} \\ \hline \boldsymbol{\chi} \end{array}\right] \tag{4.51}$$

where $\mathbf{n}$ and $\mathbf{m}$ are the plate stress resultants:

$$\mathbf{n} = \begin{bmatrix} n_{zz} \\ n_{ss} \\ n_{zs} \\ n_{zn} \end{bmatrix} = \int_n \begin{bmatrix} \sigma_{zz} \\ \sigma_{ss} \\ \tau_{zs} \\ \tau_{zn} \end{bmatrix} \mathrm{d}n, \tag{4.52}$$

$$\mathbf{m} = \begin{bmatrix} m_{zz} \\ m_{ss} \\ m_{zs} \end{bmatrix} = \int_n n \begin{bmatrix} \sigma_{zz} \\ \sigma_{ss} \\ \tau_{zs} \end{bmatrix} \mathrm{d}n, \tag{4.53}$$

the terms $\boldsymbol{\lambda}$ and $\boldsymbol{\chi}$ refer to membrane strains and curvatures respectively:

$$\boldsymbol{\lambda} = \begin{bmatrix} \lambda_{zz} \\ \lambda_{ss} \\ \lambda_{zs} \\ \lambda_{zn} \end{bmatrix} = \begin{bmatrix} \varepsilon_{zz}^{(M)} \\ \varepsilon_{ss}^{(M)} \\ \gamma_{zs}^{(M)} \\ \gamma_{zn}^{(M)} \end{bmatrix} \tag{4.54}$$

$$\boldsymbol{\chi} = \begin{bmatrix} \chi_{zz} \\ \chi_{ss} \\ \chi_{zs} \end{bmatrix} = \begin{bmatrix} \hat{\varepsilon}_{zz}^{(B)} \\ \hat{\varepsilon}_{ss}^{(B)} \\ \hat{\gamma}_{zs}^{(B)} \end{bmatrix} \tag{4.55}$$

and,

$$\mathbf{A} = [A_{jk}], \tag{4.56}$$

$$\mathbf{D} = [D_{jk}]. \tag{4.57}$$

It should be noted that, given that γ_{zn} only has a membrane contribution (see Eqs. (4.5)-(4.11)), matrices $\mathbf{A}$ and $\mathbf{D}$ have different dimensions. Specifically, $\mathbf{A}$ is a [4x4] matrix while $\mathbf{D}$ is [3x3].

The correction proposed in Approach B to the plate stiffness components consists on condensing the second row in Eq. (4.51), thus imposing a null normal stress resultant n_{ss} in the transverse direction, which completely defines the constitutive relation of the beam model.

The laminated beam

Composite laminates are formed by stacking layers of different composite materials or different fiber orientation. In this sense, the constitutive relations developed in the previous section can be extended to the laminated case by considering each layer as an orthotropic plate. One way to do this is by considering a heterogeneous laminated plate (that is, the generic laminated wall) as a statically equivalent single layer having a complex constitutive behavior. This approach, which basically reduces a problem that is in principle three-dimensional to a two-dimensional domain, is referred to in the literature as the Equivalent Single Layer theory.

To extend the relations presented in the previous section to the laminated case, we can consider a generic laminated plate (see Fig 4.2) of total thickness t composed of N orthotropic layers. Each layer will have its principal material coordinates $x_1^{(i)}, x_2^{(i)}, x_3^{(i)}$ oriented at an angle $\theta^{(i)}$ with respect to the laminate coordinate z in a manner analogous to that presented in Fig. 4.1. For the i-th layer we have $n \in \left[n^{(i)} - t^{(i)}/2, n^{(i)} + t^{(i)}/2\right]$, being $n^{(i)}$ the n-coordinate of the midplane of the layer and $t^{(i)}$ its thickness, as shown in Fig

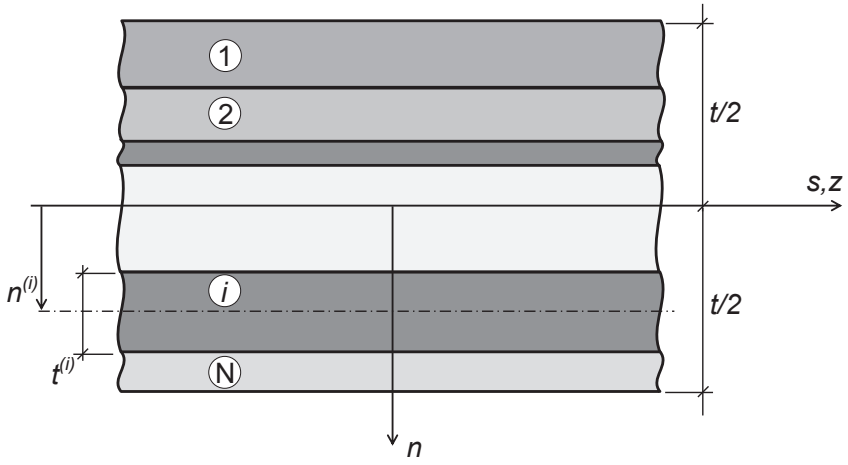

Figure 4.2: Reference system and layer numbering used for a laminated plate.

4.2.

The constitutive relation for the i-th orthotropic layer in the laminate coordinates, that is the local reference system n, s, z, is of the form:

$$\boldsymbol{\sigma}^{(i)} = \tilde{\mathbb{C}}_P^{(i)} \boldsymbol{\varepsilon}, \tag{4.58}$$

where $\boldsymbol{\sigma}^{(i)}$ is the vector of stresses over the generic layer. Although the strains are continuous through the thickness of the laminate plate ($\boldsymbol{\varepsilon}$ is unique for all layers), stresses are not, since each layer has its own material properties given by $\tilde{\mathbb{C}}_P^{(i)}$. Hence, to determine the plate constitutive relations, layer-wise integration is required. The plate stress resultants can then be written as:

$$\mathbf{n} = \begin{bmatrix} n_{zz} \\ n_{ss} \\ n_{zs} \\ n_{zn} \end{bmatrix} = \sum_{i=1}^{N} \int_{n^{(i)}-t^{(i)}/2}^{n^{(i)}+t^{(i)}/2} \begin{bmatrix} \sigma_{zz}^{(i)} \\ \sigma_{ss}^{(i)} \\ \tau_{zs}^{(i)} \\ \tau_{zn}^{(i)} \end{bmatrix} \mathrm{d}n, \tag{4.59}$$

$$\mathbf{m} = \begin{bmatrix} m_{zz} \\ m_{ss} \\ m_{zs} \end{bmatrix} = \sum_{i=1}^{N} \int_{n^{(i)}-t^{(i)}/2}^{n^{(i)}+t^{(i)}/2} n \begin{bmatrix} \sigma_{zz}^{(i)} \\ \sigma_{ss}^{(i)} \\ \tau_{zs}^{(i)} \end{bmatrix} \mathrm{d}n, \tag{4.60}$$

and the membrane, membrane-bending, and bending plate stiffness terms take the form (in the hypothesis of homogeneous layers):

$$A_{jk} = \sum_{i=1}^{N} t^{(i)} \, \tilde{\mathbb{C}}_{P\,jk}^{(i)}, \tag{4.61}$$

$$B_{jk} = \sum_{i=1}^{N} n^{(i)} t^{(i)} \, \tilde{\mathbb{C}}_{P\,jk}^{(i)}, \tag{4.62}$$

$$D_{jk} = \sum_{i=1}^{N} \left({n^{(i)}}^2 t^{(i)} + \frac{{t^{(i)}}^3}{12} \right) \tilde{\mathbb{C}}_{P\,jk}^{(i)}, \tag{4.63}$$

thus completely defining the constitutive relation for the laminate case. Notice that, in this case, B_{jk} are generally non-null, unless a symmetric stacking sequence is considered.

4.2 An alternative approach to obtain the constitutive law of the beam model

While the GBT formulation presented the previous section has been consistently used in the recent literature for composite beams (see for example [30], [49], and [50]) the justification for the particular corrections to the plate constitutive relation is somewhat lacking in terms of rigorousness. The condensation of n_{ss} addresses one of the kinematic constraints of the GBT, but ignores others. Also,

seemingly unrelated treatments are given to the isotropic and orthotropic cases for a problem that, in principle, should be the same, that is the overstiffness of the beam model due to kinematic constraints. To resolve these inconsistencies, a more comprehensive approach is presented here. The proposed approach is based on the rational derivation of the constitutive relationship from a stress assumption which reflects the internal constraints inherent to the GBT in the general case. In other words, firstly a stress representation that mirrors the GBT kinematics is assumed and then the constitutive relations are derived from the complementary strain energy. With this in mind, let us briefly recall the main assumptions behind each of the mode families introduced in Chapter 2:

Fundamental modes These modes are based on a piece-wise linear warping function $\boldsymbol{\varphi}$ in the generic wall. The Vlasov assumption of null γ_{zs} translates into a constant value of $\boldsymbol{\mu}$ over the s coordinate. The function of in-plane transverse displacements $\boldsymbol{\psi}$ is cubic over each wall.

Local modes These modes do not contribute to out-of-plane displacements, which means $\boldsymbol{\varphi}$ is null. As in the previous family of modes, shear strain γ_{zs} is null and so is $\boldsymbol{\mu}$ everywhere in the section. Function $\boldsymbol{\psi}$ is cubic over each wall.

Shear modes These may be either basic or additional shear modes. In both cases, in-plane displacements are null (thus $\boldsymbol{\mu}$ and $\boldsymbol{\psi}$ are null) and cross-section warping functions $\boldsymbol{\varphi}$ and $\boldsymbol{\varphi}^h$ are

piece-wise linear.

The particular mode functions described above engender a series of kinematic constraints: the fact that $\boldsymbol{\mu}$ is always constant over s means that $\varepsilon_{ss}^{(M)}$ (see Eq. (4.7)) will always be null, while $\gamma_{zs}^{(M)}$ (see Eq. (4.9)) will at most be constant over s. In addition to this, $\hat{\gamma}_{zn}^{(B)}$, ε_{nn} and γ_{sn} are always null stemming from the displacement field of the GBT formulation. From these considerations, we can define three distinct types of kinematic constraint present in the GBT:

Type 1 The first type of constraint is that in which a certain strain component is completely null. This is the case for $\varepsilon_{nn} = 0$ and $\gamma_{sn} = 0$.

Type 2 The second kind of constraint is based on only one part of a strain component being null, either the membrane strain or the curvature. For this type we have the conditions $\varepsilon_{ss}^{(M)} = 0$ and $\hat{\gamma}_{zn}^{(B)} = 0$.

Type 3 In this case no part of the strain component is null, but the approximation over the generic wall is poor. This is the case for $\gamma_{zs}^{(M)}$, which can only be constant over s when using fundamental modes.

To illustrate this, let us restate the strain field using the definitions for the membrane strains and curvatures found in Eqs. (4.54) and (4.55):

$$\varepsilon_{zz} = \lambda_{zz} + n\,\chi_{zz}, \tag{4.64}$$

$$\varepsilon_{ss} = n\,\chi_{ss}, \tag{4.65}$$

$$\varepsilon_{nn} = 0, \tag{4.66}$$

$$\gamma_{sn} = 0, \tag{4.67}$$

$$\gamma_{zn} = \lambda_{zn}, \tag{4.68}$$

$$\gamma_{zs} = \lambda_{zs} + n\,\chi_{zs}. \tag{4.69}$$

Based on the equations above, a way to address the kinematic constraints in Eqs. (4.64)-(4.69) is to mirror those constraints over the stress field, thus resolving the Type 1 and Type 2 cases. This approach would result in the assumption of a stress field of the form:

$$\sigma_{zz} = \frac{n_{zz}}{t} + n\frac{m_{zz}}{j}, \tag{4.70}$$

$$\sigma_{ss} = n\frac{m_{ss}}{j}, \tag{4.71}$$

$$\sigma_{nn} = 0, \tag{4.72}$$

$$\tau_{sn} = 0, \tag{4.73}$$

$$\tau_{zn} = \frac{n_{zn}}{t}, \tag{4.74}$$

$$\tau_{zs} = \frac{n_{zs}}{t} + n\frac{m_{zs}}{j}, \tag{4.75}$$

where the terms n_{jk} and m_{jk} are the plate stress resultants defined in Eqs. (4.52) and (4.53) and $j = t^3/12$. From this initial assumption, the complementary strain energy density Ψ per unit area can be written as:

$$\Psi = \frac{1}{2} \int_n \boldsymbol{\sigma}^T \mathbb{H}_P \boldsymbol{\sigma} \, \mathrm{d}n, \tag{4.76}$$

where

$$\mathbb{H}_P = \tilde{\mathbb{C}}_P^{-1}, \tag{4.77}$$

is the compliance matrix in the local reference system. This expression can then be differentiated with respect to the plate stress resultants to obtain their corresponding membrane strain and curvature terms:

$$\lambda_{jk} = \frac{\mathrm{d}\Psi}{\mathrm{d}n_{jk}}, \tag{4.78}$$

$$\chi_{jk} = \frac{\mathrm{d}\Psi}{\mathrm{d}m_{jk}}, \tag{4.79}$$

where the indexes j and k refer to the n, s, z directions. These definitions allow the writing of the membrane strains and curvatures as functions of the stress resultants, thus defining a constitutive law of the form:

$$\left[\begin{array}{c} \boldsymbol{\lambda} \\ \hline \boldsymbol{\chi} \end{array}\right] = \left[\begin{array}{c|c} \mathbf{H}_M & \mathbf{0} \\ \hline \mathbf{0} & \mathbf{H}_B \end{array}\right] \left[\begin{array}{c} \mathbf{n} \\ \hline \mathbf{m} \end{array}\right] \tag{4.80}$$

where the indexes M and B refer to the membrane and bending parts of the problem respectively. The terms in matrices $\mathbf{H}_M$ and $\mathbf{H}_B$ are given by Eqs. (4.78) and (4.79). For the reader's convenience, the same symbols $\boldsymbol{\lambda}$ and $\mathbf{n}$ have been kept to denote the vectors of membrane strains and normal stress resultants, but it

should be noted that in this case these are [3x1] vectors instead of [4x1] as they were in the previous section. This difference stems from the fact that in this approach the n_{ss} stress component is missing from the very beginning. It should also be noted that there is no coupling between the membrane and bending parts. Given that the only assumption made is the mirrored application of the kinematic constraints onto the stress field, this approach is equivalent to the conventional GBT treatments for both the isotropic and orthotropic cases. Indeed, it can be shown that evaluating the compliance matrices defined in (4.80) for the isotropic case leads to the membrane-bending separation, whereas doing it for an orthotropic material results in a constitutive matrix condensed in the way shown in Section 4.1.2.

4.2.1 The laminated case

In the case of a laminated beam, a different stress field is needed, since the kinematic constraints of the GBT model are defined for the complete laminate and not for the single generic layer. Specifically, for the generic i-th layer, the following stress assumption is used:

$$\sigma_{zz}^{(i)} = S_{zz}^{(i)} + nM_{zz}^{(i)}, \tag{4.81}$$

$$\sigma_{ss}^{(i)} = S_{ss}^{(i)} + nM_{ss}^{(i)}, \tag{4.82}$$

$$\sigma_{nn}^{(i)} = 0, \tag{4.83}$$

$$\tau_{sn}^{(i)} = 0, \tag{4.84}$$

$$\tau_{zn}^{(i)} = \frac{n_{zn}^{(i)}}{t^{(i)}}, \tag{4.85}$$

$$\tau_{zs}^{(i)} = S_{zs}^{(i)} + nM_{zs}^{(i)}. \tag{4.86}$$

where $S_{jk}^{(i)}$ and $M_{jk}^{(i)}$ stand respectively for the membrane and bending parts of their corresponding stress component. These expressions are defined as:

$$S_{jk}^{(i)} = -\frac{12n^{(i)}\left(m_{jk}^{(i)} - n^{(i)}n_{jk}^{(i)}\right) - {t^{(i)}}^2 n_{jk}^{(i)}}{{t^{(i)}}^3} \tag{4.87}$$

$$M_{jk}^{(i)} = \frac{12\left(m_{jk}^{(i)} - n^{(i)}n_{jk}^{(i)}\right)}{{t^{(i)}}^3} \tag{4.88}$$

While the above stress assumption may seem overly complicated, it is in fact written in a manner analogous to Eqs. (4.70)-(4.75). By using this stress assumption, it can be easily realized that the following conditions hold:

$$\mathbf{n}^{(i)} = \begin{bmatrix} n_{zz}^{(i)} \\ n_{ss}^{(i)} \\ n_{zs}^{(i)} \\ n_{zn}^{(i)} \end{bmatrix} = \int_{n^{(i)}-t^{(i)}/2}^{n^{(i)}+t^{(i)}/2} \begin{bmatrix} \sigma_{zz}^{(i)} \\ \sigma_{ss}^{(i)} \\ \tau_{zs}^{(i)} \\ \tau_{zn}^{(i)} \end{bmatrix} \mathrm{d}n, \tag{4.89}$$

$$\mathbf{m}^{(i)} = \begin{bmatrix} m_{zz}^{(i)} \\ m_{ss}^{(i)} \\ m_{zs}^{(i)} \end{bmatrix} = \int_{n^{(i)}-t^{(i)}/2}^{n^{(i)}+t^{(i)}/2} n \begin{bmatrix} \sigma_{zz}^{(i)} \\ \sigma_{ss}^{(i)} \\ \tau_{zs}^{(i)} \end{bmatrix} \mathrm{d}n, \tag{4.90}$$

that is, $n_{jk}^{(i)}$ is the stress resultant of the generic layer and $m_{jk}^{(i)}$ is the resultant moment of the generic i-th layer referred to the midline of the laminated plate (see Fig. 4.2). It should be noted here

that the membrane part of $\sigma_{ss}^{(i)}$ is generally not null, unlike in the stress assumption used for the orthotropic plate in the previous section. This inclusion of $n_{ss}^{(i)}$ allows a description of the normal stress σ_{ss} that is layer-wise linear over the laminated plate and discontinuous across layers. With this stress assumption, we can write the complementary strain energy density $\Psi^{(i)}$ per unit area of the generic i-th layer in the same manner as in the previous section:

$$\Psi^{(i)} = \frac{1}{2} \int_{n^{(i)}-t^{(i)}/2}^{n^{(i)}+t^{(i)}/2} \boldsymbol{\sigma^{(i)}}^T \mathbb{H}_P^{(i)} \boldsymbol{\sigma^{(i)}} \, \mathrm{d}n, \tag{4.91}$$

with $\mathbb{H}_P^{(i)} = \tilde{\mathbb{C}}_P^{(i)-1}$ being the compliance matrix of the generic layer. Taking advantage of Eqs. (4.89) and (4.90), we can write the strains in function of the stress resultants for the generic i-th layer:

$$\lambda_{jk} = \frac{\mathrm{d}\Psi^{(i)}}{\mathrm{d}n_{jk}^{(i)}}, \tag{4.92}$$

$$\chi_{jk} = \frac{\mathrm{d}\Psi^{(i)}}{\mathrm{d}m_{jk}^{(i)}}. \tag{4.93}$$

The resulting constitutive law for the generic layer has the form:

$$\left[\begin{array}{c} \boldsymbol{\lambda} \\ \hline \boldsymbol{\chi} \end{array}\right] = \left[\begin{array}{c|c} \mathbf{H}_M^{(i)} & \mathbf{H}_C^{(i)} \\ \hline {\mathbf{H}_C^{(i)}}^T & \mathbf{H}_B^{(i)} \end{array}\right] \left[\begin{array}{c} \mathbf{n}^{(i)} \\ \hline \mathbf{m}^{(i)} \end{array}\right] \tag{4.94}$$

where, in addition to the membrane and bending matrices $\mathbf{H}_M^{(i)}$ and $\mathbf{H}_B^{(i)}$, a coupling matrix $\mathbf{H}_C^{(i)}$ is present. Here, it should be noted that $\boldsymbol{\lambda}$ and $\mathbf{n}^{(i)}$ are [4x1] vectors since no stress component has been discarded.

The compliance matrix in Eq. (4.94) can be inverted to obtain a constitutive law analogous to that of Eq. (4.51) with the main difference being that in this case the coupling sub-matrix $\mathbf{B}^{(i)}$ is generally non-null. This gives:

$$\left[\begin{array}{c} \mathbf{n}^{(i)} \\ \hline \mathbf{m}^{(i)} \end{array}\right] = \left[\begin{array}{c|c} \mathbf{A}^{(i)} & \mathbf{B}^{(i)} \\ \hline \mathbf{B}^{(i)^T} & \mathbf{D}^{(i)} \end{array}\right] \left[\begin{array}{c} \boldsymbol{\lambda} \\ \hline \boldsymbol{\chi} \end{array}\right] \tag{4.95}$$

Once the constitutive law of the generic layer is defined, we can use Eqs. (4.59) and (4.60) together with Eqs. (4.89) and (4.90) to obtain the laminate plate stress resultants:

$$\mathbf{n} = \sum_{i=1}^{N} \mathbf{n}^{(i)}, \tag{4.96}$$

$$\mathbf{m} = \sum_{i=1}^{N} \mathbf{m}^{(i)}, \tag{4.97}$$

and, by means of the constitutive law in Eq. (4.95), we can write the constitutive law of the laminated plate:

$$\mathbf{n} = \sum_{i=1}^{N} \left(\mathbf{A}^{(i)}\right) \boldsymbol{\lambda} + \sum_{i=1}^{N} \left(\mathbf{B}^{(i)}\right) \boldsymbol{\chi}, \tag{4.98}$$

$$\mathbf{m} = \sum_{i=1}^{N} \left(\mathbf{B}^{(i)^T}\right) \boldsymbol{\lambda} + \sum_{i=1}^{N} \left(\mathbf{D}^{(i)}\right) \boldsymbol{\chi}, \tag{4.99}$$

or, in matrix form:

$$\left[\begin{array}{c} \mathbf{n} \\ \hline \mathbf{m} \end{array}\right] = \left[\begin{array}{c|c} \bar{\mathbf{A}} & \bar{\mathbf{B}} \\ \hline \bar{\mathbf{B}}^T & \bar{\mathbf{D}} \end{array}\right] \left[\begin{array}{c} \boldsymbol{\lambda} \\ \hline \boldsymbol{\chi} \end{array}\right] \tag{4.100}$$

with:

$$\bar{\mathbf{A}} = \sum_{i=1}^{N} \mathbf{A}^{(i)} \tag{4.101}$$

$$\bar{\mathbf{B}} = \sum_{i=1}^{N} \mathbf{B}^{(i)} \tag{4.102}$$

$$\bar{\mathbf{D}} = \sum_{i=1}^{N} \mathbf{D}^{(i)} \tag{4.103}$$

The only thing remaining to do is imposing the condition of null n_{ss} on the laminated plate. To do this, the sum of all the single layer contributions to n_{ss} is to be made equal to zero. One way to achieve this condition is to express the N-th contribution to the normal transversal stress as a function of the rest. This gives:

$$n_{ss}^{(N)} = -\sum_{i=1}^{N-1} n_{ss}^{(i)} \tag{4.104}$$

This final condition, added to the initial stress assumption, completely defines the constitutive law for a laminated case. As with the basic orthotropic case, this approach is equivalent to the conventional GBT treatment of condensing the constitutive matrix.

4.3 Shear correction factors

As shown in the previous section, the corrections to the constitutive relation, while somewhat improving the solution, don't completely resolve the kinematic constraints present in the GBT model. The presence of null strain components is indeed accounted for in the new proposed approach, but there is another significant constraint

in the way shear deformability γ_{zs} is described. The fact that warping is introduced as piece-wise linear for the fundamental modes means that λ_{zs} can only be constant over the s coordinate. This results in an inherently poor description of shear, which in turn generates overstiffness of the model. One way of attenuating this problem is the introduction of shear correction factors to adjust the cross-section stiffness matrix, thus improving the elasto-kinematic approximation of λ_{zs} in a manner analogous to that of the Timoshenko beam theory. With this in mind, following the separation of stress components introduced in Eqs. (4.70)-(4.75), we can write the membrane compliance matrix introduced in Eq. (4.80) explicitly as:

$$\mathbf{H}_M = \begin{bmatrix} H_{M\,11} & H_{M\,12} & 0 \\ H_{M\,12} & H_{M\,22} & 0 \\ 0 & 0 & H_{M\,33} \end{bmatrix} \tag{4.105}$$

which in turn allows writing the complementary in-plane membrane energy per unit area as:

$$\Phi = \frac{1}{2}(H_{M\,11}\, n_{zz}^2 + 2H_{M\,12}\, n_{zz}\, n_{zs} + H_{M\,22}\, n_{zs}^2) \tag{4.106}$$

where the contribution n_{zn} is dismissed and the constraint of null n_{ss} has been imposed. The stress resultants in Eq. (4.106) (and thus the complementary in-plane membrane energy Φ) can be calculated in two different ways: either elasto-kinematically by means of the constitutive relation or by using the stress recovery procedure

presented in Chapter 3. Given that Φ must be the same regardless of the way in which it is calculated, the following equalities can be written:

$$\int_s n_{zs}^{REC}\,\mathrm{d}s = \kappa_1 \int_s n_{zs}^{EK}\,\mathrm{d}s \tag{4.107}$$

$$\int_s \left(n_{zs}^{REC}\right)^2\,\mathrm{d}s = \kappa_2 \int_s \left(n_{zs}^{EK}\right)^2\,\mathrm{d}s, \tag{4.108}$$

thus defining the shear corrections factors κ_1 and κ_2. In the expressions above the apex REC stands for "recovered" and indicates that the stress resultant n_{zs} is calculated by means of the recovery procedure of Chapter 3. On the other hand, the apex EK denotes a stress resultant that is obtained by elasto-kinematic means. The shear factors thus obtained can then be applied to the compliance terms in Eq. (4.80) in order to obtain a corrected compliance matrix. The compliance matrix that is to be modified from the constitutive law is denoted below with superposed bar:

$$\bar{\mathbf{H}}_M = \begin{bmatrix} H_{M\,11} & \kappa_1 H_{M\,12} & 0 \\ \kappa_1 H_{M\,12} & \kappa_2 H_{M\,12} & 0 \\ 0 & 0 & H_{M\,33} \end{bmatrix} \tag{4.109}$$

and should replace the $\mathbf{H}_M$ in Eq. (4.80). However, the complementary shear energy evidently depends on the solution state, which in itself is susceptible to the shear correction factors. Since κ_1 and κ_2 cannot be known a priori, an iterative procedure must be followed to actually determine $\bar{\mathbf{H}}_M$ and solve the problem:

- Set an initial value for the shear corrections factors, i.e. $\kappa_1 = \kappa_2 = 1$.
- Obtain a first solution and calculate n_{zs}^{EK} and n_{zs}^{REC}.
- Obtain the shear correction factors κ_1 and κ_2 by means of Eqs. (4.107) and (4.108).
- Use Eq. (4.109) to adjust the cross-section stiffness matrix and obtain a new solution.
- Using the new solution, calculate new shear correction factors κ_1 and κ_2. If the difference between the previous and the new correction factors is less than a fixed tolerance, then exit the procedure. Otherwise, repeat the previous step.

4.4 Some examples

Some examples will be presented in this section to illustrate the different corrections proposed to the constitutive relation. First, the effect of the proposed approaches on the solution for an isotropic case will be presented. Later on, a series of tests using first an orthotropic and later a laminated material will be shown. Finally, an example to illustrate the effect of shear correction factors will be discussed. Hereinafter, the conventional GBT approach based on separate membrane and bending constitutive laws will be denoted simply as "GBT", while the correction to the plate constitutive relation based on the condensation of n_{ss} will be referred to

as "Condensation". Also, the results obtained with the proposed rewriting of the kinematic constraints over the stress field will be called "'Proposed approach". Finally, the results obtained with a shear deformable shell model are included as a benchmark and are denoted as "Shell".

4.4.1 An isotropic beam

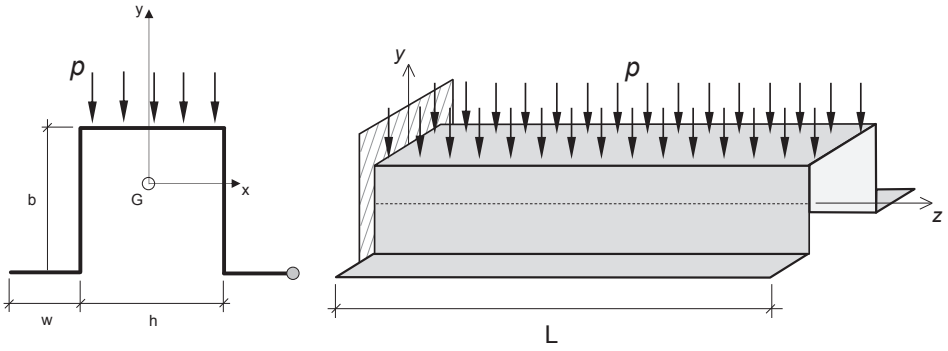

Figure 4.3: Isotropic case: a hat-section cantilever beam under transversal load.

A first example to show the validity of the proposed approach in the case of an isotropic material is presented here. A cantilever hat profile under a uniform surface load (see Fig. 4.3) is modelled using both the conventional GBT membrane-bending constitutive relation and the new approach proposed in this chapter. In both cases, only the natural nodes with their associated shear deformability are considered. For comparison, the results obtained with a shell finite element model are included as well. In this test, the material is steel, the surface load is $p = 1\,N/cm^2$, and the dimensions of the profile are $b = 10\,cm$, $h = 10\,cm$, $w = 5\,cm$, $t = 0.3\,cm$,

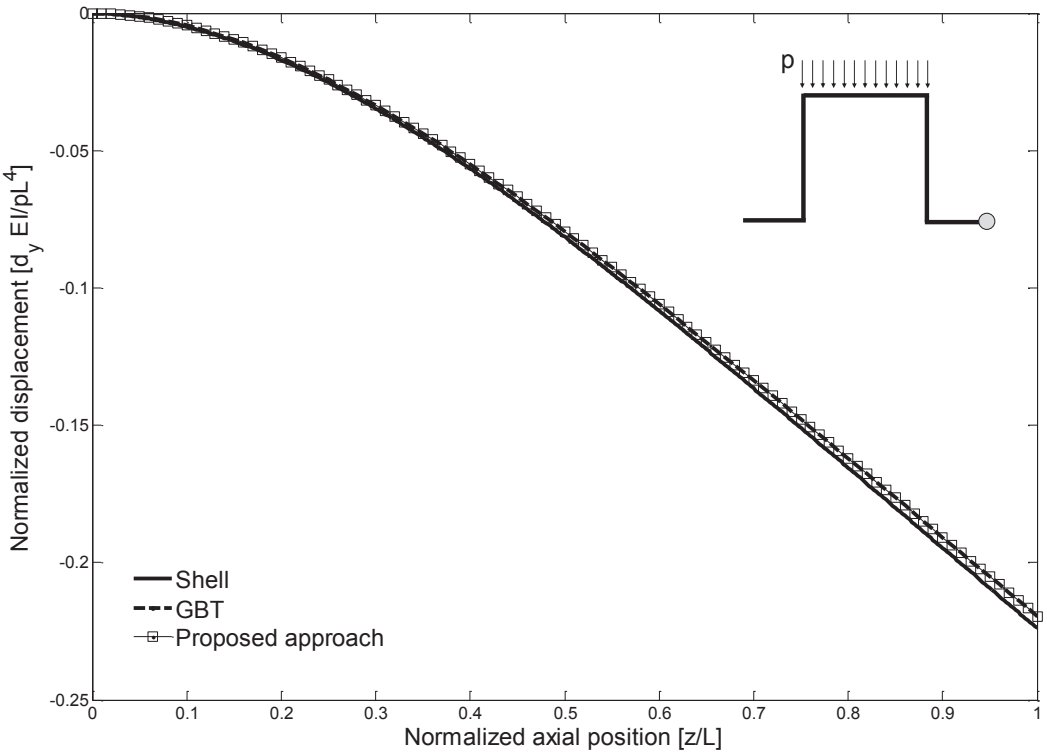

Figure 4.4: Isotropic case: Normalized y-displacement of node 6.

$L = 200\,cm$.

Fig. 4.4 shows the normalized displacement of the cross-section node marked in Fig. 4.3 with a circle along the beam axial direction. As expected, it can be seen that the proposed approach produces results that exactly match those obtained via the conventional membrane-bending constitutive relation. It can also be noted that both solutions show good agreement with the shell finite element model.

4.4.2 An orthotropic beam

To test the performance of the different orthotropic GBT formulations, a cantilever C-beam with lips was considered (see Fig. 4.5)

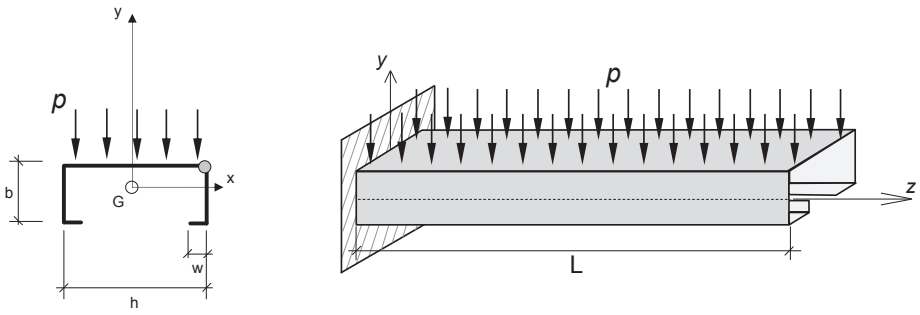

Figure 4.5: Orthotropic case: a C-section cantilever beam under transversal load.

with a uniform surface load applied over the web. The dimensions of the profile are: $b = 10\,cm$, $h = 16\,cm$, $w = 4\,cm$, $t = 0.3\,cm$, $L = 200\,cm$. The load applied is $p = 1\,N/cm^2$. The material used is a Carbon-Fiber-Reinforced-Polymer (CFRP) and has the following properties: $E_1 = 170GPa$, $E_2 = 33GPa$, $E_3 = 5.2GPa$, $\nu_{12} = 0.036$, $\nu_{13} = 0.25$, $\nu_{23} = 0.171$, $G_{12} = 9.4GPa$, $G_{13} = 8.3GPa$, $G_{23} = 3.3GPa$. Four different material orientations are presented, and the angle θ denotes the counter-clockwise rotation of the fibers with respect to the beam axis: $\theta = 0$, $\theta = \pi/2$, $\theta = \pi/6$, and $\theta = \pi/3$. The six fundamental modes with their associated shear deformability are considered in the GBT solution. The attention is focused on the normalized displacement of the cross-section node (hereinafter Node 4) marked in Fig. 4.5.

Fig. 4.6 shows the normalized y-displacement of node 4 for $\theta = 0$. In this case, all of the possible approaches advanced in this chapter closely match the three-dimensional solution. Indeed, the absence of coupling (since some of the trigonometric terms in Eq. (4.19) are null for $\theta = 0$) between the material properties in the z

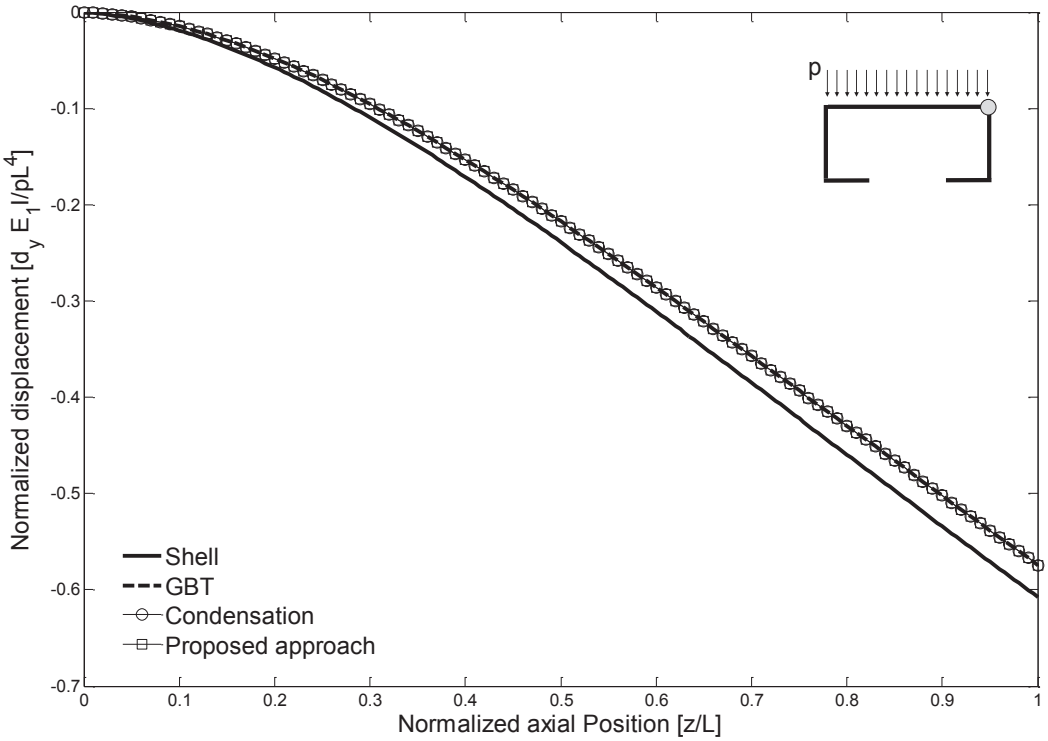

Figure 4.6: Orthotropic case: normalized y-displacement of node 4, $\theta = 0$.

and s directions means all of the proposed solutions are equivalent.

In Fig. 4.7 the normalized y-displacement of node 4 is showed for a material in which fibers are perpendicular to the beam axis ($\theta = \pi/2$). As in the previous case, all the proposed solutions closely match the three-dimensional model. Again, the lack of coupling terms in the constitutive relation means that all solutions proposed are equivalent.

Fig. 4.8 shows the normalized y-displacement of node 4 for a case in which the material fibers are rotated by an angle $\theta = \pi/6$ with respect to the beam axis. In this case a clear difference is present between the different formulations. Firstly, it can be seen the traditional GBT approach of considering an uncoupled constitutive matrix for the membrane deformations results in an overstiff model.

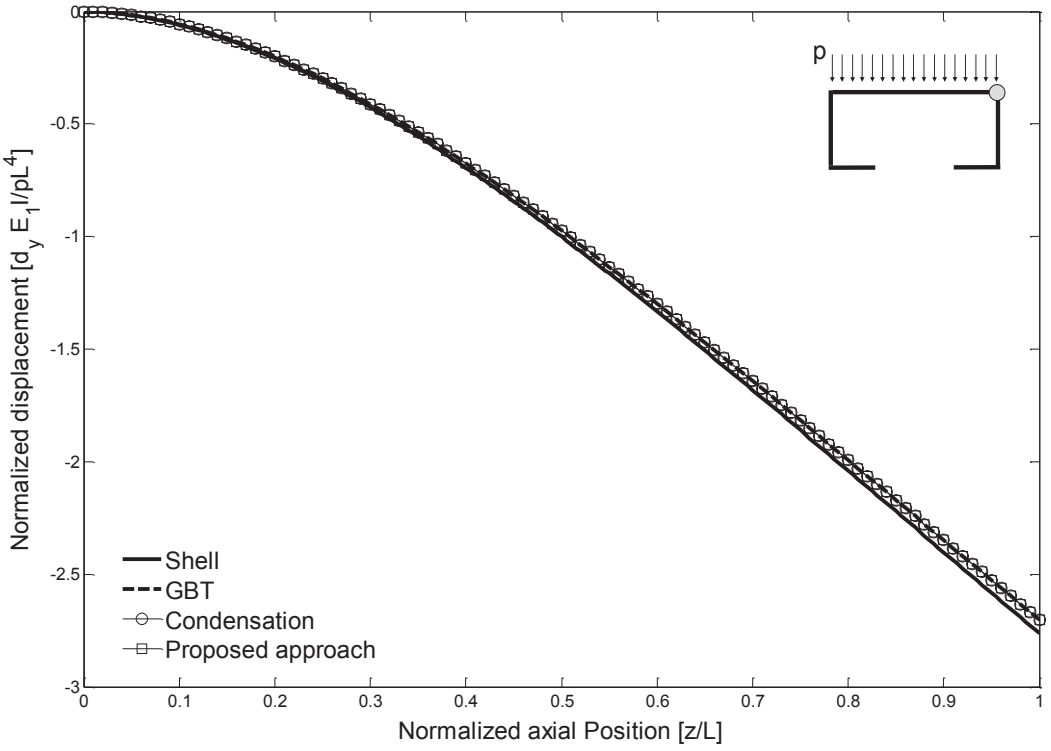

Figure 4.7: Orthotropic case: normalized y-displacement of node 4, $\theta = \pi/2$.

The standard condensation procedure partially solves this problem and brings the GBT solution closer to the three-dimensional one. The proposed approach exactly matches the condensation of n_{ss} as expected.

Fig. 4.9 portrays a situation similar to the previous test. In this case the material fibers are rotated at an angle of $\theta = \pi/3$ degrees with respect to the beam axis. As before, the classical GBT membrane-bending separation results in an overstiff model whereas the enforcement of the kinematic constraints, whether by means of the condensation of n_{ss} or by the proposed approach, have the same effect of relaxing the stiffness of the solution. Also in this case, the proposed approach to the constitutive relations is equivalent with the condensation treatment.

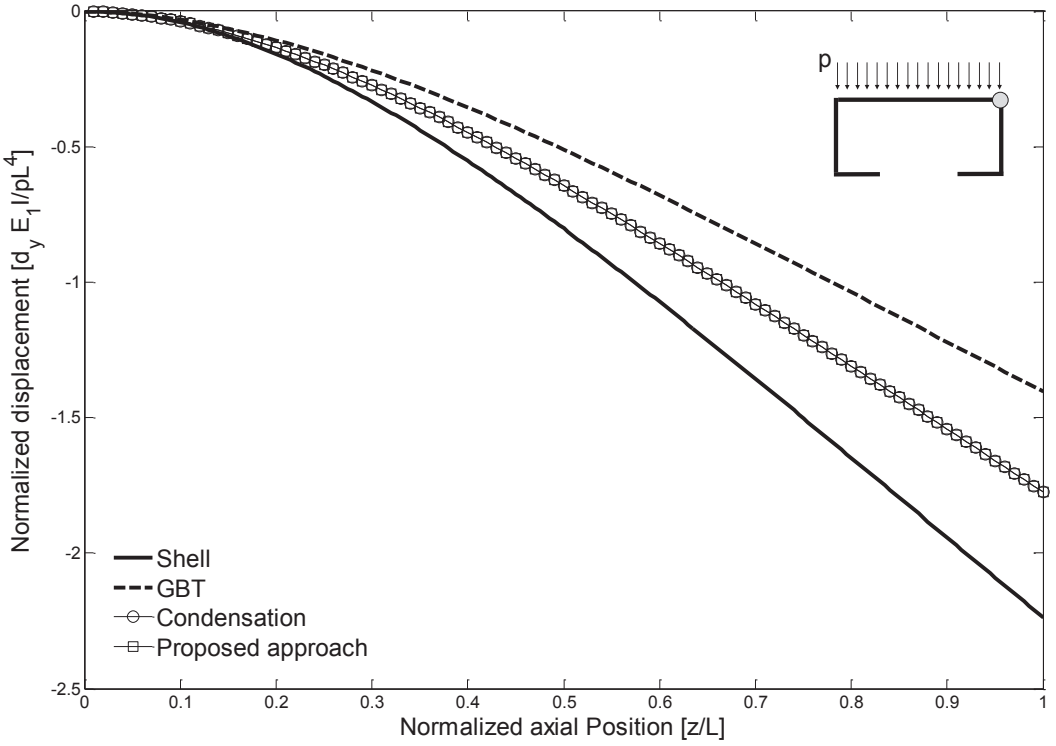

Figure 4.8: Orthotropic case: normalized y-displacement of node 4, $\theta = \pi/6$.

4.4.3 A laminated beam

The results of extending the different approaches presented above to the case of a laminated composite will be presented in this test. The same problem of a cantilever C-beam with lips (see Fig. 4.5) with a uniform surface load applied over the web was used for this test, but in this case the beam walls are formed by stacking three orthotropic layers, all of the same thickness but with different fiber orientations. The dimensions of the profile are: $b = 10\,cm$, $h = 16\,cm$, $w = 4\,cm$, $t = 0.3\,cm$, $L = 200\,cm$. The load applied is $p = 1\,N/cm^2$. The material used for all layers is a CFRP with the following mechanical properties: $E_1 = 170GPa$, $E_2 = 33GPa$, $E_3 = 5.2GPa$, $\nu_{12} = 0.036$, $\nu_{13} = 0.25$, $\nu_{23} = 0.171$, $G_{12} = 9.4GPa$, $G_{13} = 8.3GPa$,

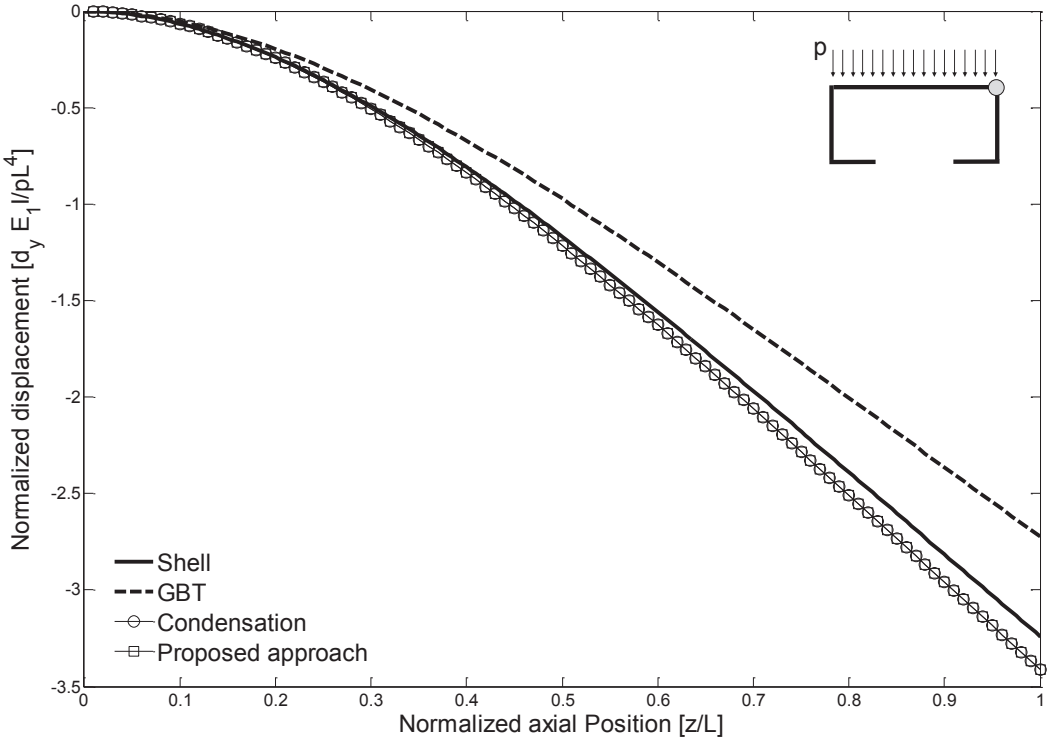

Figure 4.9: Orthotropic case: normalized y-displacement of node 4, $\theta = \pi/3$.

$G_{23} = 3.3GPa$. Two different stacking sequences are presented: first, a symmetrical sequence is used with the fiber orientation for each layer being $\theta = [\pi/3; \pi/6; \pi/3]$ and later an unsymmetrical sequence $\theta = [0; \pi/6; \pi/3]$ is used. The six fundamental modes with their associated shear deformability are considered in this example and the normalized displacement of node 4 (shown in Fig. 4.5) is reported.

Fig. 4.10 shows the normalized y-displacement of node 4 for the stacking sequence $[\pi/3; \pi/6; \pi/3]$. It can be seen that the conventional GBT approach of separating membrane and bending constitutive relations produces a model that is overstiff in the same way as the single-layer orthotropic beam already shown. The proposed approach improves this situation and stands in better agreement with

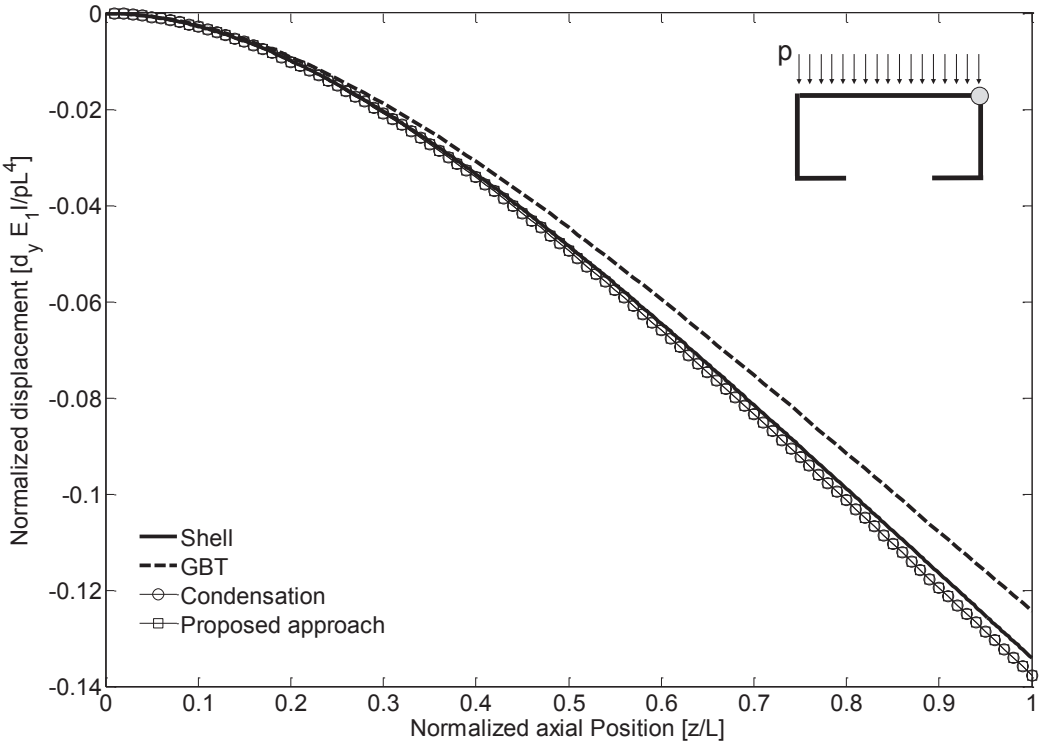

Figure 4.10: Laminated case: normalized y-displacement of node 4, stacking sequence $[\pi/3; \pi/6; \pi/3]$.

the shell solution. The condensation of n_{ss} matches the proposed approach, as expected. It should be noted that in this case the membrane-bending stiffness matrix $\mathbf{B}$ is null due to the symmetry of the stacking sequence.

Fig. 4.11 refers to the stacking sequence $[0; \pi/6; \pi/3]$ and presents a situation similar to the previous case. Again, the normalized y-displacement of node 4 is shown, and the conventional GBT formulation results in a stiffer model. The results obtained from the proposed approach closely match the shell finite element solution and again coincide with those obtained by means of the condensation of the transversal membrane stress n_{ss}.

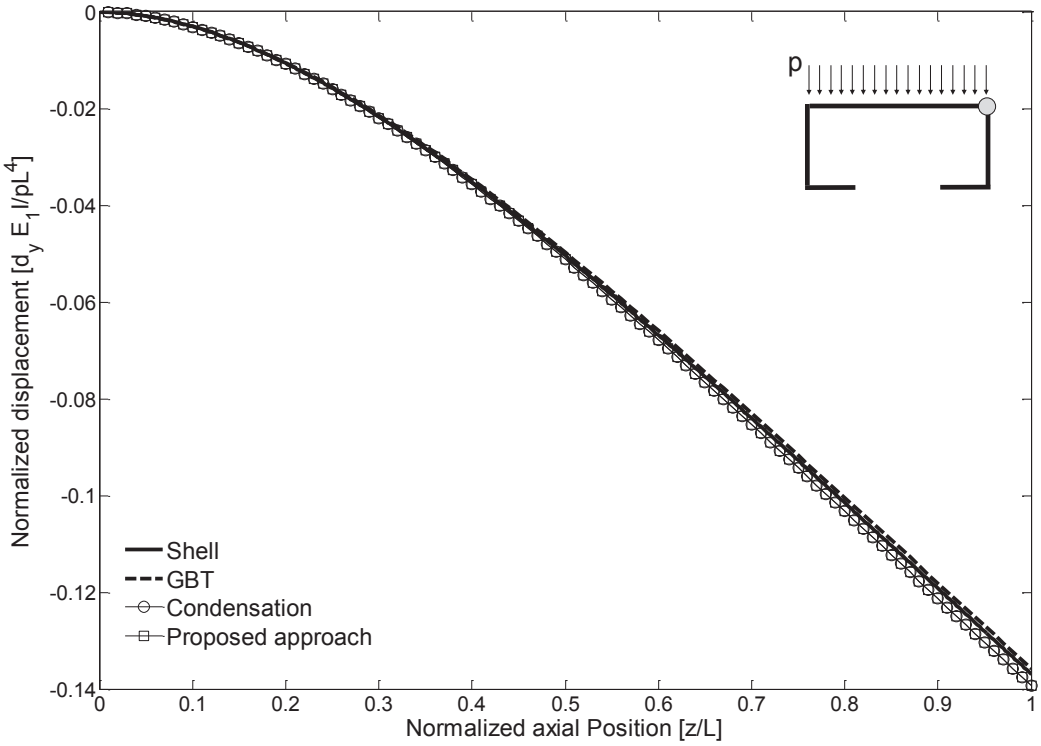

Figure 4.11: Laminated case: normalized y-displacement of node 4, stacking sequence $[0; \pi/6; \pi/3]$.

4.4.4 Shear correction factors

To show the effect of the shear correction factors, the example of the cantilever Z-profile presented in Chapter 3 is revisited. A transversal distributed load is applied at the upper flange, as shown in Fig. 4.12. The material is steel and the dimensions are: $b = 4cm$, $h = 12cm$, $w = 1.5cm$, $t = 0.18cm$, $L = 120cm$.

The convergence rate of the iterative procedure is illustrated in Fig. 4.13, which shows the value of the complementary in-plane membrane energy per unit area Φ over successive iterations. The shear correction factors obtained for this example after the iteration process are $\kappa_1 = 0.7047$ and $\kappa_2 = 0.0064$. The effect of

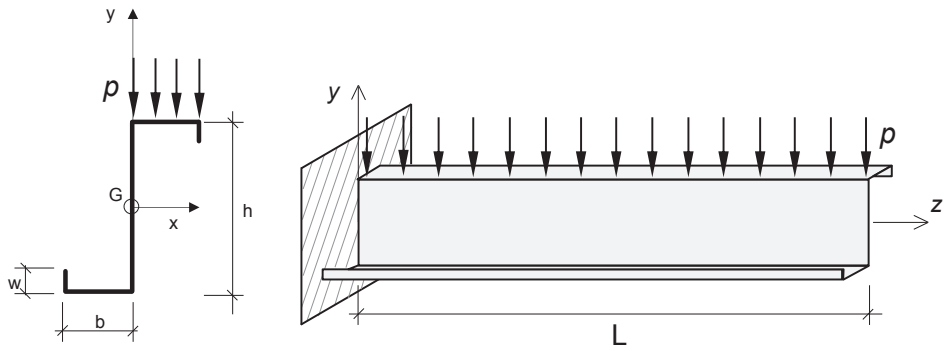

Figure 4.12: Shear correction factors: a Z-section cantilever beam under transversal load.

this correction is shown in Fig. 4.14 where the distribution of the elasto-kinematic shear stress τ_{zs} over the section midline is presented with (denoted as "Elasto-kinematic w κ") and without (denoted as "Elasto-kinematic w/o κ") the shear correction factors. As can be seen, the inclusion of said factors has a significant effect on the solution and helps to correct the poor elasto-kinematic description of shear. By this adjustment of the constitutive relation, the elasto-kinematic shear stress distribution more closely approximates the results of the recovery procedure, which in themselves follow closely a fully three-dimensional solution, and both give the same energy contribution.

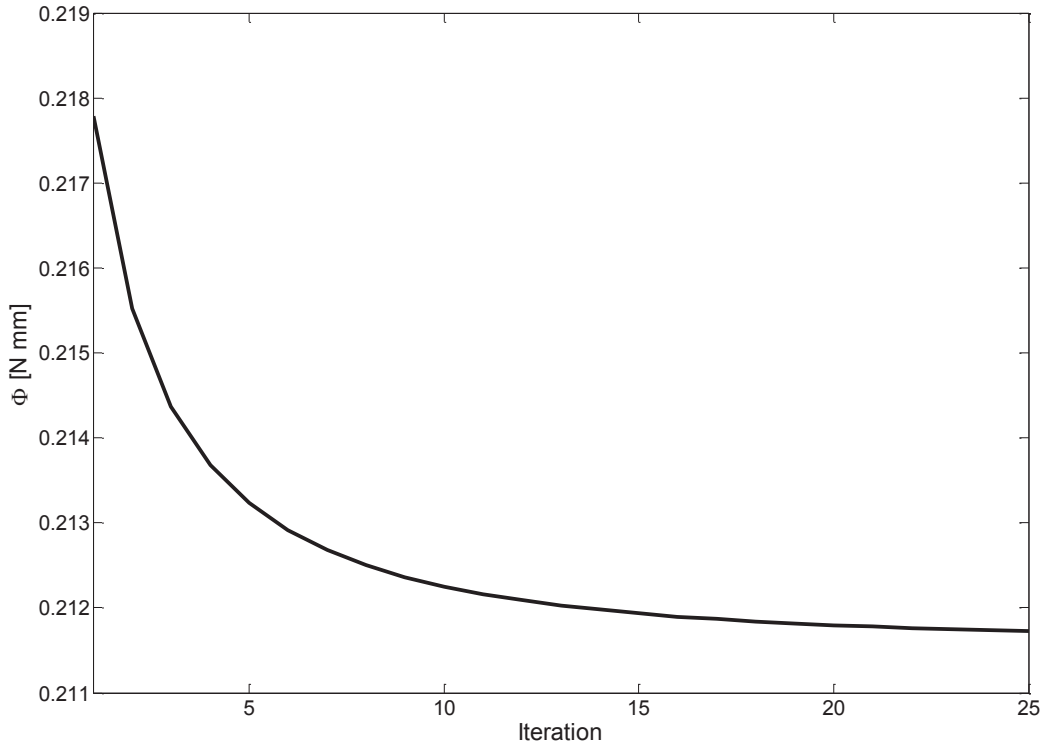

Figure 4.13: Shear correction factors: Convergence rate of the complementary in-plane membrane energy per unit area.

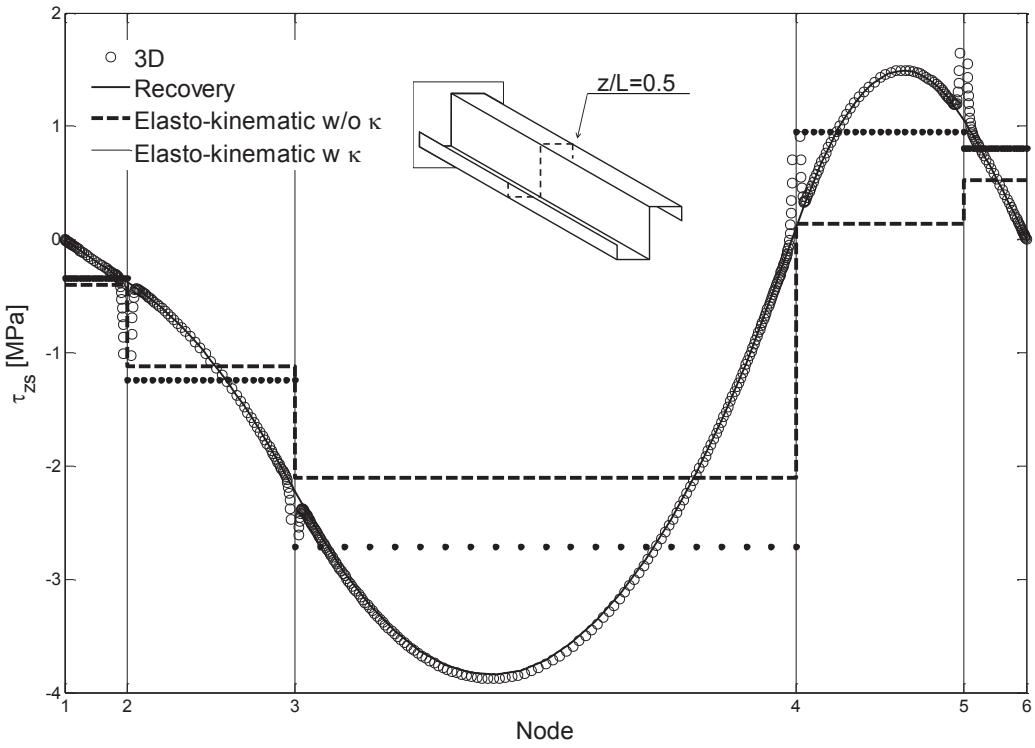

Figure 4.14: Shear correction factors: effect of the shear correction factors κ_1 and κ_2 on the distribution of τ_{zs} over the cross-section midline.

Conclusions

The analysis of thin-walled beams is a rich and complex area of knowledge. Whether attention is directed toward cold-formed profiles, composite beams, or some other form of these structural elements, the particular mechanics that must be described require rigorous and precise treatment. Moreover, the current trends in engineering call for the usage of thin-walled beams in increasingly diverse contexts, each one with a particular set of critical conditions that must be met even in extreme environments. Economical factors also push the limits of application of thin-walled beams, requiring always to do more with less, and driving innovation for cheaper and more structurally efficient structural elements. All these factors engender a need for precise and efficient calculation tools that can not only provide accurate results at a low computational cost, but also be readily used by engineers following standard structural design practices. In this work, a solution for these exigencies has been advanced in the form of a numerical implementation of the Generalized Beam Theory (GBT).

After an introduction to the mechanics of thin-walled beams and a quick review of some of the most well-known approaches

to describe the behaviour of these elements, a novel formulation of the GBT is presented. This formulation contains the classic shear-deformable GBT available in the literature and contributes an additional description of cross-section warping that is variable along the wall thickness besides along the wall midline. Shear deformation is introduced in such a way that the classical shear strain components of the Timoshenko beam theory are recovered exactly. According to the new kinematics proposed, a reviewed form of the cross-section analysis procedure is devised, based on a unique modal decomposition. After the modal decomposition, it is possible to: (i) clearly distinguish bending deflections from deflections due to shearing strains and (ii) recover classical beam degrees of freedom and standard beam theories as special cases.

After the new formulation for the GBT is advanced, a procedure for a posteriori reconstruction of all the three-dimensional stress components in the finite element analysis of thin-walled beams using the GBT has been presented. The reconstruction is simple and based on the use of three-dimensional equilibrium equations and of the RCP procedure. Numerical results show that the procedure allows to effectively recover local stress profiles which match those of three-dimensional solid finite element models, without any need for correcting procedure to meet boundary conditions on bottom/top faces of the walls.

Finally, once the stress reconstruction procedure is presented, a study of several existing issues on the constitutive relations in the

GBT is carried. Firstly, attention is drawn to the current practice of: (i) considering separate constitutive laws for the membrane and bending parts of the model in isotropic beams and (ii) using a single constitutive law for orthotropic profiles with a condensation of the transverse normal stress in the direction of the cross-section midline. The apparent inconsistency between these two approaches is resolved by proposing a constitutive law based on mirroring the kinematic constraints of the GBT model into a specific stress field assumption. It is shown that this method is equally valid for isotropic and orthotropic beams and coincides with each of the conventional approaches. Later on, an analogous procedure is presented for the case of laminated beams. Lastly, as a way to improve an inherently poor description of shear deformability in the GBT, the introduction of shear correction factors is proposed. These factors are obtained by means of an iterative procedure and are shown to improve the energy contribution of the shear strain to the GBT model.

Bibliography

[1] EN 1993-1-3:2006(E) Part 1-3 Supplementary rules for cold formed members and sheeting., CEN.

[2] Standards Australia and Standard new Zealand. Cold-formed steel structures AS/NZS 4600, 1996.

[3] AISI, North American Specifications. Appendix 1: design of cold-formed steel structural members using the direct strenght method. In: 2004 supplement to the North American specifications for the design of cold-formed steel structures., American Iron and Steel Institution, Washington (DC),2004.

[4] UNI EN 1993-1-3, Progettazione delle strutture in acciaio - Parte 1-3: Regole generali- Regole supplementari per l'impiego dei pro
lati e delle lamiere sottili piegati a freddo.

[5] V.Z. Vlasov, Thin-Walled Elastic Beams, Monson, Jerusalem, 1961.

[6] F. Bleich, Buckling Strength of metal structures, McGraw-Hill, New York, 1952

[7] S.P. Timoshenko, J. M. Gere, Theory of Elastic Stability, McGraw-Hill, New York, 1961.

[8] Y.J. Kang, C.H. Yoo, Thin-walled curved beams I: formulation of nonlinear equations, Journal of Engineering Mechanics Division, 120 (EM10) (1994), pp. 2072–2101

[9] M.H. Kim, B.C. Min, M.W. Suh, Spatial stability of non-symmetric thin walled curved beams, I: analytical approach, Journal of Engineering Mechanics-ASCE 126 (2000) 497-505.

[10] J.F. Wilson, Y. Wang, I. Threfall, Responses of near optimal continuous horizontally curved beams to transit loads, Journal of Sound Vibrations 222 (1999) 565-575.

[11] L.T. Stavridis, G.T. Michaltsos, Eigenfrequency analysis of thin walled girders curved in plan, Journal of Sound and Vibration, 227 (1999) 383–396.

[12] M. Capurso, Sul calcolo delle travi in parete sottile in presenza di forze e distorsioni, La ricerca scientifica 6 (1964) 241-286.

[13] M. Capurso, Influenza delle componenti di scorrimento nella deformazione delle travi di parete sottile con sezione aperta, Giornale del Genio Civile 122 (1984) 127-144.

[14] M.T. Piovan, V.H. Cortínez, R.E. Rossi, Out-of-plane vibrations of shear deformable continuous horizontally thin-walled curved beams, Journal of Sound and Vibration, 237 (2000) 101–118.

[15] A.S. Gendy, F. Saleeb, Vibration-analysis of coupled extensional–flexural–torsional modes of curved beams with arbitrary thin-walled sections, Journal of Sound and Vibrations, 174 (1994) 261–274.

[16] M.Y. Kim, S.B. Kim, N.I. Kim, Spatial stability of shear deformable curved beams with non-symmetric thin walled sections, I: stability formulation and closed form solutions, Computers and Structures, 83(2005) 2525–2241

[17] R.P. Schardt, Verallgemeinerte Technische Biegetheorie, Springer, Berlin, 1989.

[18] R.P. Schardt, Generalized Beam Theory - an adequate method for coupled stability problems, Thin-Walled Structures, 19 (1994) 161-180.

[19] P. Dinis, D. Camotim, N. Silvestre, GBT formulation to analyse the buckilng behavior of thin-walled members with arbitrarily "branched" open cross-sections, Thin-Walled Structures 44 (2006) 20-38.

[20] N. Silvestre, Generalised beam theory to analyse the buckling behavior of circular cylindrical shells and tubes, Thin-Walled Structures 45 (2007) 185-198.

[21] R. Goncalves, P. Dinis, D. Camotim, GBT formulation to analyse the first-order and buckling behavior of thin-walled

members with arbitrary cross-sections, Thin-Walled Structures 47 (2009) 583-600.

[22] J.M. Davies, P. Leach, D. Heinz, Second-order Generalized Beam Theory, Journal of Constructional Steel Research 31 (1994) 221-241.

[23] N. Silvestre, D. Camotim, GBT buckling analysis of pultruded FRP lipped channel members, Computers and Structures 81 (2003) 1889-1904.

[24] D. Camotim, C. Basaglia, N. Silvestre, GBT buckling analysis of thin-walled steel frames: A state-of-the-art report, Thin Walled Structures 48 (2010) 726-743.

[25] G. Ranzi, A. Luongo, A new approach for thin-walled member analysis in the framework of GBT, Thin-Walled Structures 49 (2011) 1404-1414.

[26] S. de Miranda, R. Miletta, A. Ruggerini, F. Ubertini, On the numerical modeling of thin-walled cold-formed roof systems, in: Proceedings of the IV European Conference on Computational Mechanics, Paris, France, May 2010.

[27] S. de Miranda, R. Miletta, A. Ruggerini, F. Ubertini, Progettazione e calcolo di sistemi di copertura formati a freddo, Costruzioni Metalliche 3 (2011) 43-53.

[28] M. Braham, A. Ruggerini, F. Ubertini, A numerical model

for roof detailing of cold-formed purlin-sheeting systems, Stahlbau 77 (2008) 238-246.

[29] N. Silvestre, D. Camotim, Nonlinear Generalized Beam Theory for cold-formed steel members, International Journal of Structural Stability and Dynamics 3 (2003) 461-490.

[30] N. Silvestre, D. Camotim, Influence of sheardeformation on the local and global buckling behaviour of composite thin-walled members, in: Thin-walled structures: advances in research, design and manufacturing technology (conference proceedings – Loughborough, 22–24/6), J. Loughlan (Ed.), Institute of Physics Publishing, Bristol, 2004, 659-668.

[31] S. de Miranda, A. Gutiérrez, R. Miletta, F. Ubertini, A generalized beam theory with shear deformation, Thin-walled Structures 67 (2013) 88-100.

[32] C.E.S. Cesnik, D.H. Hodges, VABS: A new concept for composite rotor blade cross-section modelling. Journal of the American Helicopter Society 42(1997) 27–38

[33] V.V. Volovoi, D.H. Hodges, V.L. Berdichevsky, V.G. Sutyrin, Asymptotic theory for static behavior of elastic anisotropic I-beams, International Journal of Solids and Structures 36 (1999) 1017–1043

[34] D. Camotim, N. Silvestre, C. Basaglia, R. Bebiano, GBT-based buckling analysis of thin-walled members with non-

standard support conditions, Thin-Walled Structures 46 (2008) 800-815.

[35] S. de Miranda, A. Gutiérrez, R. Miletta, Equilibrium-based reconstruction of three-dimensional stresses in GBT, Thin-walled Structures 74 (2014) 146-154

[36] F. Ubertini, Patch recovery based on complementary energy, International Journal for Numerical Methods in Engineering 59 (2004) 1501-1538.

[37] A. Benedetti, S. de Miranda, F. Ubertini, A posteriori error estimation based on the superconvergent recovery by compatibility in patches, International Journal for Numerical Methods in Engineering 67 (2006) 108-131.

[38] F. Daghia, S. de Miranda, F. Ubertini, E. Viola, A hybrid stress approach for laminated composite plates within the First-order Shear Deformation Theory, International Journal of Solids and Structures 45 (2008) 1766-1787.

[39] S. de Miranda, K. Garikipati, L. Molari, F. Ubertini, A simple solution strategy for coupled piezo-diffusion in elastic solids, Computational Mechanics 44 (2009) 191–203.

[40] G. Castellazzi, S. de Miranda, F. Ubertini, Adaptivity based on the recovery by compatibility in patches, Finite Element in Analysis and Design 46 (2010) 379-390.

[41] G. Castellazzi, S. de Miranda, F. Ubertini, Patch based stress recovery for plate structures, Computational Mechanics 47 (2011) 379-394.

[42] S. de Miranda, L. Patruno, F. Ubertini, Transverse stress profiles reconstruction for finite element analysis of laminated plates, Composite Structures 94 (2012) 2706-2715.

[43] F. Daghia, S. de Miranda, F. Ubertini, Patch based recovery in finite element elastoplastic analysis, Computational Mechanics 52 (2013) 827-836.

[44] N. Bauld Jr., L. Tzeng, A Vlasov theory for fiber-reinforced beams with thin-walled open cross sections, International Journal of solids and structures 20 (1984) 277-297.

[45] X. Wu, C. Sun, Simplified theory for composite thin-walled beams. AIAA J. 30(1992) 2945–2951.

[46] R. Chandra, I. Chopra, Structural response of composite beams and blades with elastic couplings, Composites Engineering 2 (1992) 347-374.

[47] C. Kim, S. White, Thick-walled composite beam theory including 3-D elastic effects and torsional warping, International journal of Solids and Structures 34 (1997) 4237-4259.

[48] N. Silvestre, D. Camotim, First-order generalized beam theory for arbitrary orthotropic materials, Thin-Walled Structures 40 (2002) 755-789.

[49] N. Silvestre, D. Camotim, GBT-based local and global vibration analysis of loaded composite open-section thin-walled members, International Journal of Structural Stability and Dynamics 6 (2006) 1-29.

[50] N.M.F. Silva, N. Silvestre, On the influence of material couplings on the linear and bickling behavior of I-section composite columns, International Journal of Structural Stability and Dynamics 7 (2007) 243-272.

[51] N.M.F. Silva, N. Silvestre, D. Camotim, GBT formulation to analyse the buckling behaviour of FRP composite open-section thin-walled columns, Composite Structures 93 (2010) 79-92.

[52] F. Auricchio, E. Sacco, A mixed-enhanced finite element for the analysis of laminated composite plates, International Journal for Numerical Methods in Engineering, 44 (1999) 1481-1504

[53] N.W. Murray, Introduction to the Theory of Thin-Walled Structures, Oxford University Press, New York, 1984.

[54] L. De Lorenzis, A. La Tegola, Static behavior of pultruded fiber-reinforced polymer thin-walled beams, Composite Structures 60 (2003) 231-244.

[55] L. De Lorenzis, A. La Tegola, Effect of the actual distribution of applied stresses on global buckling of isotropic and trans-

versely isotropic thin-walled members: Numerical examples, Composite Structures 71 (2005) 83-100.

[56] L.V. Kantorovich, V. I. Kyrlov, Approximate method of higher analysis, Interscience Publishers, New York, 1958.

[57] Y.K. Cheung, L. G. Tham, The Finite Strip Method, CRC Press, Florida, 1997.

[58] S. Adany, N. Silvestre, B.W. Schafer, D. Camotim, GBT and cFSM: two modal approaches to the buckling analysis of unbranched thin-walled members, Advanced Steel Construction - An International Journal 5 (2009) 195-223.

[59] B. W. Schafer, S. Ádány, Buckling analysis of cold-formed steel members using CUFSM: conventional and constrained finite strip methods, in: Eighteenth international specialty conference on cold-formed steel structures, 2006.

[60] B. W. Schafer, Finite strip stability solutions for general boundary conditions and the extension of the constrained finite strip method, in: Trends in civil and structural engineering computing, Topping BHV, Costa Neves LF, Barros RC, editors, Stirlingshire, 2009.

[61] M.T. Piovan, V.H. Cortínez, Mechanics of thin-walled curved beams made of composite materials, allowing for shear deformability. Thin-Walled Structures 45 (2007) 759-789

[62] A.H. Sheikh, O.T. Thomsen, An efficient beam element for the analysis of laminated composite beams of thin-walled open and closed cross sections. Composites Science and Technology 68 (2008) 2273-2281

[63] N.I. Kim, D.K. Shinb, M.Y. Kim, Exact solutions for thin-walled open-section composite beams with arbitrary lamination subjected to torsional moment, Thin-Walled Structures 44 (2006) 638-654

[64] J.N. Reddy, Mechanics of laminated composite plates and shells: theory and analysis, CRC Press, Boca Raton, 2004.